THESE TERMS GOVERN YOUR USE OF THIS DOCUMENT

Your use of this Ontario Geological Survey document (the "Content") is governed by the terms set out on this page ("Terms of Use"). By downloading this Content, you (the "User") have accepted, and have agreed to be bound by, the Terms of Use.

Content: This Content is offered by the Province of Ontario's *Ministry of Northern Development and Mines* (MNDM) as a public service, on an "as-is" basis. Recommendations and statements of opinion expressed in the Content are those of the author or authors and are not to be construed as statement of government policy. You are solely responsible for your use of the Content. You should not rely on the Content for legal advice nor as authoritative in your particular circumstances. Users should verify the accuracy and applicability of any Content before acting on it. MNDM does not guarantee, or make any warranty express or implied, that the Content is current, accurate, complete or reliable. MNDM is not responsible for any damage however caused, which results, directly or indirectly, from your use of the Content. MNDM assumes no legal liability or responsibility for the Content whatsoever.

Links to Other Web Sites: This Content may contain links, to Web sites that are not operated by MNDM. Linked Web sites may not be available in French. MNDM neither endorses nor assumes any responsibility for the safety, accuracy or availability of linked Web sites or the information contained on them. The linked Web sites, their operation and content are the responsibility of the person or entity for which they were created or maintained (the "Owner"). Both your use of a linked Web site, and your right to use or reproduce information or materials from a linked Web site, are subject to the terms of use governing that particular Web site. Any comments or inquiries regarding a linked Web site must be directed to its Owner.

Copyright: Canadian and international intellectual property laws protect the Content. Unless otherwise indicated, copyright is held by the Queen's Printer for Ontario.

It is recommended that reference to the Content be made in the following form: <Author's last name>, <Initials> <year of publication>. <Content title>; Ontario Geological Survey, <Content publication series and number>, <total number of pages>p.

Use and Reproduction of Content: The Content may be used and reproduced only in accordance with applicable intellectual property laws. *Non-commercial* use of unsubstantial excerpts of the Content is permitted provided that appropriate credit is given and Crown copyright is acknowledged. Any substantial reproduction of the Content or any *commercial* use of all or part of the Content is prohibited without the prior written permission of MNDM. Substantial reproduction includes the reproduction of any illustration or figure, such as, but not limited to graphs, charts and maps. Commercial use includes commercial distribution of the Content, the reproduction of multiple copies of the Content for any purpose whether or not commercial, use of the Content in commercial publications, and the creation of value-added products using the Content.

Contact:

FOR FURTHER INFORMATION ON	PLEASE CONTACT:	BY TELEPHONE:	BY E-MAIL:
The Reproduction of Content	MNDM Publication Services	Local: (705) 670-5691 Toll Free: 1-888-415-9845, ext. 5691 (inside Canada, United States)	Pubsales@ndm.gov.on.ca
The Purchase of MNDM Publications	MNDM Publication Sales	Local: (705) 670-5691 Toll Free: 1-888-415-9845, ext. 5691 (inside Canada, United States)	Pubsales@ndm.gov.on.ca
Crown Copyright	Queen's Printer	Local: (416) 326-2678 Toll Free: 1-800-668-9938 (inside Canada, United States)	Copyright@gov.on.ca

LES CONDITIONS CI-DESSOUS RÉGISSENT L'UTILISATION DU PRÉSENT DOCUMENT.

Votre utilisation de ce document de la Commission géologique de l'Ontario (le « contenu ») est régie par les conditions décrites sur cette page (« conditions d'utilisation »). En téléchargeant ce contenu, vous (l'« utilisateur ») signifiez que vous avez accepté d'être lié par les présentes conditions d'utilisation.

Contenu : Ce contenu est offert en l'état comme service public par le *ministère du Développement du Nord et des Mines* (MDNM) de la province de l'Ontario. Les recommandations et les opinions exprimées dans le contenu sont celles de l'auteur ou des auteurs et ne doivent pas être interprétées comme des énoncés officiels de politique gouvernementale. Vous êtes entièrement responsable de l'utilisation que vous en faites. Le contenu ne constitue pas une source fiable de conseils juridiques et ne peut en aucun cas faire autorité dans votre situation particulière. Les utilisateurs sont tenus de vérifier l'exactitude et l'applicabilité de tout contenu avant de l'utiliser. Le MDNM n'offre aucune garantie expresse ou implicite relativement à la mise à jour, à l'exactitude, à l'intégralité ou à la fiabilité du contenu. Le MDNM ne peut être tenu responsable de tout dommage, quelle qu'en soit la cause, résultant directement ou indirectement de l'utilisation du contenu. Le MDNM n'assume aucune responsabilité légale de quelque nature que ce soit en ce qui a trait au contenu.

Liens vers d'autres sites Web : Ce contenu peut comporter des liens vers des sites Web qui ne sont pas exploités par le MDNM. Certains de ces sites pourraient ne pas être offerts en français. Le MDNM se dégage de toute responsabilité quant à la sûreté, à l'exactitude ou à la disponibilité des sites Web ainsi reliés ou à l'information qu'ils contiennent. La responsabilité des sites Web ainsi reliés, de leur exploitation et de leur contenu incombe à la personne ou à l'entité pour lesquelles ils ont été créés ou sont entretenus (le « propriétaire »). Votre utilisation de ces sites Web ainsi que votre droit d'utiliser ou de reproduire leur contenu sont assujettis aux conditions d'utilisation propres à chacun de ces sites. Tout commentaire ou toute question concernant l'un de ces sites doivent être adressés au propriétaire du site.

Droits d'auteur : Le contenu est protégé par les lois canadiennes et internationales sur la propriété intellectuelle. Sauf indication contraire, les droits d'auteurs appartiennent à l'Imprimeur de la Reine pour l'Ontario.
Nous recommandons de faire paraître ainsi toute référence au contenu : nom de famille de l'auteur, initiales, année de publication, titre du document, Commission géologique de l'Ontario, série et numéro de publication, nombre de pages.

Utilisation et reproduction du contenu : Le contenu ne peut être utilisé et reproduit qu'en conformité avec les lois sur la propriété intellectuelle applicables. L'utilisation de courts extraits du contenu à des fins *non commerciales* est autorisé, à condition de faire une mention de source appropriée reconnaissant les droits d'auteurs de la Couronne. Toute reproduction importante du contenu ou toute utilisation, en tout ou en partie, du contenu à des fins *commerciales* est interdite sans l'autorisation écrite préalable du MDNM. Une reproduction jugée importante comprend la reproduction de toute illustration ou figure comme les graphiques, les diagrammes, les cartes, etc. L'utilisation commerciale comprend la distribution du contenu à des fins commerciales, la reproduction de copies multiples du contenu à des fins commerciales ou non, l'utilisation du contenu dans des publications commerciales et la création de produits à valeur ajoutée à l'aide du contenu.

Renseignements :

POUR PLUS DE RENSEIGNEMENTS SUR	VEUILLEZ VOUS ADRESSER À :	PAR TÉLÉPHONE :	PAR COURRIEL :
la reproduction du contenu	Services de publication du MDNM	Local : (705) 670-5691 Numéro sans frais : 1 888 415-9845, poste 5691 (au Canada et aux États-Unis)	Pubsales@ndm.gov.on.ca
l'achat des publications du MDNM	Vente de publications du MDNM	Local : (705) 670-5691 Numéro sans frais : 1 888 415-9845, poste 5691 (au Canada et aux États-Unis)	Pubsales@ndm.gov.on.ca
les droits d'auteurs de la Couronne	Imprimeur de la Reine	Local : 416 326-2678 Numéro sans frais : 1 800 668-9938 (au Canada et aux États-Unis)	Copyright@gov.on.ca

©1986 Government of Ontario
Printed in Ontario, Canada

ONTARIO GEOLOGICAL SURVEY

Open File Report 5610

Exploration Technology Development Fund Grant No. 010 Advanced Hardware and Software Development for Ground EM Prospecting

by

J.C. Macnae and Y. Lamontagne

1986

Parts of this publication may be quoted if credit is given. It is recommended that reference to this publication be made in the following form:

Macnae, J.C., and Lamontagne, Y.

1986: Exploration Technology Development Fund, Grant 010, Advanced Hardware and Software Development for Ground EM Prospecting, Ontario Geological Survey Open File Report 5610, 40p., 4 tables, 29 figures, and 2 appendices.

Ministry of
Northern Development
and Mines

Ontario

Ontario Geological Survey

OPEN FILE REPORT

Open File Reports are made available to the public subject to the following conditions:

This report is unedited. Discrepancies may occur for which the Ontario Geological Survey does not assume liability. Recommendations and statements of opinions expressed are those of the author or authors and are not to be construed as statements of government policy.

This Open File Report is available for viewing at the following locations:

(1) Mines Library
Ministry of Northern Development and Mines
8th floor, 77 Grenville Street
Toronto, Ontario M5S 1B3

(2) The office of the Regional or Resident Geologist in whose district the area covered by this report is located.

Copies of this report may be obtained at the user's expense from a commercial printing house. For the address and instructions to order, contact the appropriate Regional or Resident Geologist's office(s) or the Mines Library. Microfiche copies (42x reduction) of this report are available for $2.00 each plus provincial sales tax at the Mines Library or the Public Information Centre, Ministry of Natural Resources, W-1640, 99 Wellesley Street West, Toronto.

Handwritten notes and sketches may be made from this report. Check with the Mines Library or Regional/Resident Geologist's office whether there is a copy of this report that may be borrowed. A copy of this report is available for Inter-Library Loan.

This report is available for viewing at the following Regional or Resident Geologists' offices:

All Regional/Resident Geologists' Offices.

The right to reproduce this report is reserved by the Ontario Ministry of Northern Development and Mines. Permission for other reproductions must be obtained in writing from the Director, Ontario Geological Survey.

V.G. Milne, Director
Ontario Geological Survey

EXPLORATION TECHNOLOGY DEVELOPMENT FUND

Final Research Report

Foreword

The Exploration Technology Development Program was created in the Fall of 1981 as part of the Ontario Government's Board of Industrial Leadership and Development program to assist in areas of mineral exploration and research. The intention of this program is to encourage the advancement of exploration geophysics and geochemistry through mission-oriented joint ventures with industry.

It is the intent of this Program to finance 60 percent of approved project activities to a maximum government contribution of $150,000/year.

A requirement of the Exploration Technology Development Program is that grant recipients submit a final report concerning project activities while receiving a grant. A final report is defined as a comprehensive summary stating the findings obtained during the tenure of the grant, together with supporting data.

It is not the intent of the Ontario Geological Survey to formally publish the final reports for wide distribution but rather to encourage the recipients of grants to seek publication in appropriate scientific journals whenever possible. The Survey, however, also has an obligation to ensure that the results of the research are made available to the public at an early date. Although final reports are the property of the applicants and the sponsoring agencies, they may also be placed on open file. This report is intended to meet this obligation.

No attempt has been made to edit the report, the technical content of which is entirely the responsibility of the authors.

V.G. Milne
Director
Ontario Geological Survey.

TABLE OF CONTENTS

	Page
Preface	v
Abstract	ix
Introduction	1
Section 1 - Borehole Utem Development Report 1: "Fibre optic data links for borehole EM application"	3
Section 2 - Borehole Utem Development Report 2: "Field testing of the prototype UTEM 3 borehole system"	17
Section 3 - Interpretation Development Report: "Interpretation aids for EM exploration"	28
Section 4 - Development Of A High Power Transmitter: "High power transmitter"	37
List of Captions for Tables and Figures	
Appendix 1 - Signal To Noise Optimisation For EM Measurement Report 1: "Noise processing techniques for timedomain EM systems"	*
Appendix 2 - Signal To Noise Optimisation For EM Measurement Report 2: "Survey design for milticomponent EM systems"	**

* Paper scheduled for publication in July 1984 issue of Geophysics.

** Paper published in the March 1984 issue of Geophysics.

ABSTRACT

A borehole system using a fibre optic data link was designed, constructed and tested in the field. This project had two distinct aspects: instrumentation and field surveys, which are both reported separately. EM interpretation aids were developed to make full use of EM measurements. These consist of scale model data including more complex models, such as conductors under overburden, irregular overburden, and syncline-anticline structures. A computer program was also developed to make it possible to use the model data and a bank of model data to fit field anomalies on a microcomputer.

ADVANCED HARDWARE AND SOFTWARE DEVELOPMENT FOR GROUND EM PROSPECTING

by

J.C. MACNAE

Y. LAMONTAGNE

INTRODUCTION

Improvements in exploration techniques can now be separated into two broad fields: hardware improvements regarding development in electronic instumentation and mechanical systems, and software improvements dealing mostly with data processing and presentation. There is also the

Manuscript approved for publication by V.G. Milne, Director, Ontario Geological Survey, March 20, 1986.
This report is published by permission of V.G. Milne, Director, Ontario Geological Survey.

indistinct zone of firmware development involving hardware-oriented microprogramming in microprocessor controlled systems. The UTEM developments include all three of these aspects. In hardware development, the largest project was the design and construction of the borehole UTEM system using a fibre optic link and an automatic servo-winch system. Section 1 is a report on this project. Field testing of the system and development of the software tools to reduce and diplay the data, display the primary field in the plane of the borehole, and adjust the borehole position has been a separate project recently completed making use of the prototype hardware. These developments are reported in section 2 of this report.

To assist in the interpretation effort, a comprehensive series of model type curves were generated using a scale modelling apparatus and numerical model ling. The models and their use in the interpretation and fitting of field data are discussed in section 3.

A comprehensive study into the design of a high voltage/high power transmitter has been completed. The design objectives are for a transmitter operating as a high frequency switch mode regulator and capable of current regulation with a bandwidth of 15 kHz. The section entitled "a high voltage switch-mode transmit ter" reports on this effort.

Grant 010 Advanced Hardware and Software Development for Ground Em Prospecting:

Part 1 - Fibre Optic Data Links for Borehole EM Application

Y. Lamontagne and J. Macnae

Lamontagne Geophysics Ltd., 49 Spadina Ave., Toronto M5V 2J1

Submitted to GSC for publication in Proceedings of "Borehole Geophysics" Conference

ABSTRACT

A borehole EM system using a fibre optic cable has been designed, constructed and tested in field surveys. In this system, a large loop on the surface generates a magnetic field and the down-hole sensor detects the field distorted by the ground. It was decided that a fibre optic link would best suit the system because of the problems associated with conventional electrical cables in a down-hole application, particularly with respect to common mode signals, cable channeling and signal degradation. Although these problems can be overcome with difficulty with electrical cables, fibre optic cable does not have any potential for similar problems. As well, fibre optic cable has an additional advantage in that it is lighter in weight and lower in cost than conventional shielded electrical cable. These advantages must be balanced against the cost of additional down-hole electronics and battery operation however, leading to a more expensive probe than is usual for borehole systems. Our results show that a fibre optic cable of this design can be used in many borehole applications particulary where the data rate is high and where signal degradation can be a problem.

INTRODUCTION

With the success of the UTEM system in surface applications (West et al,1984, Lamontagne,1975), it became clear that there was a need for an EM sensor which could be lowered into boreholes. Some of the unique characteristics of the system made adaptation to a borehole system perhaps more difficult than for other systems. These difficulties arise from the unusually large bandwidth of the UTEM system and the unique fact that the transmitter is always on during measurements. An additional problem posed by a borehole system, is the spurious response likely to be caused by the long cable connecting the sensor to the surface equipment. The way in which this problem was solved by the use of a fibre optic cable, and the additional advantages and drawbacks of this technology, are the subject of this paper.

CONVENTIONAL ELECTRICAL CABLE PROBLEMS

Initial analysis of existing borehole systems indicated that the task of supressing stray coupling effects to the required accuracy over the desired bandwidth was almost impossible using conventonal electrical cable. Some initial tests by Dyck (1981) using a conventional borehole probe confirmed this suspicion. Three main areas of difficulty were detected in this analysis which are summarized in Table 1.

Common mode interferences

With a transmitter loop excited by several hundred volts at the surface, it is difficult to achieve a sufficiently high common mode rejection ratio, and the complete system balance needed to avoid spurious responses where conductive zones provide an electrical link to parts of the loop by capacitive or resistive coupling. Some of the very sharp responses often seen even on late channels when crossing minor conductive zones, are probably caused by these effects.

Cable related signal degradation

Over a long electrical cable, mechanical and/or environmental effects caused by motion of the cable, flowing water, mechanical stress, temperature differences etc. can introduce noise signals or change the electrical characteristics of the line (e.g. resistance), thus affecting any critical adjustment of common mode rejection.

Current channeling in the cable

When the probe depth is very large, a long shielded cable acts as a long antenna which can channel appreciable currents which are capacitively coupled to it. This disturbance in the induced current flow is more acute for early sampling times, where, depending on the symmetry of the channeled current flow in the vicinity of the probe, a variety of artificial responses may result.

These effects can not only introduce stray responses, but can also affect the system gain and fidelity, which would be interpreted as long time constant responses in UTEM.

THE NEED FOR AN ALL-DIELECTRIC LINK

From the start, the possibility of using fibre optic transmission was considered as a way around all these problems. Since an optical link can be all dielectric, complete electrical isolation can be realized, thus avoiding common mode problems and cable channeling effects. Also, one way to avoid signal degradation is signal encoding which is not only necessary for an optical link, but also can be done without introducing much noise in driving the long transmission line, as would be the case for electrical transmission (Hewlitt Packard, 1978).

When the possibility was studied further, there appeared a number of further advantages in the use of an optical link. A good number of disadvantages were also discovered, mostly having to do with the use of a new technology. Both are summarized in Table 2.

Design problems associated with the use of a fibre optic cable

Once the decision to use a fibre optic cable had been taken, it became necessary to find satisfactory solutions for various aspects of system design. These can be summarized as follows:

- incompatibility of presently available standard fibre optic with high hydrostatic pressure tolerance and tensile strength needed in logging operations
- method of digital data encoding to be used
- modifications required to a conventional winch to accommodate the special requirements of a fibre optic cable
- types of electro-optical transducers required to modulate and demodulate the optical carrier used to transmit the "H" field signal from the borehole sensor.

The first two of these are discussed below and the third is addressed in the subsequent section which describes the overall system.

Cable construction

It was found surprisingly, that fibre optic cables can be considerablly cheaper than electrical cables for a comparable data handling capability. They are also much lighter since no metallic members are needed. The effective density of a fibre optic cable is near 1, giving it a near zero weight in a water filled borehole. This means that the winch system must only support the weight of the probe. One of the main difficulties encountered at the beginning was that there existed no fibre optic cable capable of withstanding a sufficiently high pressure without damage. This was due to the fact that in normal construction, the cables are made to resist crushing rather than hydrostatic pressure. It was then necessary to specify a special cable that could withstand high pressures and also have a greater tensile strength to weight ratio than usual. After several attempts, we arrived at a construction which could be made by our supplier and had the required properties. The normal fibre optic cable construction is shown in Figure 1 and consists of:

A. Tough outer jacket.(high density polyethylene)

B. Soft plastic inner jacket to help cushion crushing loads.

C. Strength member.(usually braided Kevlar)

D. Rigid buffer tube.(air filled)

E. Fibre

The special fibre optic cable custom designed for borehole/high pressure work has a modified construction:

A. Tough outer jacket as above.

C. Heavier Kevlar strength member.

D. Semi-rigid buffer tube.

F. Freeze proof gel filling with density of 1.

G. Fibre spiraling in buffer tube.

The overall cable diameter and weight is reduced and the tensile strength/ weight is greater than for a standard cable. The physical properties are summarized in Table 3.

THE OVERALL SYSTEM

The system consists of the following functional blocks:

- down-hole probe
- optical link
- winch assembly
- winch controller

Probe

The sensor is physically distinct from the other down-hole electronics as shown in Figure 2. Only an axial magnetic sensor has been constructed so far, but an electric field sensor and transverse magnetic sensors will be implemented in the future.

Optical link

The analogue-digital-analogue data link (Figure 3) contains a signal encoder, optical transmitter, fibre optic cable, optical receiver and decoder. Physically, the encoder is in the borehole, as is the optical transmitter. The optical receiver is in the hub of the removable winch spool and the decoder is in the controller box. The signal going through the slip-rings is thus a digital pulse coded electrical signal. The decoder reproduces the analogue signal for normal sampling by the receiver. The analogue signal at surface lags that down hole by 20 s; this time delay is caused by encoding, decoding and transmission through the 2 km of fibre optic cable.

Winch assembly

The winch system was designed to include all components necessary for complete automation of the system (Figure 4). The winch is driven by a servo motor and brake system. Optical shaft encoders are used to measure the probe position and the tension on the cable. The rack-and-pinion tensiometer also acts as a shock absorber. It is comprised of a pulley mounted on a spring-loaded arm. The spool and pulleys were made reasonably large in diameter to avoid undue bending of the fibre optic cable. The winch has a maximum torque limit set by the hardware, but this corresponds to actual cable tensions varying over a range of 2.7:1, depending on how full

the spool is. For this reason, a tensiometer is needed. The speed and braking of the winch is regulated by the winch contoller unit. An upper tension limit is entered on the keyboard of the contoller and determines the threshold at which the winch will slow down or stop to reduce the actual tension on the cable. This normally occurs when the probe is being pulled up. While the probe is being lowered, the tension is maintained by the contoller above a fixed 5% minimum limit.

Winch controller

This unit provides intelligence for the whole system, although its main purpose is to control the winch. The controller can be operated manually from the keyboard or set automatically. The keyboard layout is shown schematically in Figure 5 and illustrates the controller operation functions. One set of entries is necessary to initialize the controller and a second set permits on-line intervention by the operator.

Entries which initialize the controller:

VMAX: sets the maximum velocity of the probe in cm/sec (limit of 150)

TENSION: sets the maximum tension in percent of probe weight in air

HOLE: sets the hole depth (controller will refuse to go to any greater depth)

SET: initializes the depth register from the keyboard

Entries which permit on-line intervention by operator:

DEPTH: enters probe target depth (initiates movement of probe upon entry)

STOP: controlled stop (gradually slows winch to a complete stop)

MAN: emergency manual stop

START: re-initiates movement of the probe toward current target depth (used after STOP or MAN or automatic stoppage)

In addition to the essential functions outlined above, the following functions are provided for convenience in routine keyboard operation:

INCR: sets depth increment

UP: moves probe up by depth increment (INCR)

DOWN: moves probe down by depth increment (INCR)

THRESH: sets an anomaly threshold depth above which automatic detailing is performed

The probe speed is limited to the value specified by VMAX and by the tension monitoring system. During descent, the tension is maintained above 5% probe air weight whereas during ascent the tension limit is entered by the operator. When approaching these limits the winch is slowed by the controller, which regulates the rate of descent or ascent of the probe to keep the tension on the cable within the specified limits. Thus, the winch acts as a slip clutch during probe ascent and prevents cable spillage during probe descent. The contoller digital loop characteristics are such that the speed is regulated steadily when the drag is viscous in nature.

A conservative hole depth limit is usually entered before logging a hole. Once the probe reaches that depth, the controller warns the operator. The hole depth is then increased and the maximum velocity reduced until the controller detects the bottom of the hole by means of the tensiometer and stops the winch. In a greasy hole, the same mechanism slows down the probe during probe descent in order to keep a slight tension on the cable. The whole cable retains some tension in such cases since the fibre optic cable itself has a null buoyancy in water.

The signal connection from the down-hole coil to the UTEM 3 receiver is identical to that from the UTEM 3 surface coil. There is also an interface for automatic logging in which the winch controller unit can signal the UTEM 3 receiver to start reading and, upon completion of the reading, move the probe to

a new depth. In both keyboard and automatic operation, the usual UTEM response and depth data (together with the standard header information) are stored on magnetic cassette in the receiver.

FIELD TESTING

Figure 6 shows the results from the first hole logged with the UTEM borehole system. The data collected in this hole did not include any compensation for the 20 s delay of the analogue-digital-analogue link, which caused the large response on channel 8. A subsequent receiver program modification corrects for this time delay.

CONCLUSIONS

The development of a fibre optic data link proved to be more of a challenge than initially anticipated. However, the technological problems have now been solved, and the data link should prove to be a cheap, lightweight alternative to electrical wire data links with none of the usual problems of common mode rejection, capacitive pickup or grounding. Many other applications for the data link such as borehole IP measurements are likely developments in the near future.

ACKNOWLEDGEMENTS

Development of the borehole system at Lamontagne Geophysics was supported by Cominco Ltd., Texasgulf Inc., Kidd Creek Mines, St. Joe American, Sulpetro Minerals and the Ontario Geological Survey through a ETOF grant GR-010 to Lamontagne Geophysics. The careful work of two critical reviewers is also gratefully noted.

REFERENCES

Dyck, A.V., 1981. A method for quantitative interpretation of wide-band, drill-hole EM surveys in mineral exploration; PhD thesis, University of Toronto, available as RAG 23, Geophysics Laboratory, University of Toronto.

Hewlett Packard, 1978. Digital transmission with the HP Fibre Optic System; Application note 1000, Hewlett Packard, Palo Alto, California.

Lamontagne, Y., 1975. Applications of wideband, time-domain EN measurements in mineral exploration; PhD thesis, University of Toronto, available as RAG 7, Geophysics Laboratory, University of Toronto.

West, G.F., Macnae, J.C. and Lamontagne, Y., 1984. A time-domain system measuring the step-response of the ground; Geophysics (submitted, expected publication July 1984).

GRANT 010 Advanced Hardware and Software Development for Ground Em Prospecting:

Part 2 - Field Testing of the Prototype UTEM 3 Borehole System

Y.Lamomtagne, H.Urbanski and R.Huxter

Lamontagne Geophysics Ltd., 49 Spadina Ave., Toronto M5V 2J1

INTRODUCTION

A series of test borehole surveys was carried out as a comprehensive test of the new protoype UTEM 3 borehole system. These tests allowed us to first test the functionality of the system and also its capabilities in a variety of field situations. Some of the boreholes were surveyed at the Gertrude site near Sudbury because there exist comparative data from other borehole systems (A.V.Dyck, 1981), whereas others were surveyed to test the deep hole capability of the system. These tests also provided us with the field data necessary for the development of data reduction software for use with our field computer.

FIELD OPERATION

Transport to site

The UTEM borehole system was carried to the test site by means of a four wheel drive vehicle. It was necessary in some instances, however, to backpack the equipment for several hundred meters when road access was not available. The winch, including loaded cable spool, can be carried over such distances using simple carrying poles which are attached to the winch frame. Over longer distances it may be preferable to transport the winch assembly (22 kg) and full cable spool (30 kg) separately. The system can be easily installed by two

persons, but, at the expense of more individual trips, a single person could also carry the system over short distances and operate it. The heaviest component of the system used in the test surveys was the 1500 W motor generator required to operate the winch and UTEM 3 transmitter.

Installation

The components of the borehole system necessary for field surveys are:

- the winch assembly
- the cable spool (incudes optical decoder located in the hub of the spool, and optical transmitter housing)
- the downhole components (includes separate optical encoder tube and sensor)
- the boom assembly (disassembles into two sections for transport)
- the controller unit
- a 115 volt, 1500 W motor generator

Installation of the system requires roughly 15 minutes. As the last step in the installation procedure, two sections of the encoder tube (encoder and optical transmitter) are connected together providing power for the probe. An '0' ring seals the two threaded sections of the connector but this is not critical as both the encoder and transmitter housings are themselves pressure sealed from the connector compartment. Figure 1 shows the system ready for measurement and a closeup

of the controller unit keyboard.

Start up procedure

The winch is connected to the controller unit, powered and brake applied before the dowh-hole components are placed into the hole. When the top of the optical transmitter housing (the uppermost part of the downhole probe) is flush with borehole collar, the current depth of the probe is entered on the controller keyboard as 7.00 metres. This is the distance between the centre of the sensor coil and the top of the optical transmitter housing and is mostly made up of a 5.0 metre section of shielded cable linking the sensor coil and optical encoder/transmitter tube.

Measuring mode operation

After the controller has been initialized and the header information recorded, the normal UTEM measuring procedure is followed. Once the desired number of cycles has been stacked and the data recorded, the probe is lowered by a selected increment using the two controller keyboard functions "DOWN" and "ENTER" or to a selected depth using the controller keyboard functions "DEPTH" nnnnn "ENTER", where nnnnn is a number. At each new depth, the measuring procedure is repeated. The depth increment and target depth may be selected at any time to a resolution of 1 centimetre. For

moderate speeds of operation, the depth closure after the probe is raised is about 0.5% of the hole depth. This makes it practical to relog the hole on the way up with a different transmitter loop configuration.

DATA PRESENTATION

Since the UTEM system measures during the transmitter "on" time, a special normalization procedure is necessary. The data are normalized by dividing by the total primary field which would exist at the measurement location in free air. Usually this total primary field is not strongly dependent on the borehole trajectory. For secondary field presentation, the calculated primary field along the borehole as a percentage of the total primary field is also subtracted. Usually, however, only channel 1 (the latest channel) is reduced in this manner. Since there may be anomalies caused by orientation/location errors if the borehole trajectory is unknown. This problem may be corrected by normalizing all earlier channels with respect to channel 1 rather than the calculated axial primary field since, in the absence of long time constant anomalies, the channel 1 response is a good approximation of the primary field.

By comparing data from more than one transmitter loop, the trajectory of the borehole may be estimated. The estimated trajectory may then be incorporated into the reduction data (this is done using an interactive feature of

the program) and the resulting, adjusted data from the different loops compared again. The process is repeated until the response appears to be corrected. Of course, it is still left to the discretion of the interpreting geophysicist whether the observed channel 1 anomaly is due to orientation/location errors or a real channel 1 response. If a real channel 1 response is suspected, it is always possible to resurvey the hole at a lower base frequency to test this hypothesis With three or more loop locations, however, it can almost certainly be determined if the borehole trajectory is the cause of the anomaly. In spite of the added geometrical complications involved, this procedure allows us to measure long time constant response not generally detectable by a conventional pulse EM system and possibly help determine the position of the borehole.

"VECPLOT" PRIMARY FIELD DISPLAY

As an aid to survey layout and understanding borehole trajectory effects, a microcomputer (VECPLOT) program was developed which can plot the direction (as vectors) and amplitude (as contours) of the primary field in any plane around the borehole. The transmitter loop location and borehole trajectory are plotted on the output to help orient the section. Figure 2 is an example of the output of VECPLOT.

EXAMPLE BOREHOLE DATA

The field data examples will be presented with only preliminary comments since the final interpretation has not yet been completed.

Gertrude site

The first example is from borehole BH9266 at Gertrude. The borehole was logged several times during the field trials of the system. Figure 2-3 shows the borehole location and transmitter loop positions. In Figure 2-4 the data obtained using the north loop are presented. The legend of symbols used to label the channel response curves is given in Table 2-1. In the convention used here an off-hole response appears as a positive anomaly. The most prominent features are two off-hole responses at 315 (A) and 435 (B) metres depth which are well known from other borehole logging done at this location (Dyck, A.V., 1981). The UTEM data show a definite migration of the deeper response and an increase in its time constant with increasing depth. The channel 1 response correlates well to responses of channels 2 through 6. If the channel 1 response is added back on to the channel 6 response (recall that it was subtracted during reduction), it would account for roughly half of the amplitude of the true anomaly of channel 6 of anomaly A. The decay also displays a definite bimodal character in the shallower anomaly with a plateau in the channel 4-5-6 responses. The data obtained using the

south transmitter loop (Figure 2-5) shows a much reduced anomaly at A and the coupling with the conductor causing anomaly B has even been reversed. But most notable is the channel 1 response over both A and B which has changed character and been reversed. Figure 2-6 is an expanded plot of the deepest part of the data of Figure 2-4 where the measurements were made every 2 metres.

Figure 2-7 shows the data from the neighbouring borehole (BH9273) using the south transmitter loop. Basically, the response is a narrow in-hole anomaly which indicates the presence of a conductor (of small effective size). The data from the same borehole but using the north transmitter loop shows that this loop configuration couples with a much larger conductive zone (Figure 2-8). Particularly intriguing is the channel 1 response which suggests the presence of a long time constant, off-hole conductor above the in-hole intersection.

In another borehole at the site, the north loop data (Figure 2-9) has a more neutral response except for a tight in-hole anomaly over a known intersection. Data obtained using the south transmitter loop (Figure 2-10) are in complete agreement with the north loop data. Judging from the small channel 1 response in the BH10621 data, it is apparent that its time constant is much shorter than in the channel 1 responses of the previous examples, but this cannot be easily determined without first inspecting the primary field reduced channel 1 data.

Site 2

The measurements at this site were made early in the field trial period before final adjustments were made to the instrument and was primarily intended to test the 2 kilometre depth capability of the system. For this reason, short stacking times were used resulting in a larger degree of scatter in the data than is usual (Figure 2-11). The most interesting feature of the data is the very large negative (-100%) channel 1 anomaly at a depth of 1760 m where there is a known sulphide intersection. The anomaly was so large, that when first encountered, the operators were convinced that the effect was due to a transmitter shutdown. The transmitter had not stopped, however, and the effect was caused by a highly conductive zone, the centre of which the primary field was unable to penetrate. The time constant of this anomaly has been estimated to be more than 100 ms.

Site 3

The location of the first borehole logged and the location of the transmitter loops are shown in Figure 2-12. The data from this borehole show an almost neutral response over the entire 1600 m depth except for a very minor in-hole anomaly which appears in various forms in the responses for each of the two loop positions (Figures 2-13 and 2-14).

In the last example, the borehole strays considerably from the south loop as a result of the great number of wedges (Figures 2-15 and 2-16). The effect of the wedges is clearly noticable in the channel 1 response from the south loop data. It is obvious that the borehole position is poorly determined, but a minor deep, off-hole response is still detectable.

CONCLUSIONS

The field trials of the prototype model of the UTEM 3 borehole system provided the down-hole UTEM data necessary for the design of effective reduction and interpretation software and demonstrated the depth capability of the system. The data illustrated several aspects of the types of response obtained from a UTEM-style survey (i.e.an EM system which measures during "transmitter on" time) when used in a down-hole environment.

ACKNOWLEDGMENTS

The early field testing and all software (reduction and interpretation) development involved in these tests were supported by the Exploration Technology Development Fund. During the final field trial survey program, the direct field costs were paid for by the Geological Survey of Canada. Alfred V. Dyck, from the Geological Survey of Canada, and Barry Drouse of INCO helped us select the boreholes to survey.

We thank the geophysical department of Internation Nickel Co. for allowing us to use the survey sites and for assistance during the field work.

REFERENCES

Dyck, A.V., 1981. A method for quantitative interpretation of wide-band, drill-hole EM surveys in mineral exploration; PhD thesis, University of Toronto, available as RAG 23, Geophysics Laboratory, University of Toronto.

Grant 010 Advanced Hardware and Software Development for Ground EM Prospecting:

Part 3 - Interpretation Aids for EM Exploration

J.C. Macnae, R. Huxter and Y. Lamontagne

Lamontagne Geophysics Ltd, 49 Spadina Ave., Toronto M5V 2J1

INTRODUCTION

In the absence of economically reliable EM modelling programs for most of the three dimensional models which are relevant to EM interpretation, the most effective way to build a wide base of model data is to use a scale model apparatus and some ingenuity in finding and making models of varied shapes and properties. Once a large data base is available, the problem is one of extracting some rules or quasi-rules from these volumes of data to be used in interpretation ,and ultimately to have it easily available for fitting field data.

SCALE MODEL PROGRAM

The scale model program was devised to complement the generally available numerical solutions, such as the "Plate" and "Sphere" programs available from the University of Toronto. Figure 3-1 shows an overview of the model shapes used. The modelling apparatus simulated a large loop system and the system response was that of the UTEM system. For each type and size of model, a variety of positions and depth relative to the loop were measured. Both vertical and in-line horizontal magnetic components were measured and presented. In all, 1800 types of curves were produced. In the case of an infinite half plane models, a numerical solution was used to compute the inductive limit(i.e. early amplitude) of the response.

The Infinite Half-Plane

A large number of infinite half plane models were measured over a wide range of position, depths, and dips. The half-plane is of particular relevance since it approximates the effect large stratigraphic conductors truncated below the overburden, or at a fault or unconformity. Shallow dipping stratigraphic conductors give particularly complex responses depending on the position of the edge relative to the loop. Figure 3-2 compares two such cases (PH:A (3-2a) vs. PH:G (3-2b) continuous normalization) for vertical magnetic field measurements. The anomalies were normalised to the primary field at each point of measurement, which is usually referred to as "continuous normalization". Normalization to the primary field at a fixed point is the basis of an alternate presentation called "point normalization". All model data are presented in both formats, but our examples here will be of continuous normalization only. The model 3-2b produces more complex responses because the conductor extends under the transmitter loop at shallow depth. Other models in this series, such as large slabs and wedges show the characteristic response of thick tabular, or pinched out conductors.

Laminated Conductors

As examples from the block/face series, the response between inductively interacting, but isolated parallel plate conductors can be of significant relevance in areas of steeply dipping geology. A particularly intriguing case occurs when the laminations run perpendicular to the loop edge (Figure 3-3a). The broad positive response of similar shape, on all channels can be mistaken for a deep horizontal conductor unless the decay characteristic is studied carefully. If the lamination runs parallel to the loop edge (Figure 3-3b), the response can be mistaken for a horizontal half-plane or a wedge dipping away from the loop unless, again, the decay is examined over a sufficiently long time range. This type of model is instructive in studying the response of large strongly interacting conductors.

Syncline/Anticline

These are models taken from the series pictured in Figure 3-1c which contains a selection of more complex models. Figure 3-4a shows the response measured on a traverse over a large plunging syncline measure near the nose of the fold. The presence of the larger width of the structure down plunge is obvious from the positive response lasting to the end of the line. The response of a broad anticline (Figure 3-4b) by comparison has a predominantly negative lobe and is much smoother than for most other models of the same depth to top.

Conversion to Other System Responses

It is possible to convert the UTEM responses to those of pulse EM system or frequency domain systems of the same geometry. This is possible because the large bandwidth of the UTEM system is generally wider than that of the other large loop systems. Some care had to be taken to obtain sufficient precision at the early channels, particularly since the model apparatus does not use high frequency preemphasis (prewhitening) as does the field UTEM3 system. Figure 3-5 shows examples of data converted to the Crone PEM system response and frequency responses for the particular half-plane model of Figure 3-2a.

Model Data as a Direct Interpretation Aid

The first use of the model data is in training the EM interpreter. Even for the relatively restricted class of models covered, the responses obtained very often have unexpected shapes over the time spectrum considered, which can call attention to the diagnostic features of the data. Very often the interpreter will find in the model data, a response which matches well his field data. If the response of an EM system can be freely scaled in time (this is possible with frequency domain data and UTEM data), each of the model data sets can be used to interpret data from a similar model with different conductivity or measured with a different system base frequency. In general, the models were scaled in such a

way that the time range measured includes as much of the range of response variation over time, or frequency as possible.

For example, Figure 3-6 illustrates the response of irregular overburden with a step decrease in conductivity. It was found sufficient to include only 8 channels to cover the whole response variation (covering a time range of 1:256), but in fact the response of the step is undetectable in channels 1 and 2 (12.8 ms and 6.4 ms sampling times, respectively). The overburden conductance was chosen as 8.1 and 3.9 S to obtain a response over most of the channels. If in fact the likely situation is that of a step variation between 1 and 0.5 S, the same model curves can be used, but would be scaled in time by a factor of 8 (i.e. 3 binary spaced channels). In this case, channel 1 to 5 would show no anomaly on the step instead of 1 and 2 only and channel 8 would show an anomaly similar to channel 5 of the model curves. Furthermore, channel 10 of the field system would show the response of channel 7 of the model curves.

Interpretation Manual

To gain maximum benefit from this arduous laboratory work, a preliminary interpretation manual is drafted, which uses the model data as a base for simple interpretation. The manual was oriented towards the UTEM system, but most of it can be applied to frequency domain data with minor adaptations. Charts and formulae are provided to interpret

the location, depth, conductivity and size of simple conductors based on converging evidence from profile anomaly shapes, absolute amplitude information and time decay shape. Figure 3-7, for example, shows a chart used in the interpretation of dip from anomaly shape.

"LIGHT TABLE" FITTING PROGRAM ON A MICROCOMPUTER

A core computer program was derived to aid EM interpretation by comparing the field response to a selected model response. This program was made for the GFC-1 microcomputer using its dual package screen graphics capabilities. The program simulates the fitting of data on a light table, with the added advantage of instant scale changes and model scaling. The field data written on one graphics plane remain fixed, whereas on the other plane, data from the disk stored bank of model data can be scanned until a suitable set of data is found to attempt more specific fitting. The model data can be translated to be coincident with the field data. The reference position of the conductor is continuously updated during this process on the alphanumeric screen in the same coordinate system as the field data. If the horizontal scale of the model data must be changed to fit the field data, this can also be done continuously. In this case, all dimensional information of the model data are also scaled (as displayed on the alphanumeric screen) in proportion and the drawing of the model cross-section is similarly scaled. Also,

the conductivity or conductance of the model is properly scaled. Time scaling is also allowed in two ways:

- in changing the system base frequency to agree with the field frequency,
- channel interpolation without a frequency change, which has the effect of changing the model conductivity.

Amplitude scaling of the profile data is permitted over a limited range. In this case the empirical relation between depth, conductor size and initial amplitude is used to alter the model depth and size, such as to produce the desired amplitude. The conductivity was also adjusted to reflect the change in conductor size. Fitting time decays is similarly done by vertical and horizontal translations, and the anomaly decay time and inductive limit are determined.

The light-table program also has the capability of rotation, which could be useful for fitting data in contour form, but no model data base exists for this yet. Table 3-1 lists the commands available to the program user.

The main requirement for this program is for fast vector graphics and computer arithmetic, such that the changes occur almost in real time on the graphics screen. The interpreter can then judge the best fit, by eye. This is done on the GFC-1 through the use of a dedicated graphics controller and dual processor organisation of the computer.

Since the development of a computerized model data base was beyond the scope of this research project only a few test model data sets are presently accessible to the program. The building of the necessary disk based model data catalogue has now been undertaken by Lamontagne Geophysics to make this program commercially useable.

CONCLUSIONS

With the availability of a large suite of scale model data curves, EM interpretation can be made easier and more reliable in :

- providing an education for the interpreter
- forming a base for interpretation rules and
- quantitatively fitting field data with the aid of a computer which automatically uses scaling rules and empirically derived relations.

Grant 010 Advanced Hardware and Software Development for Ground EM Prospecting:

Part 4 - High Power Transmitter

Y. Lamontagne and Z. Noworolski

INTRODUCTION

The aim of this project is to develop a high voltage, high power current regulating transmitter with 15 kHz bandwidth using switchmode regulation techniques. The objective specifications are for a maximum output swing of +/- 800v at a current of 16 amps; or +/- 400v at 32 amps.

POWER DESIGN ANALYSIS

Because of the difficulties in obtaining the components necessary for our first design, we were led to consider more complex designs requiring more readily available components. For this reason we have retained the services of a switchmode design consultant who made a complete analysis of the power cicuitry. As a result, a number of possible switching regulator configurations were considered which use high frequency transformers for voltage conversion. These configurations included:

Primary Control Types:

- Boost Converter Configuration
- Push-pull Bridge Configuration
- Double Converter Configuration

Secondary Control Types:

Simple Switching Regulator

Switched Shunt 2 Quadrant Regulator

Four Quadrant Regulator

Four Quadrant Bridge Regulator

Combinations of the above

A four quadrant regulator is one in which the voltage or current can be arbitrarily of the same or opposite polarity. This feature is required to prevent the self-destruction of a transmitter that could be driving a very inductive load at high power levels. Such a regulator can remove power stored in the load, as well as driving the load.

A final converter circuit was designed which makes use of both phase shift control and pulse width modulation and can operate in four quadrants. The switching frequency of the main regulator considered will be 110 kHz to achieve the required bandwidth and most semi-conductors only need to have ratings of 300v.

To produce the required extreme degree of regulation at lower frequencies, an adaptive digital loop regulator must be combined with the analogue controlled switch mode regulator. Special design considerations were given to voltage isolation, precise output current sensing, and cooling the circuitry in a sealed enclosure.

STATUS OF THE RESEARCH

The greatest difficulty in producing a prototype system was the delay in the production of the necessary high power, high voltage power MOSFET transistors which have been on special order from a manufacturer for over a year. Sample quantities of MOFSET's approaching the required specification have only recently been received. However, with our latest design revision, the specification on the required voltage specifications have been relaxed significantly, and these newly available components will be more than adequate.

CONCLUSION

For the reason stated above, the high power transmitter design is a part of our research project which has not been completed at the expiration of the E.T.D.F. support, but the design work to date will be of great use in our ongoing work on this project.

LIST OF CAPTIONS

Figure 1-1. Sections showing the construction of fibre optic cables and the layering of the optical fiber.

Figure 1-2. Schematic sketch of the down-hole components. The magnetic sensor (PROBE) is separated form the encoder module by a five metre cable. The optical transmitter housing which terminates the F.O. cable is detachable from the encoder module.

Figure 1-3. Sketch showing the transformations undergone by the signal from the sensor output through the fibre optic cable, and to the UTEM 3 receiver input.

Figure 1-4. Close-up photograph of the whinch showing the motor, gearbox, brake, and level winder.

Figure 1-5. Block diagram of the BLC-1 controller also showing the front panel functions.

Figure 1-6. Data obtained during the first field test of the UTEM borehole system at Gertrude.

Figure 2-1. Photographs of the borehole UTEM system in the field and of the controller front panel.

Figure 2-2. Example of the output of the VECPLOT program. This program maps the primary field in the section of the borehole for any loop position or size as an aid in survey layout.

Figure 2-3a. Borehole survey layout at site 1 (Gertrude) showing the positions of the boreholes and transmitter loops.

Figure 2-3b. Legend for the layout maps 2-3a and 2-12.

Figure 2-4. Plot of the reduced borehole data of BH9266 measured with the north loop. Refer to Table 2-1 for a legend of the plotting symbols. Channel 1 data, reduced by subtracting the calculated axial primary field component is plotted on the bottom scale. On the middle scale are channels 2-4 'channel 1 reduced', and on the top scale channels 4-9 also 'channel 1 reduced' at a reduced scale. The station spacings are 10, 5, and 2 m from top to bottom of the hole.

Figure 2-5. Reduced data for BH 9266, south loop.

Figure 2-6. Expanded bottom portion of Figure 2-4.

Figure 2-7. Reduced data for BH9273, south loop. The scales of the middle and top axes are reduced because of the large anomaly amplitude.

Figure 2-8. Reduced data for BH9273, north loop also with reduced scales.

Figure 2-9. Reduced data from BH10621, north loop.

Figure 2-10. Reduced data from BH 10621, south loop.

Figure 2-11. Reduced data from a 2000 m hole at site 2. Note the -100% anomaly on channel 1. The channel 1 reduction has removed this response from the other channels; this is why the early channels are near zero at this point. The mirror image anomaly is caused by the subtraction of channel 1.

Figure 2-12. Survey layout at site 3 showing the two borehole locations and the loop positions. The projection of borehole B shown on the layout is only approximate.

Figure 2-13. Reduced data from borehole A, north loop showing only a weak conductor and the conductive overburden response. The near surface response is caused by the uninsulated wire of the south loop touching the ground.

Figure 2-14. Reduced data from borehole B, south loop.

Figure 2-15. Reduced data from borehole B, south loop. Note the effect of multiple wedges on channel 1. The jumps are caused by hole direction changes at the wedges. There is a small off-hole response at the bottom of the hole.

Figure 2-16. Reduced data from borehole B, north loop. The deep off-hole response is smaller and the wedges show differently.

Figure 3-1a. Models included in the half plane, slabs and wedges series. The The position index of the halfplane models shows all the positions and dips of these models. The slab and wedge models were also measured for a variety of sizes, positions and depths.

Figure 3-1b. Models included in the block/face series. A variety of positions and depths were measured for each model.

Figure 3-1c. Models in the overburden/plate, irregular overburden, syncline/ anticline series.

Figure 3-2a. UTEM response of a horizontal half-plane model extending away from the transmitter loop.

Figure 3-2b. UTEM response of a horizontal half-plane model extending under the transmitter loop.

Figure 3-3a. UTEM response of a laminated conductor striking perpendicualr to the transmitter loop edge.

Figure 3-3b. UTEM response of a laminated conductor striking parallel to the transmitter loop edge.

Figure 3-4a. UTEM response measured on a traverse near the nose of a plunging syncline.

Figure 3-4b. UTEM response measured on a traverse over a broad anticline.

Figure 3-5. Model responses of Figure 3-2a transformed into frequency domain (real and imaginary) and into PEM ram shut-off responses.

Figure 3-6. UTEM response over a highly conductive overburden of varying thickness. These data can be scaled in time to obtain the effect of a less conductive overburden.

Figure 3-7. Interpretation chart used in the interpretation of conductor dip for conductors of varying sizes.

LONG CABLE EFFECTS

PROBLEM	EFFECT	MEASUREMENTS AFFECTED	SOLUTIONS
1- COMMON MODE	- SYSTEMATIC ERROR - NOISE	- 'ON' TIME WORSE - WIDEBAND	- BALANCED DIFFERENTIAL TRANSMISSION - SHIELDING - ELECTRICAL ISOLATION
2- SIGNAL DEGRADATION	- DISTORTION - GAIN VARIATION	- HF WORSE - 'ON' TIME	- ENCODING - CONTROLLED IMPEDANCE LINE
3- CABLE CHANNELING	- ARTIFICIAL RESPONSE	- HF H FIELD - ALL E FIELD	- ELECTRICAL ISOLATION

UTEM CHARACTERISTICS

- 'ON' TIME MEASUREMENTS
- WIDEBAND
- GAIN CALIBRATED
- E FIELD MEASUREMENTS

FIBER OPTIC LINK

ADVANTAGES

- NO LONG CABLE EFFECTS
- NO MECHANICAL EFFECTS
- HIGH THROUGHPUT
- LOW WEIGHT
- LOW COST
- LIGHTER WINCH

DISADVANTAGES

- MORE DOWN-HOLE ELECTRONICS
- BENDING RADIUS LIMIT
- TERMINATION PROBLEMS
- NEW TECHNOLOGY

CABLE SPECIFICATIONS

– OD 3.8 MM	
– ATTENUATION 5 db/km	
– WEIGHT 14 KG/KM	
– STRUCTURAL STRENGTH	3390 N (760 LBS)
– DAMAGE FREE LOADING	1160 N (260 LBS)
– BENDING RADIUS	75 MM
– DENSITY 1 G/CM^3	

FIBER OPTIC CABLES

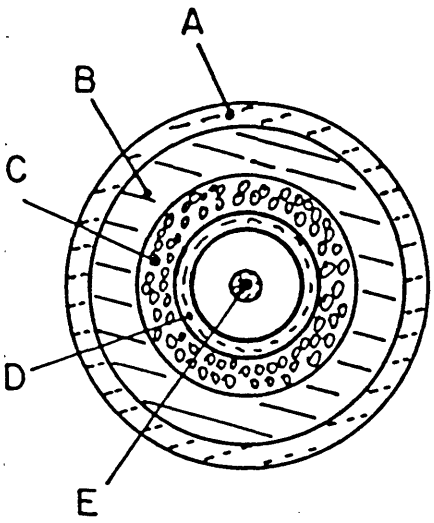

CONVENTIONAL CABLE

A- TOUGH OUTER JACKET 5.6 MM

B- SOFT INNER JACKET

C- STRENGTH MEMBER

D- HARD BUFFER TUBE 2.0 MM

E- OPTICAL FIBER

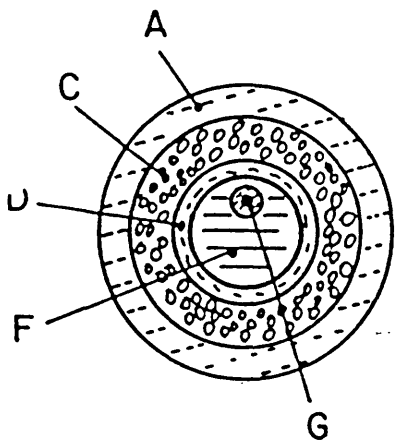

CUSTOM BOREHOLE CABLE

A- 3.8MM

F- LIQUID FILLED BUFFER TUBE

G- SPIRALING FIBER

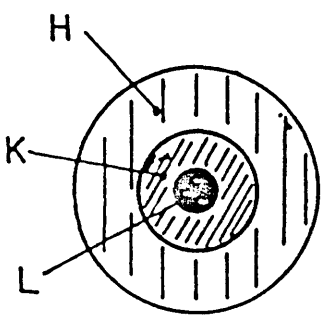

OPTICAL FIBER

H- SILICONE COATING 230 MICRON

K- GLASS CLADDING 125 "

L- GRADED INDEX GLASS CORE 50 "

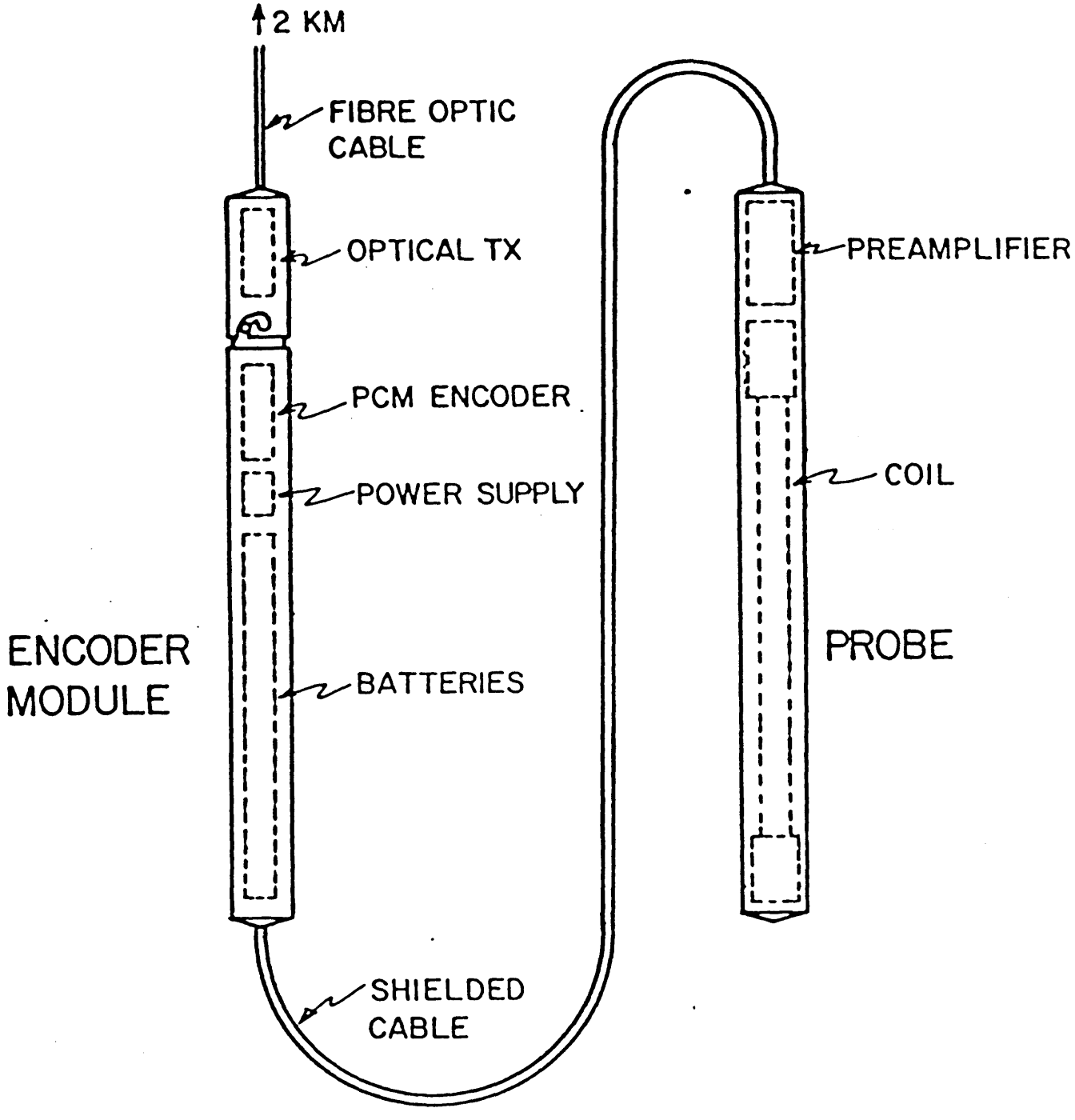

DOWN-HOLE COMPONENTS

FIGURE 1-3

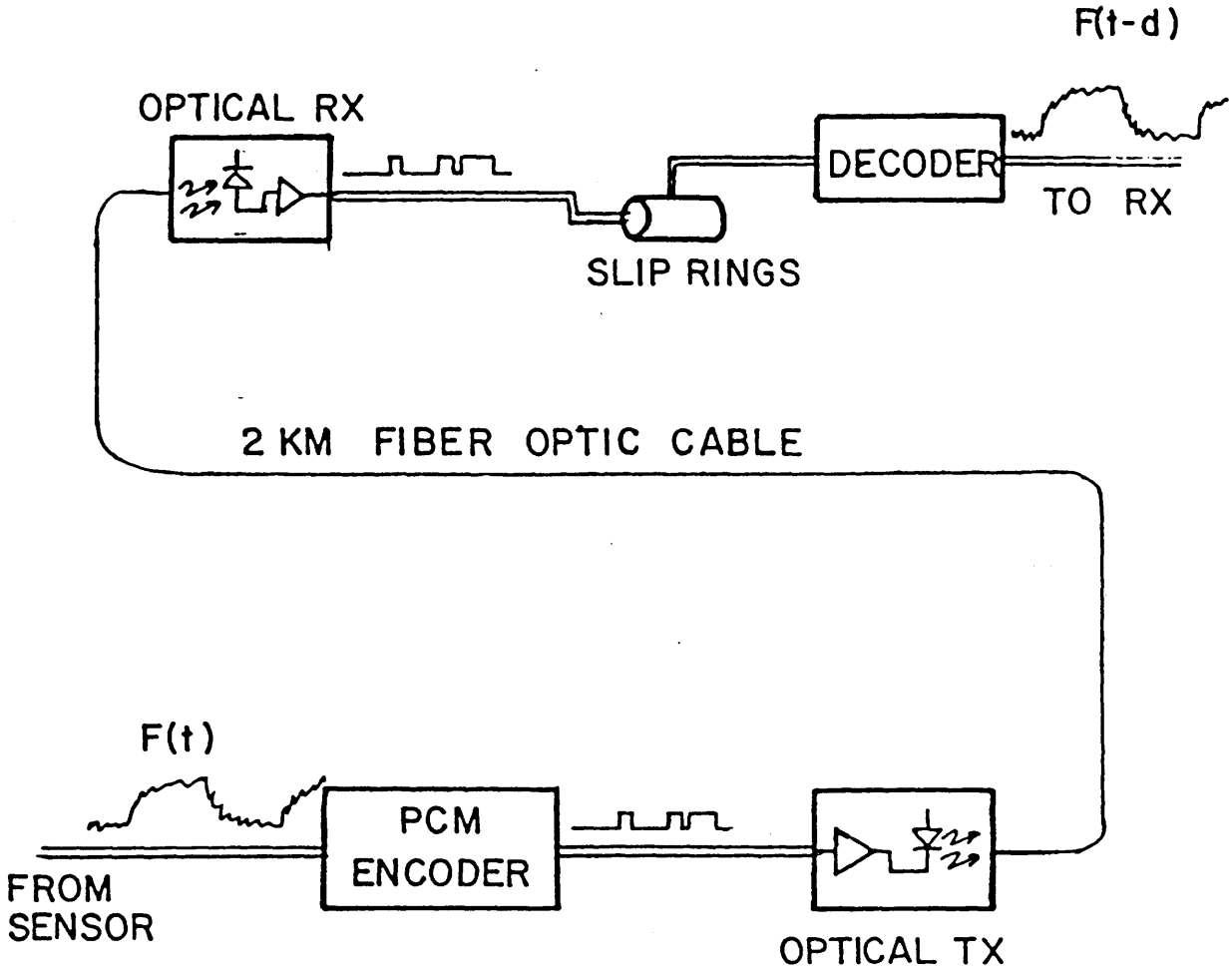

ANALOGUE-TO-ANALOGUE LINK

FIGURE 1-4

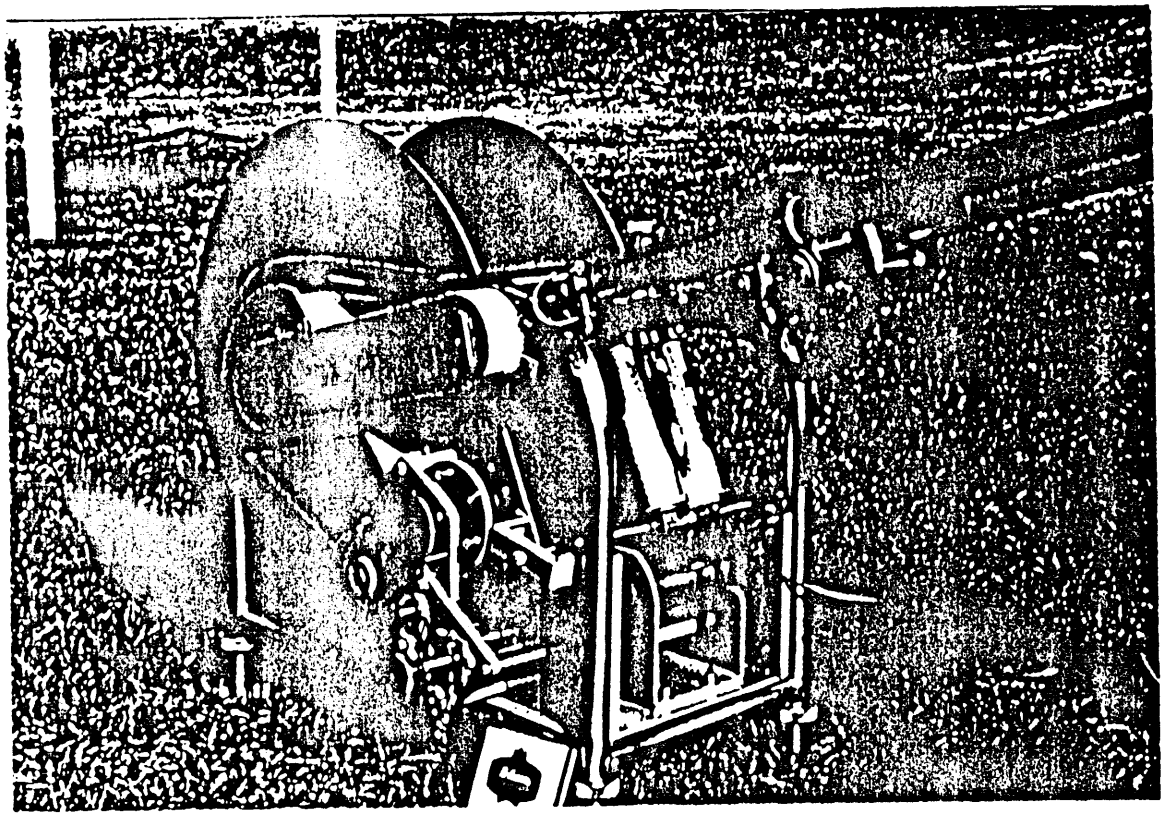

FIGURE 1-5

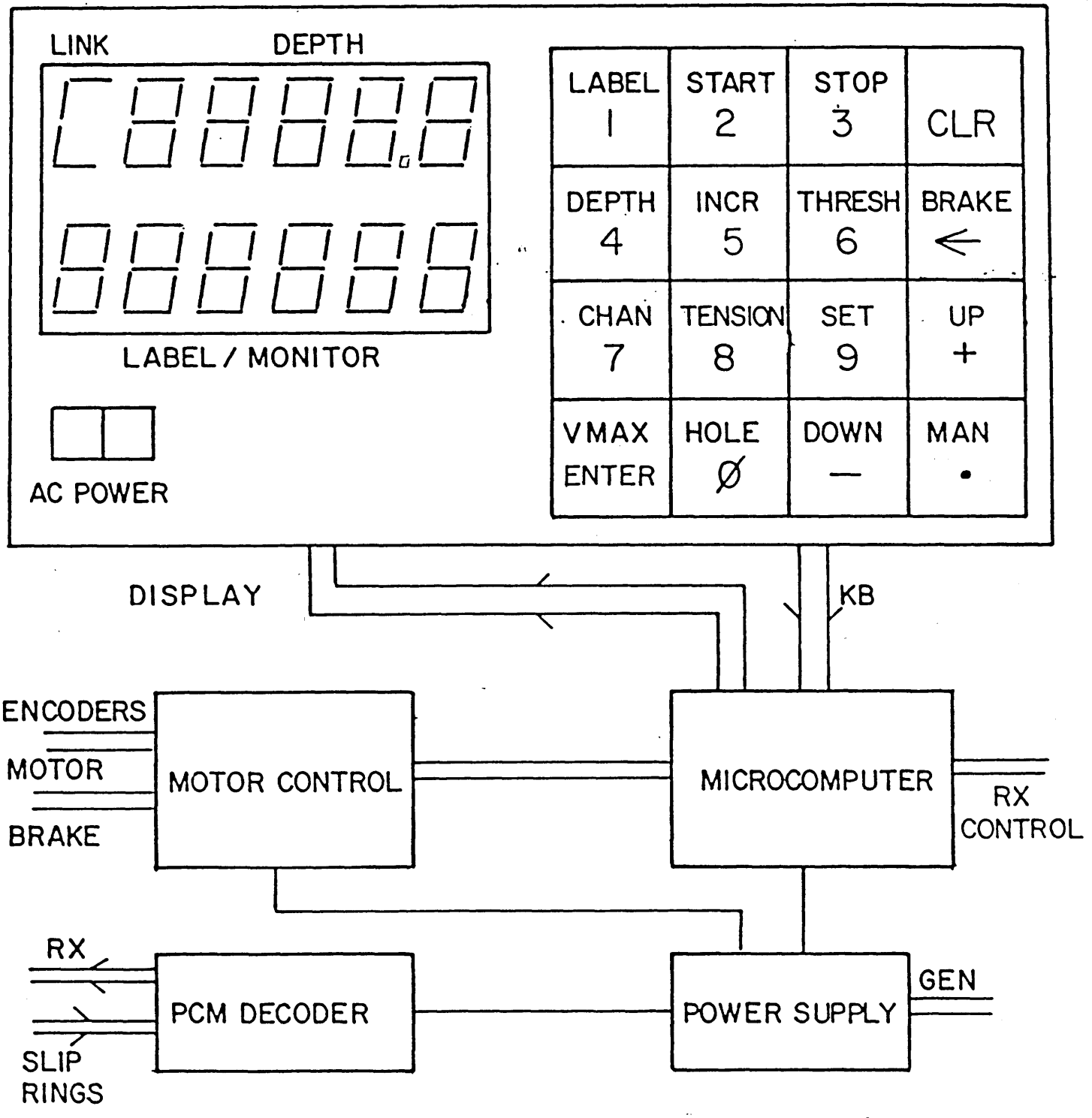

BOREHOLE SYSTEM CONTROLLER

BOREHOLE UTEM FIRST TEST

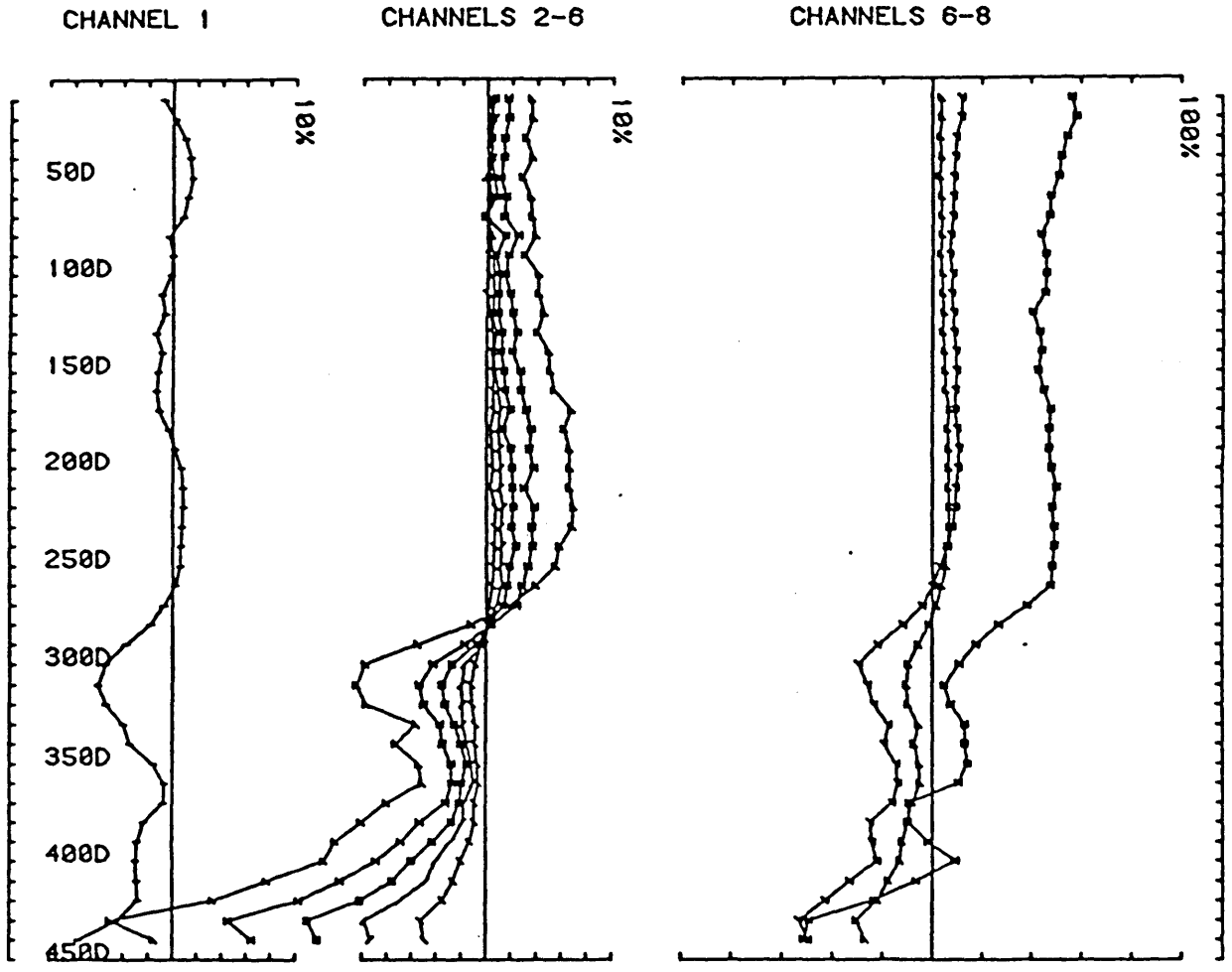

PLOT OF THE FIRST DOWN-THE-HOLE MEASUREMENTS WITH THE NEW FIBER OPTIC BOREHOLE UTEM SYSTEM DURING EQUIPMENT TESTING AT GERTRUDE.

DDH 9266 DEPTH INTERVAL: 10 M MEASUREMENT TIME: 65 MIN
LOOP: 500 M E-W BY 450 M N-S ENTIRELY TO THE NORTH OF DDH 9266
CENTRE OF SOUTH LOOP SIDE 150 M NORTH OF COLLAR

UTEM SURVEY conducted by HU AW YL Job 9266
Project Area BH TEST GERTRUDE Survey for LGL Freq(hz) 30.974

UTEM PLOTTING SYMBOLS

TABLE 2-1

CHANNEL	SYMBOL	MEAN DELAY (msec) 30Hz	15.5Hz
1		12.8	25.6
2		6.4	12.8
3		3.2	6.4
4		1.6	3.2
5		0.8	1.6
6		0.4	0.8
7		0.2	0.4
8		0.1	0.2
9		0.05	0.1
10		0.025	0.05

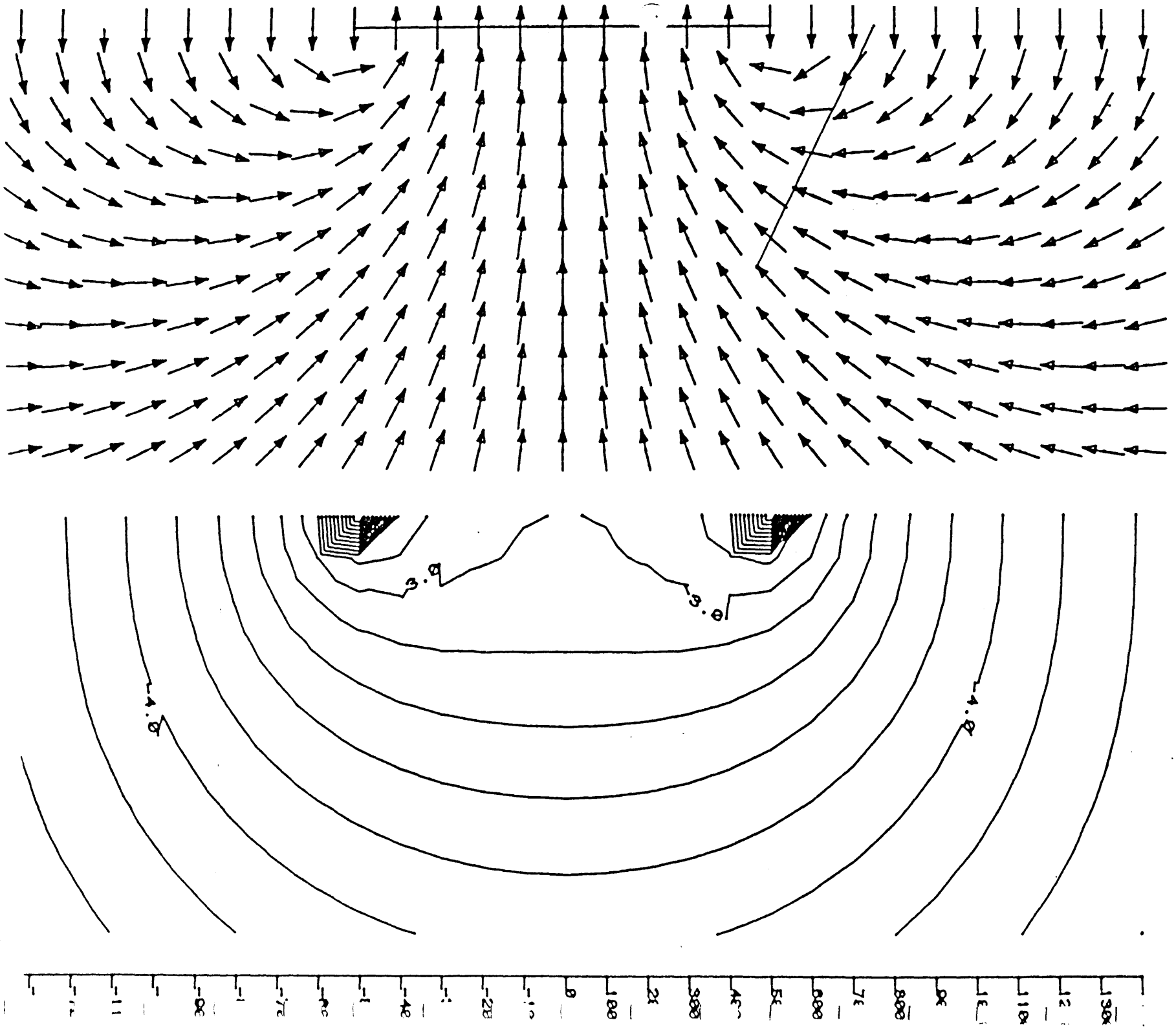

FIG. 2-2

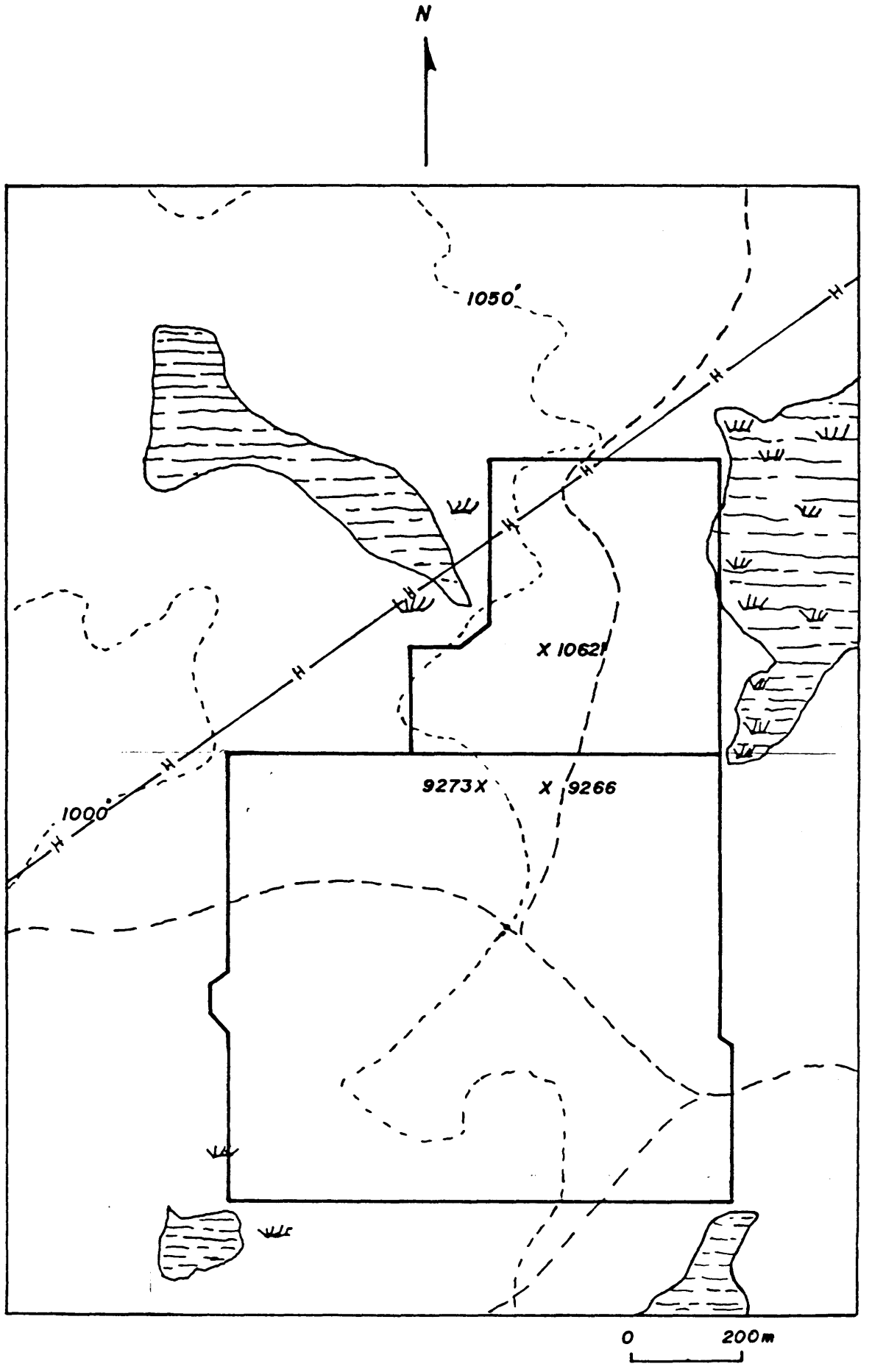
N
1050'
1000'
X 10621
9273X
X 9266
0
200m

FIG. 2-3b

MAP LEGEND

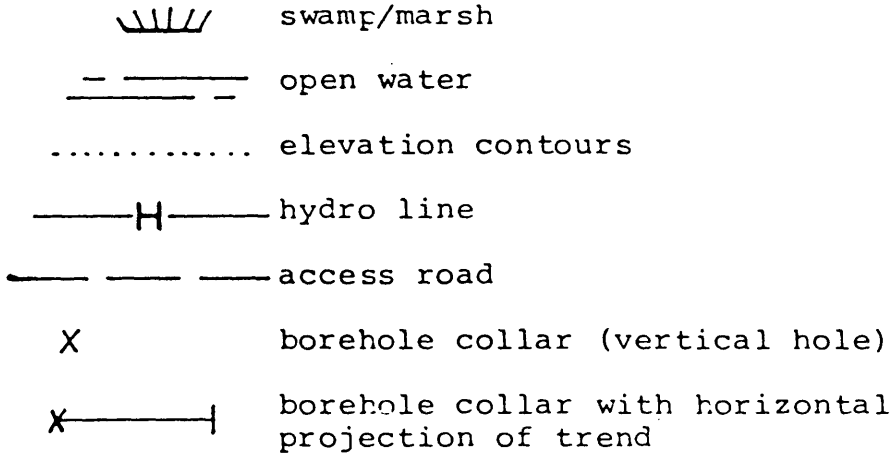

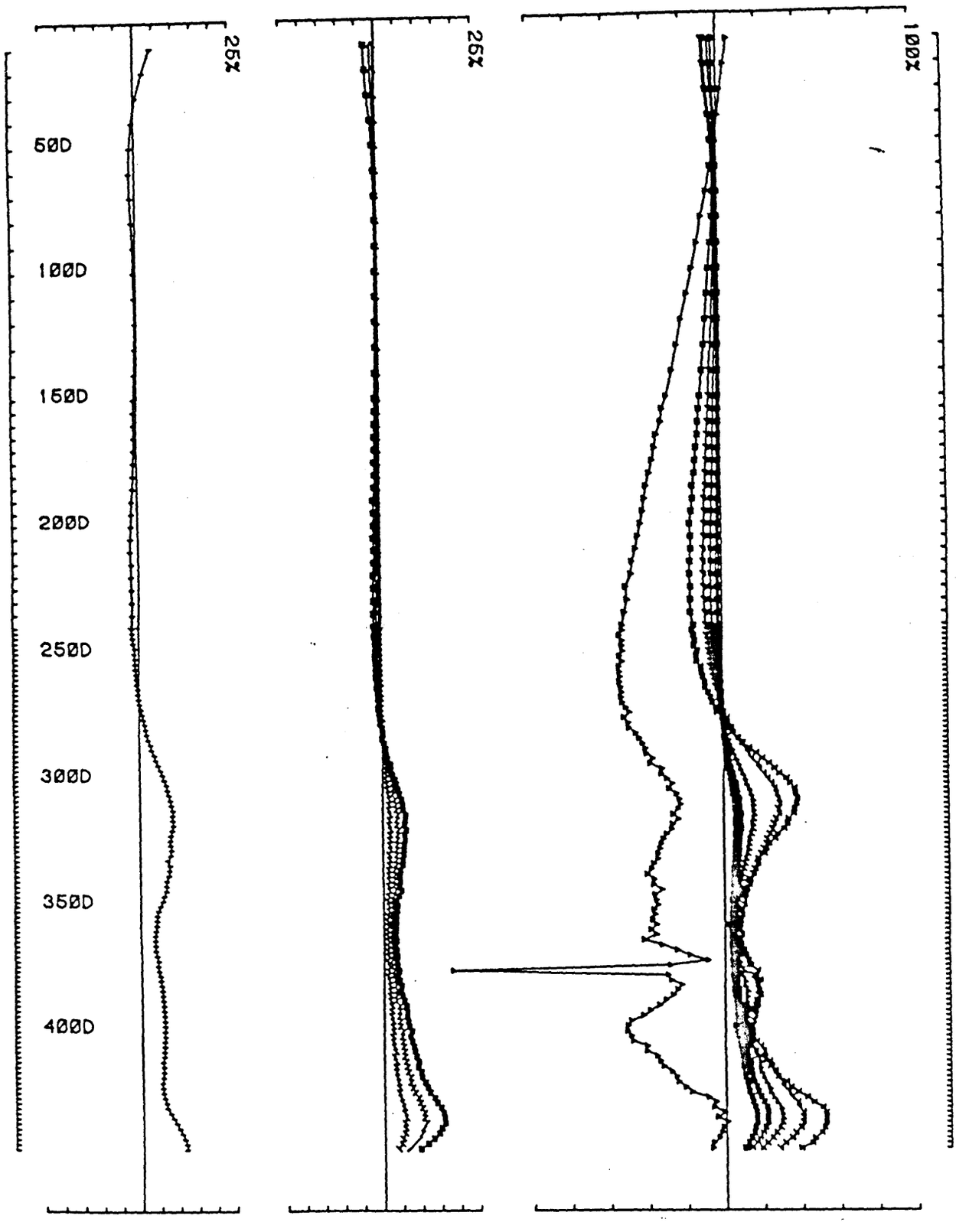

UTEM SURVEY conducted by Lamontagne Geophysics Job 9266
Project Area GERTRUDE BH 9266 NORTH LOOP Survey for GSC freq(hz) 30.974
Loopno 6604 Line GERTRUDE BH 9266 NORTH LOOP component Hx secondary Ch 1

FIG. 2-4

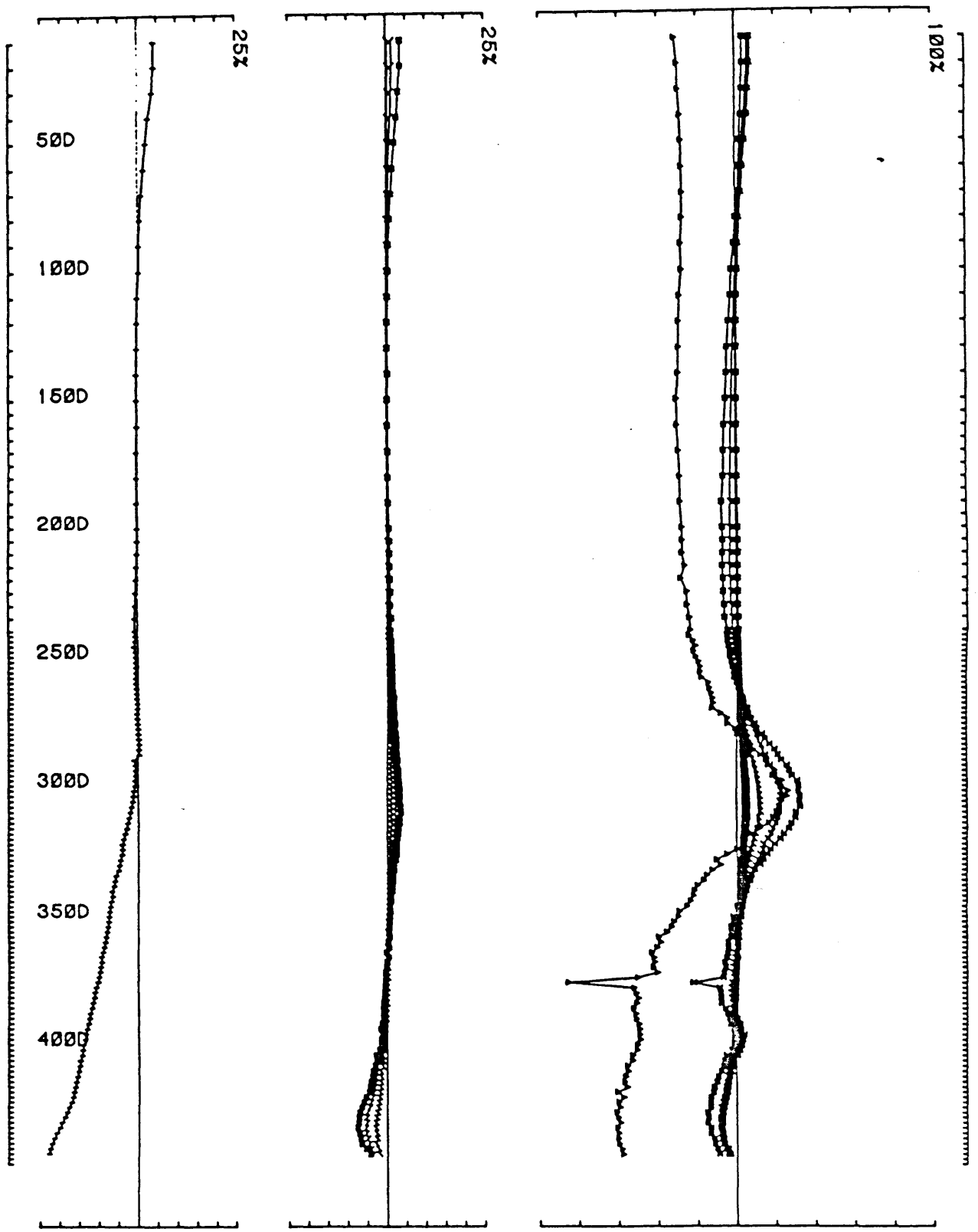

UTEM SURVEY conducted by Lamontagne Geophysics Job 9266
Project Area GERTRUDE BH 9266 SOUTH LOOP Survey for GSC freq(hz) 30.974
Loopno 6692 Line GERTRUDE BH 9266 SOUTH LOOP component Hx secondary Ch 1

FIG. 2-5

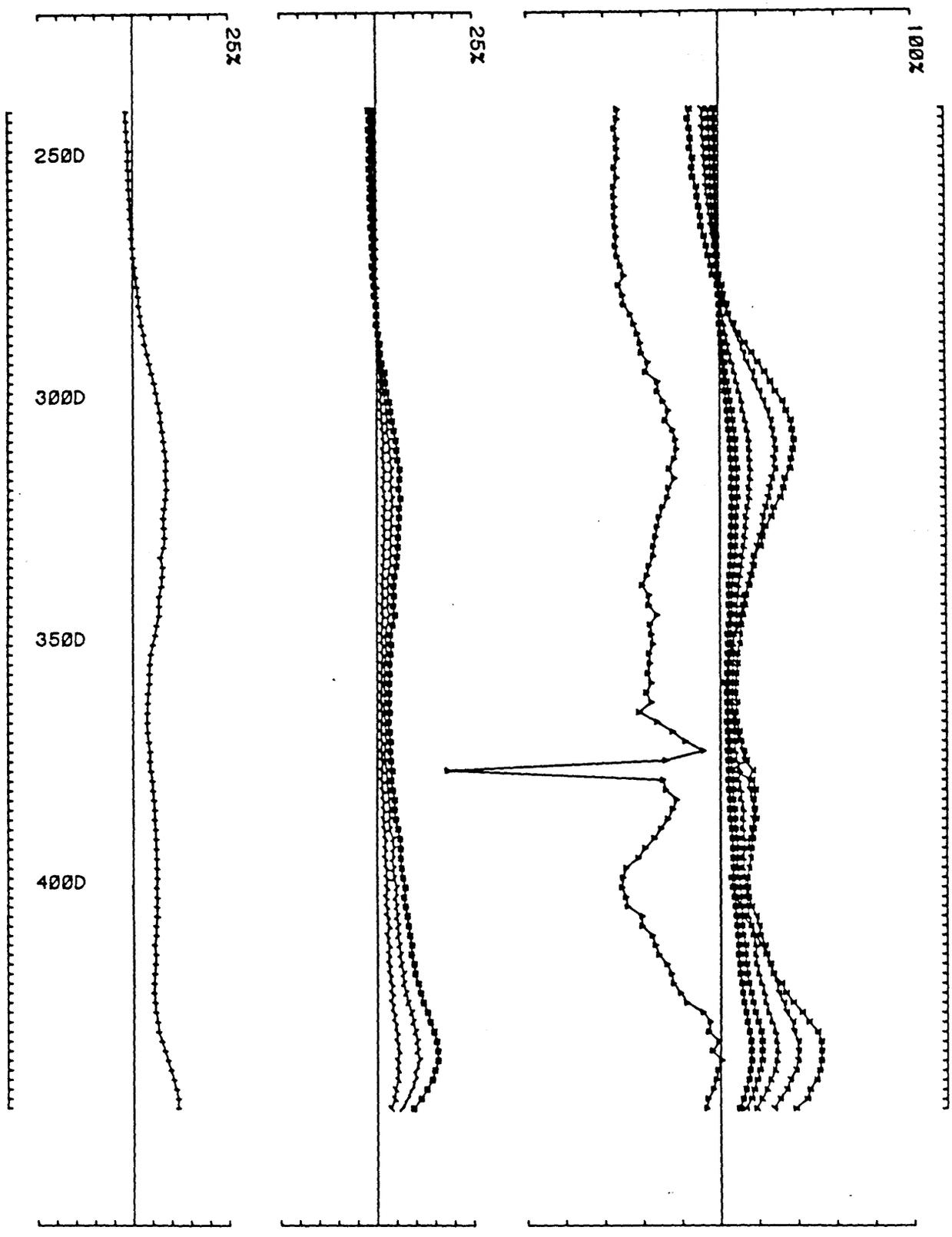

UTEM SURVEY conducted by Lamontagne Geophysics Job 9266
Project Area GERTRUDE BH 9266 NORTH LOOP Survey for GSC freq(hz) 30.974
Loopno 6604 Line GERTRUDE BH 9266 NORTH LOOP component Hx secondary Ch 1

FIG. 2-6

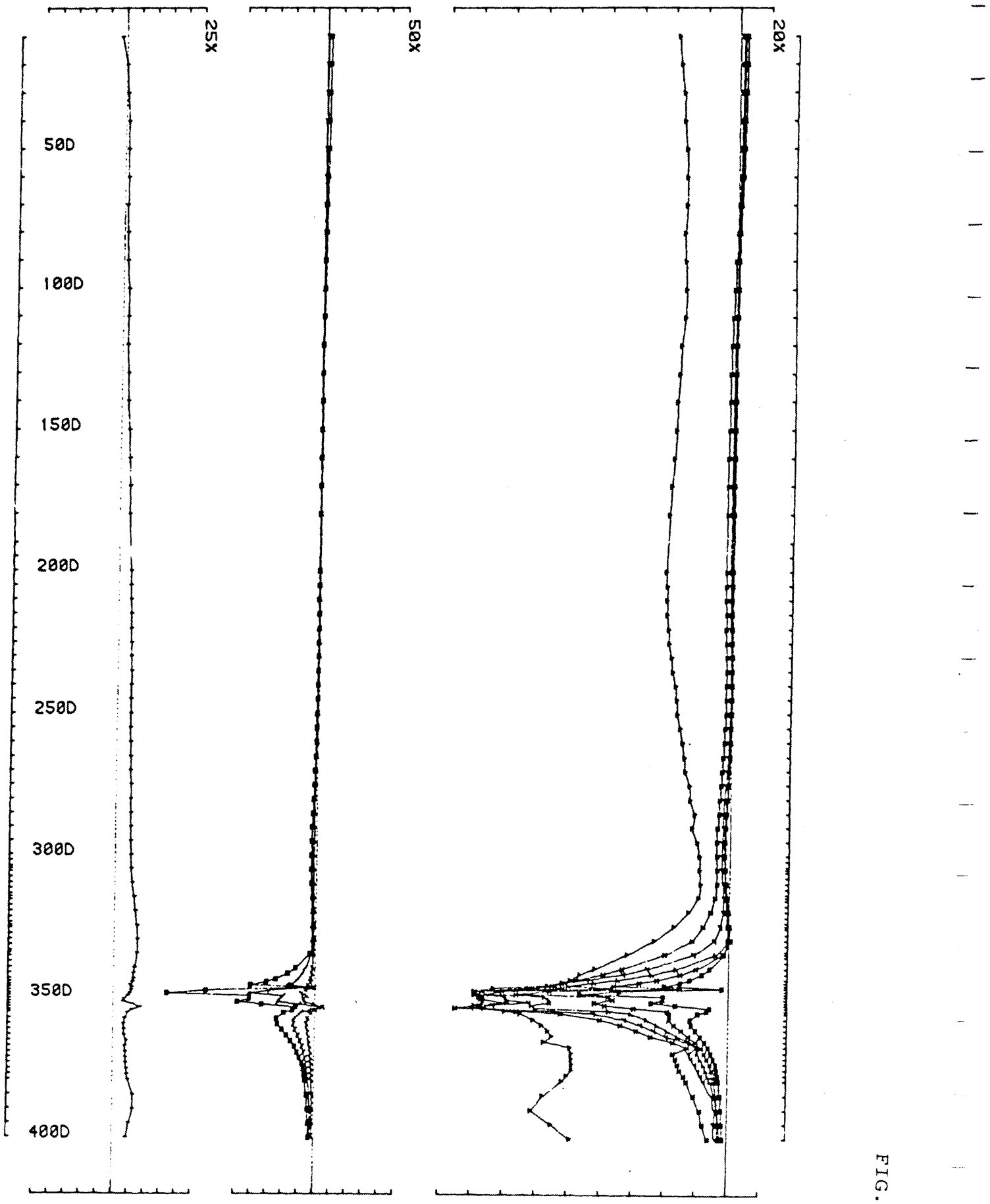

UTEM SURVEY conducted by Lamontagne Geophysics Job 9273

Project Area GERTRUDE BH 9273 SOUTH LOOP Survey for GSC freq(hz) 30.974

Loopno 7302 Line GERTRUDE BH-9273 SOUTH LOOP component Hx secondary Ch 1

FIG. 2-7

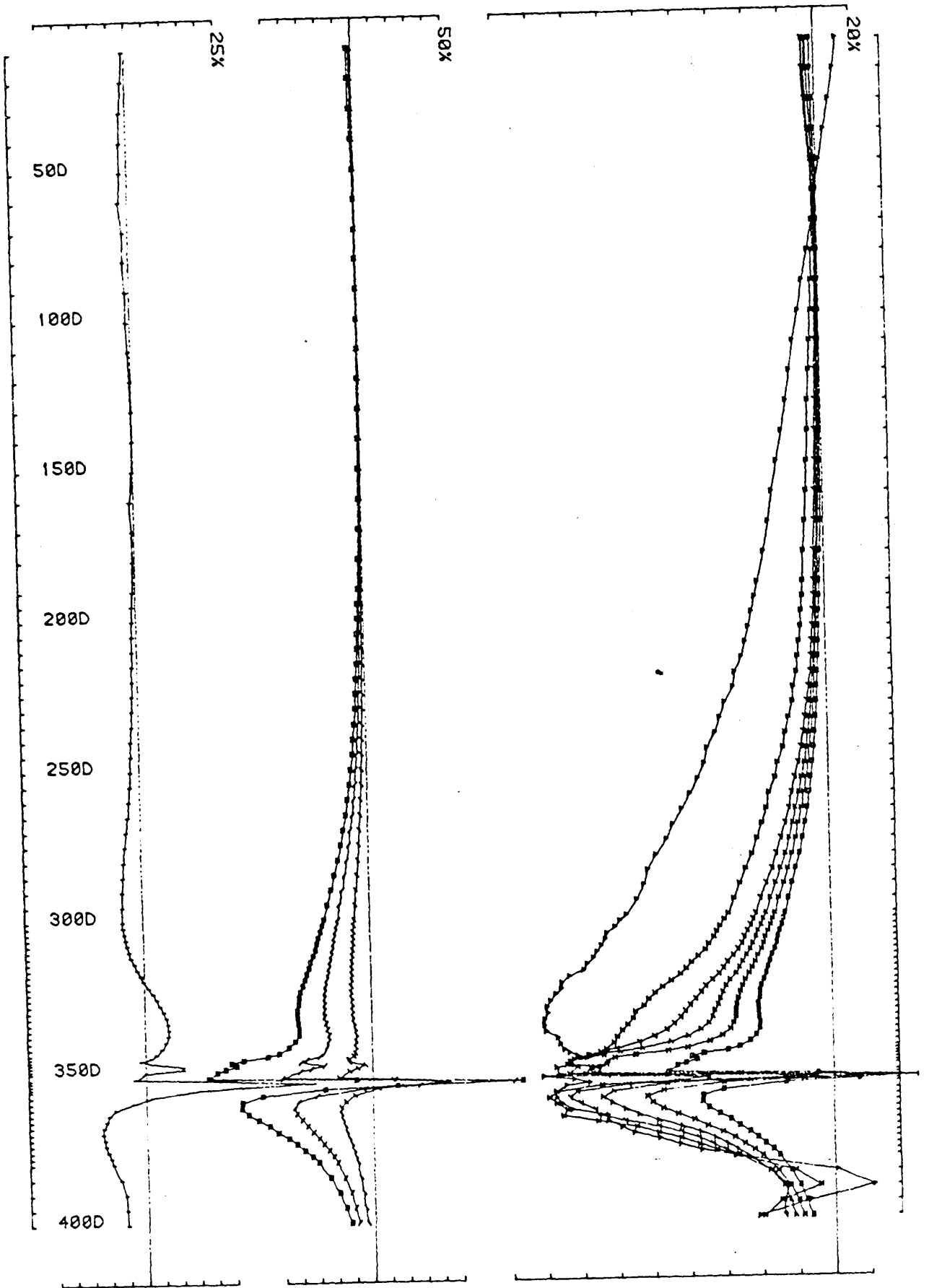

UTEM SURVEY conducted by Lamontagne Geophysics Job 9273

Project Area GERTRUDE BH 9273 NORTH LOOP Survey for GSC freq(hz) 30.874

FIG. 2-8

FIG. 2-9

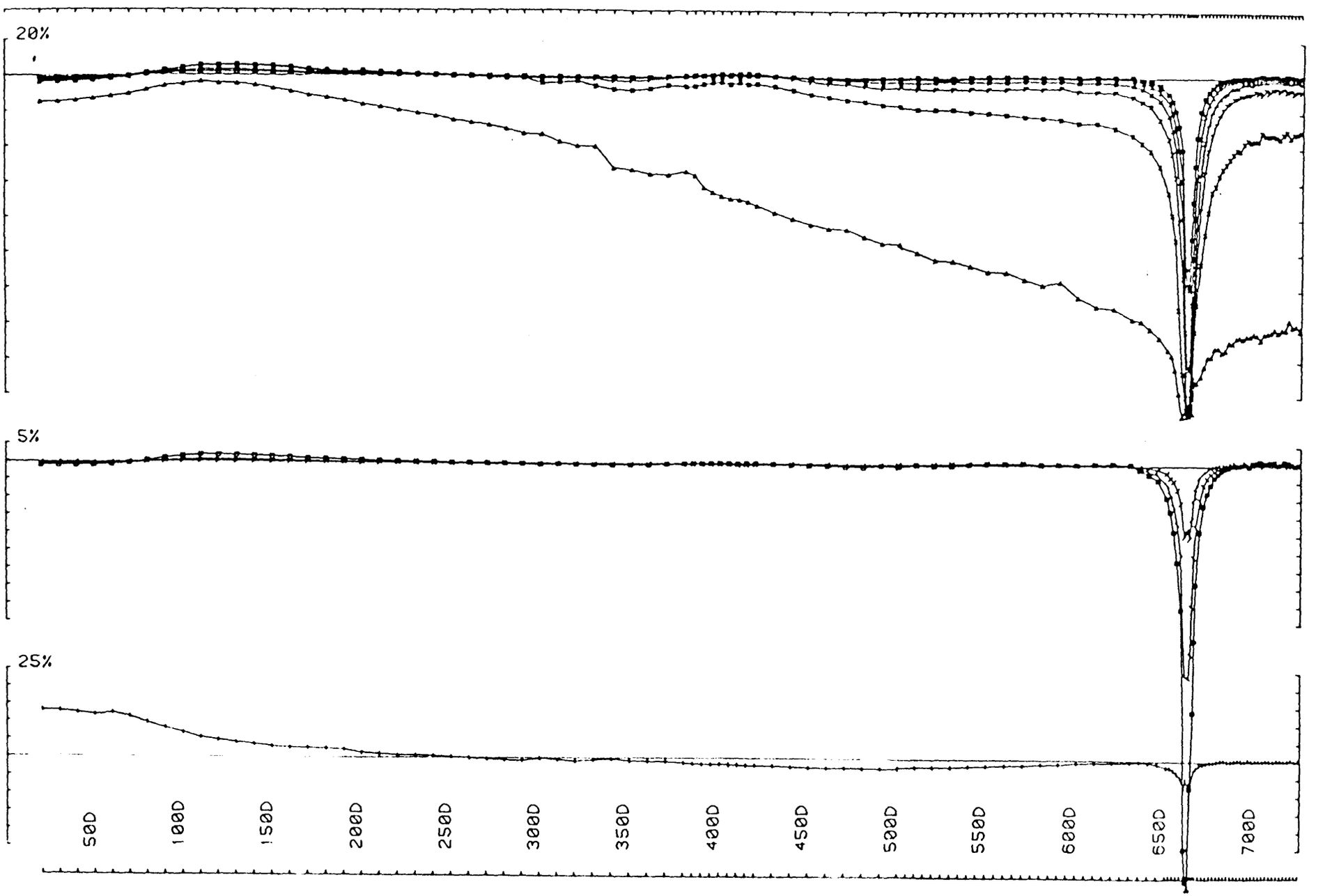
20%
5%
25%
50D
100D
150D
200D
250D
300D
350D
400D
450D
500D
550D
600D
650D
700D
UTEM SURVEY conducted by Lamontagne Geophysics Job 10621
Project Area GERTRUDE BH 10621 NORTH LOOP Survey for GSC freq(hz) 30.963

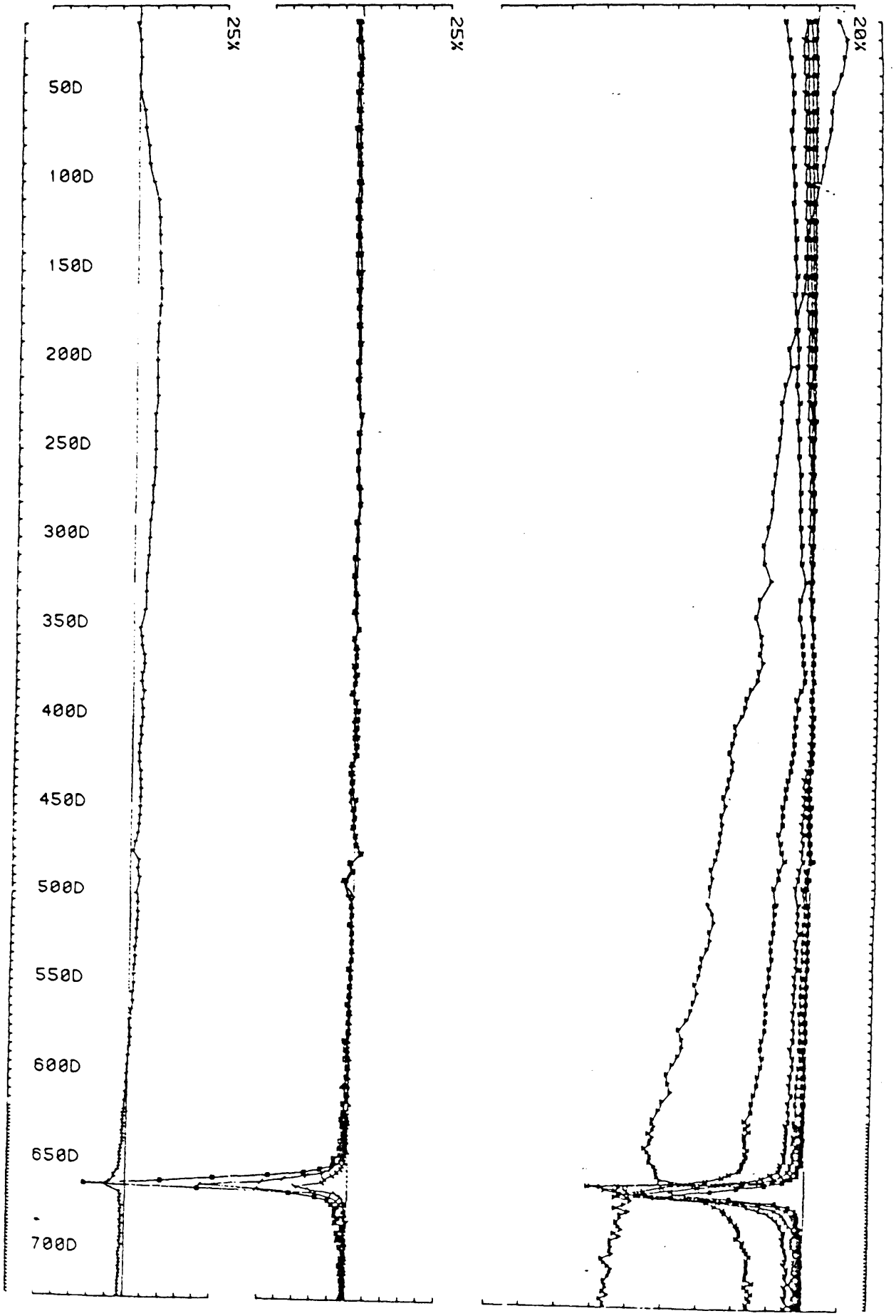

UTEM SURVEY conducted by Lamontagne Geophysics Job 10621
Project Area GERTRUDE BH 10621 SOUTH LOOP Survey for GSC freq(hz) 30.963

FIG. 2-10

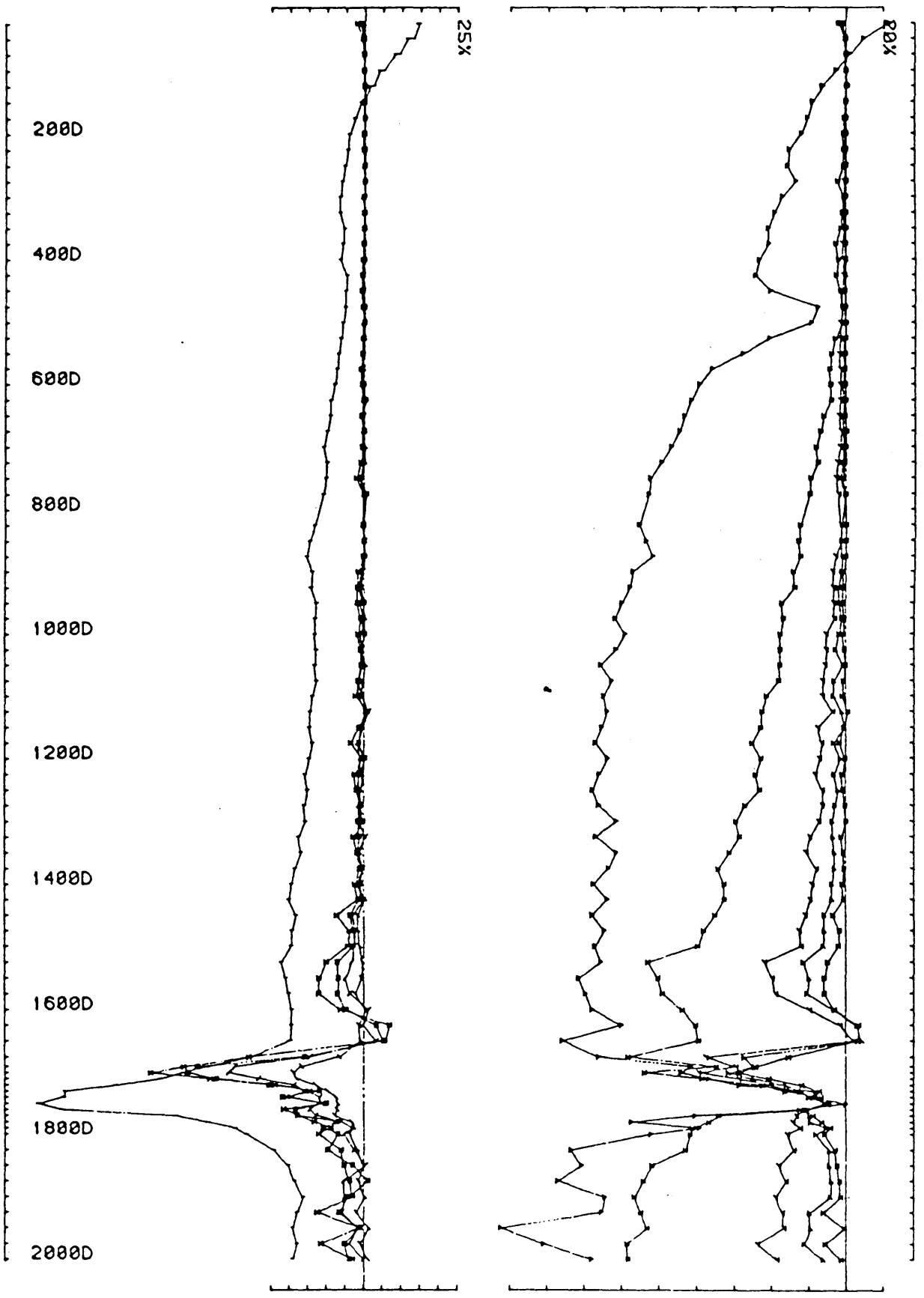

UTEM SURVEY conducted by LAMONTAGNE GEOPHYSICS HU YL RH Job 1

SITE 2

FIG. 2-11

FIG 2-12.

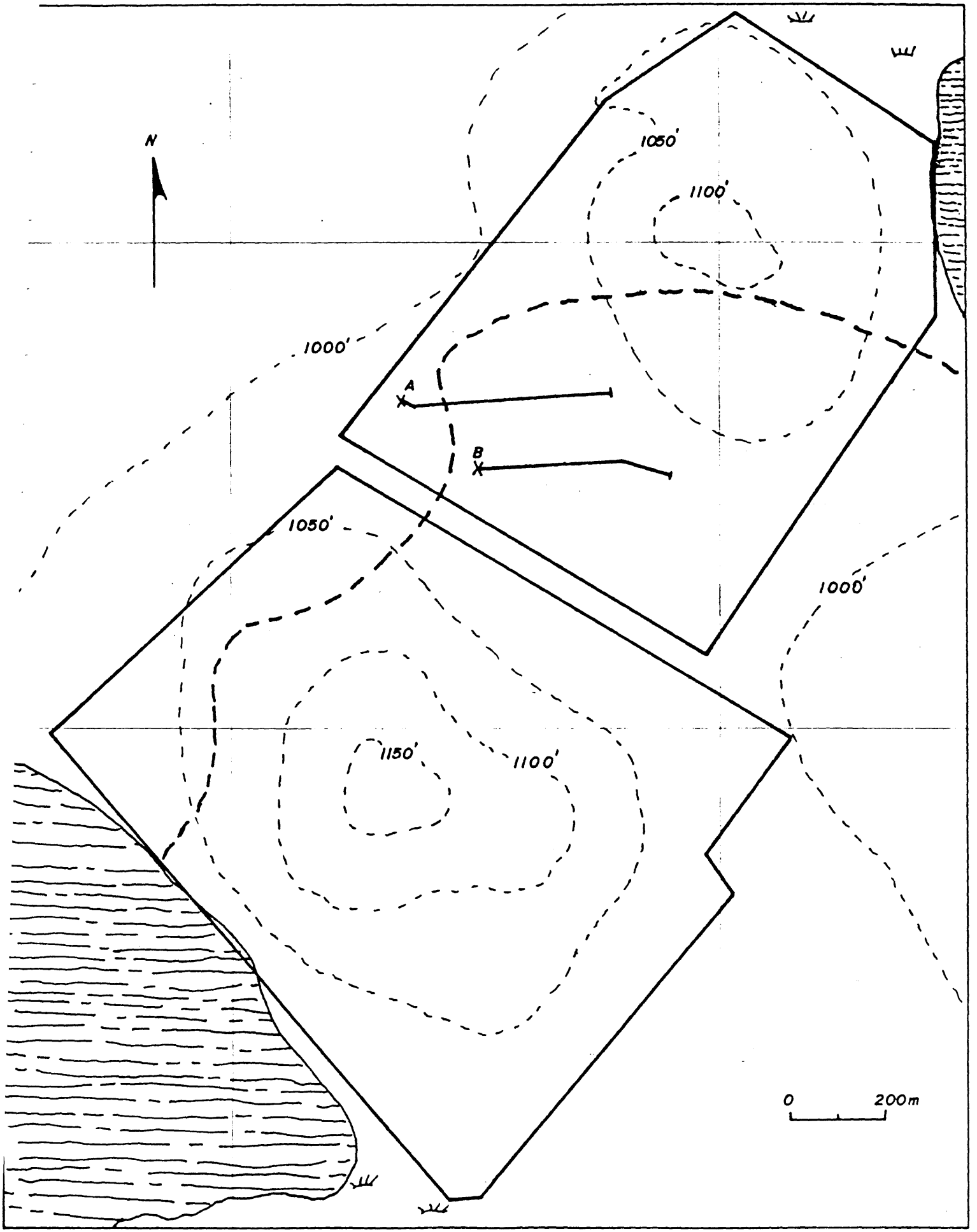

FIG. 2-12b

MAP LEGEND

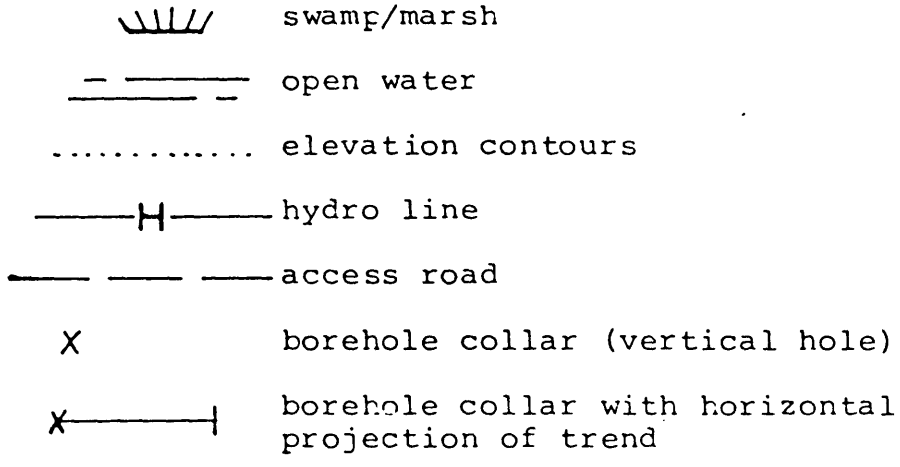

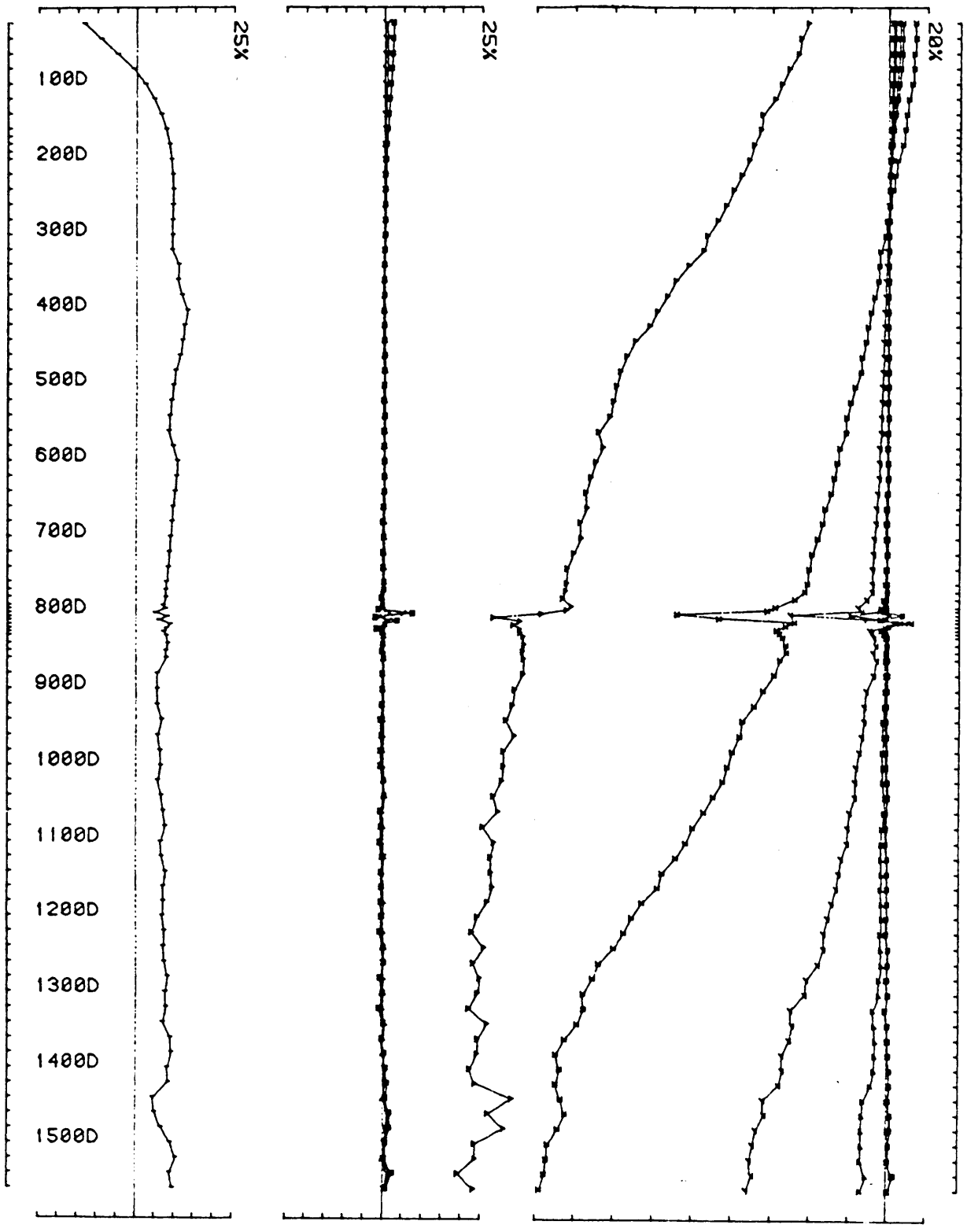

SITE 3

FIG. 2-13

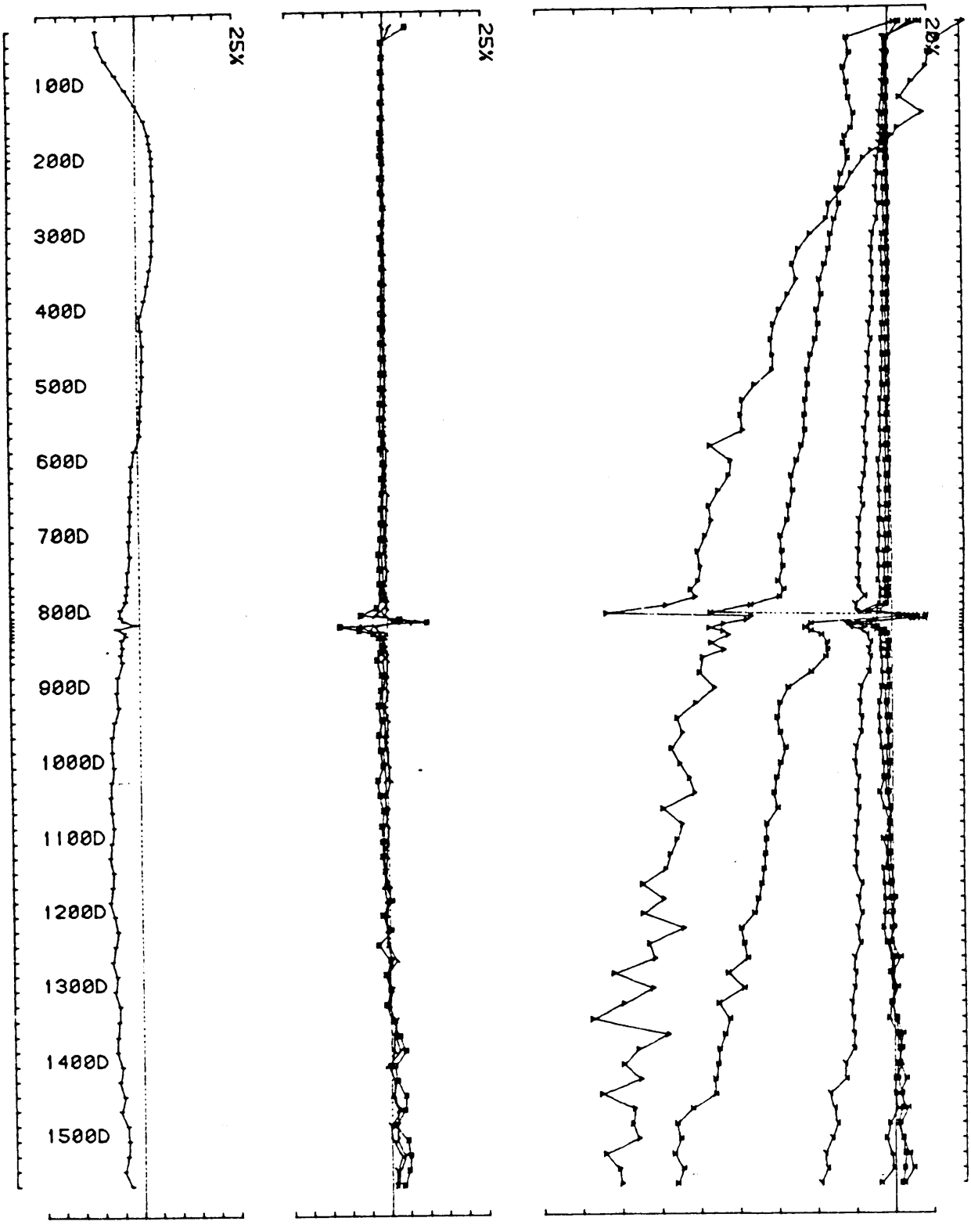

SITE 3

FIG. 2-14

FIG. 2-15

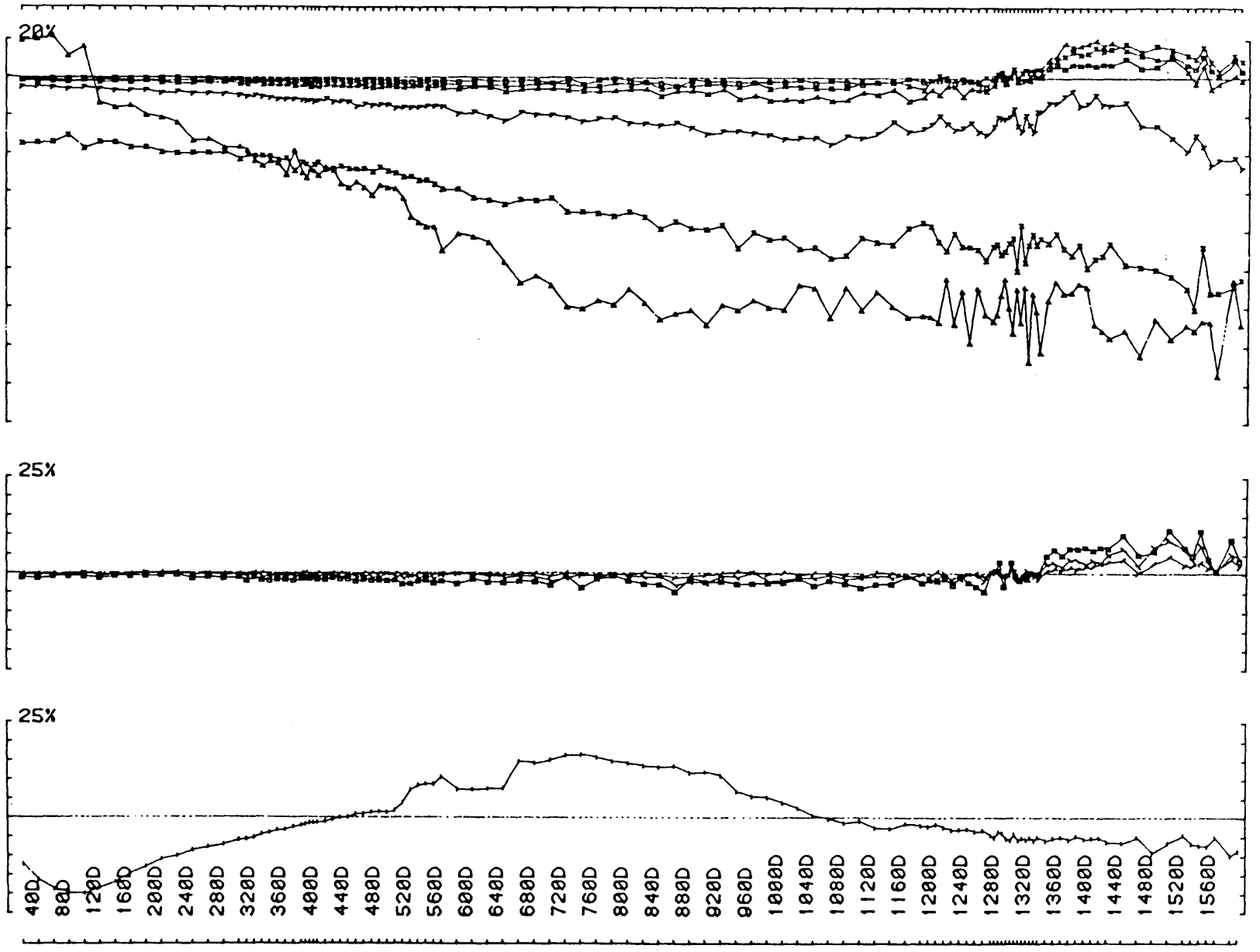

SITE 3

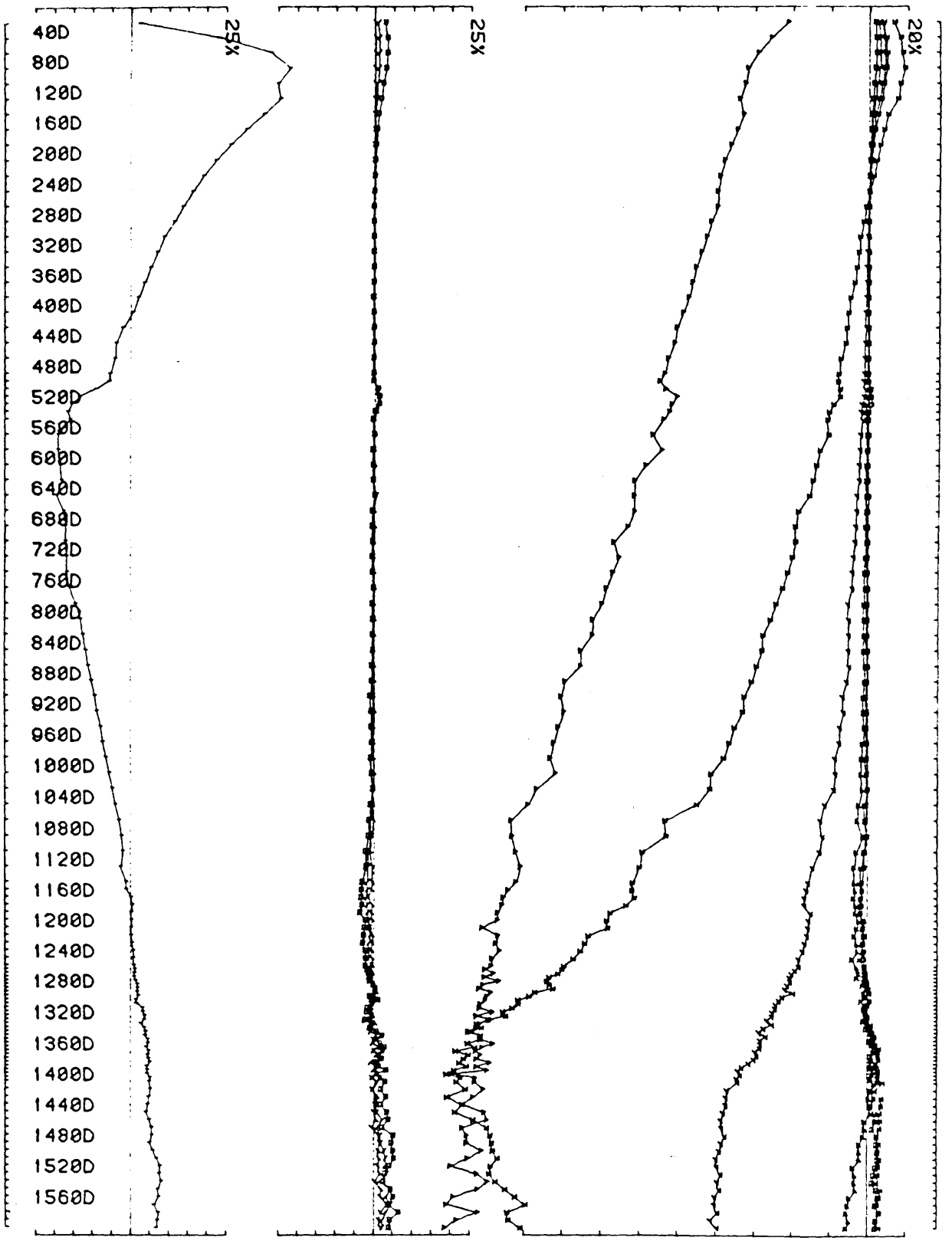

SITE 3

FIG. 2-16

LIGHT TABLE INTERACTIVE GRAPHICS COMMANDS

1) "c": locates the center of transformation on the profile
2) "o": plots original data
3) "a": uses graphics screen a
4) "b": uses graphics screen b
5) "O": overlays screen a and screen b
6) "r": solid body transformation right by input increment
7) "l": solid body transformation left by input increment
8) "u": solid body transformation up by input increment
9) "d": solid body transformation down by input increment
10) "h": horizontal compression about point picked by 'c'
11) "H": horizontal expansion about point picked by 'c'
12) "v": vertical compression about point picked by 'c'
13) "V": vertical expansion about point picked by 'c'
14) "m": mirrors using x axis
15) "M": mirrors using y axis
16) "e": erase present screen
17) "F": keeps all pre-plotted images on screen
18) "f": refreshes screen for every plot
19) "p": clockwise rotation about point picked by 'c'
20) "n": counterclockwise rotation about point picked by 'c'

OPTIONS

1) continuous alpha display of re-adjusted parameters
2) many channels per use of program each with hard plot copy
3) choice of automatic scaling or standard UTEM scaling
4) choice of plotting symbols and line type
5) autorepeat on any command key

HALF PLANE SERIES

DIPPING

STRIKING

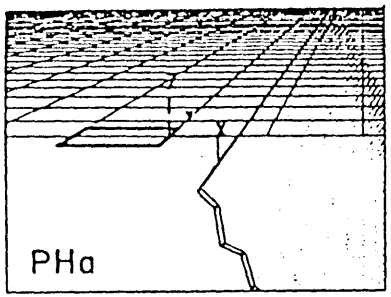

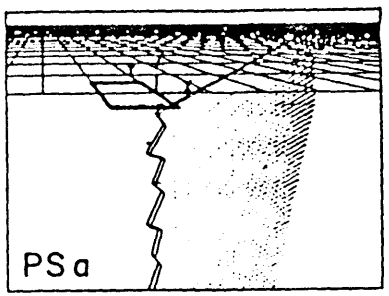

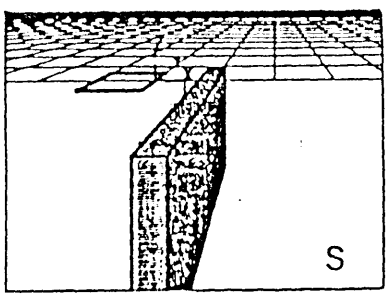

SLAB AND WEDGE MODEL SERIES

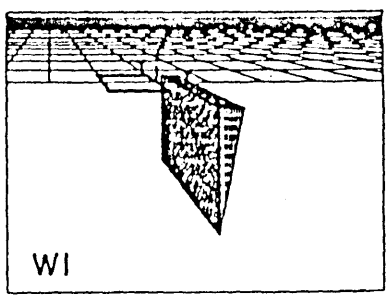

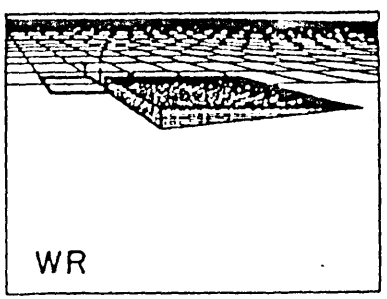

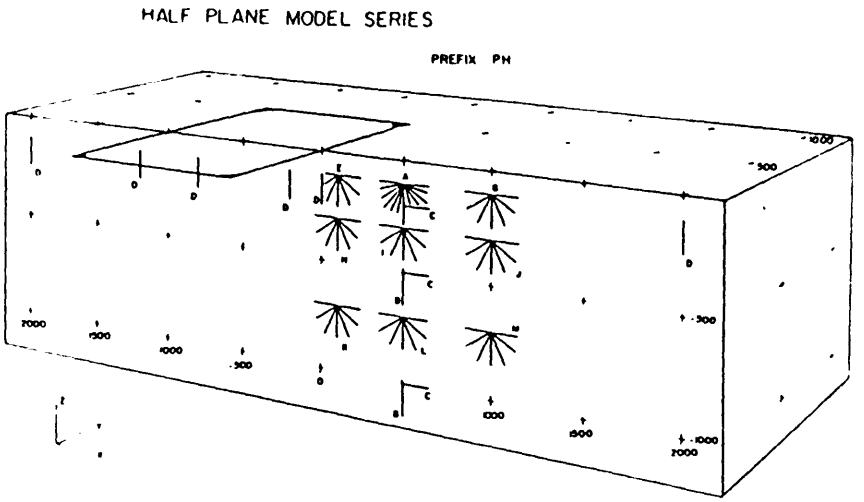

FIG. 3-1a

BLOCK/FACE MODEL SERIES

FIG. 3-1b

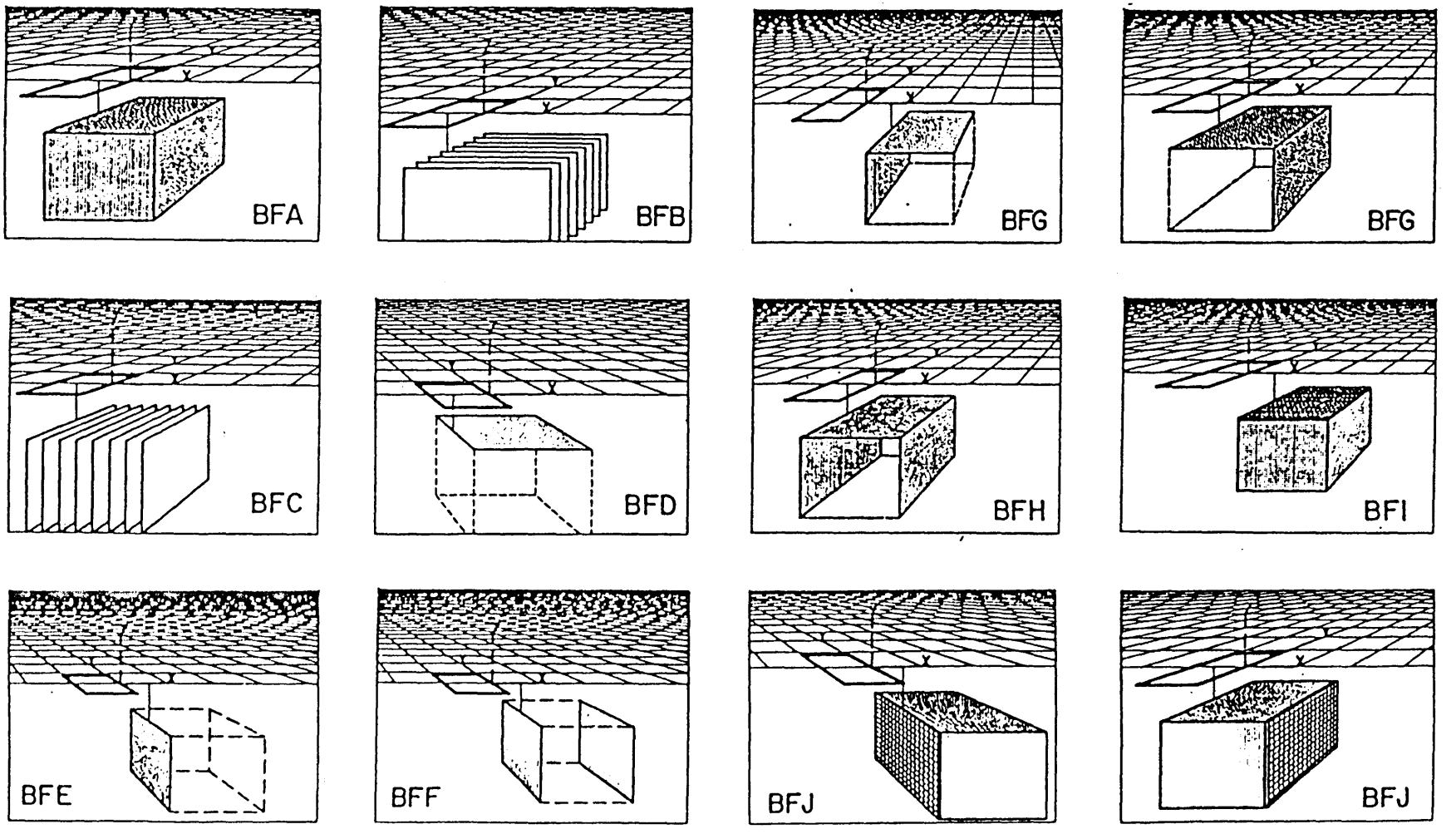

HALF PLANE ONLY OC:A

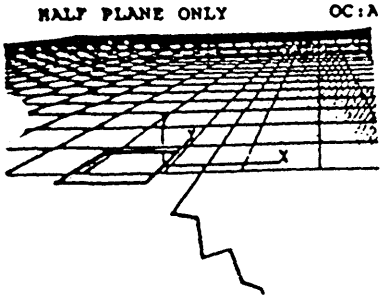

FINITE PLATE ONLY OC:B

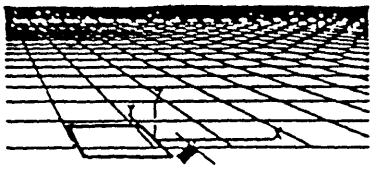

OVERBURDEN ONLY OC:C

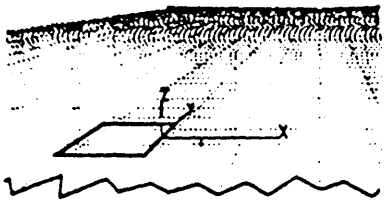

FINITE PLATE PLUS OVERBURDEN

CONTACT OC:G
NO CONTACT OC:E

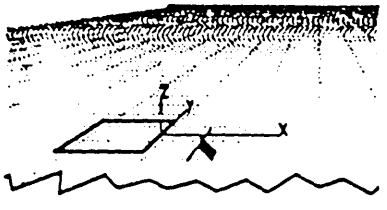

HALF PLANE PLUS OVERBURDEN

CONTACT OC:F
NO CONTACT OC:D

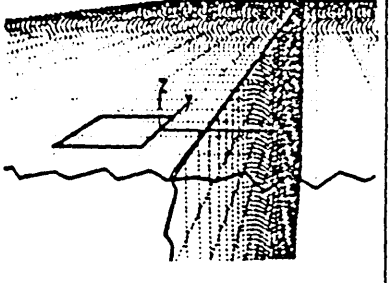

OVERBURDEN AND CONDUCTOR SERIES

FINITE OVERBURDEN OV:0

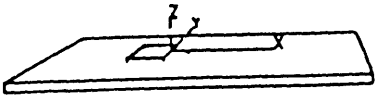

OVERBURDEN RIDGE OV:1

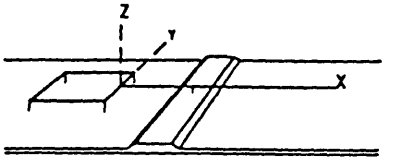

OVERBURDEN VALLEY OV:2

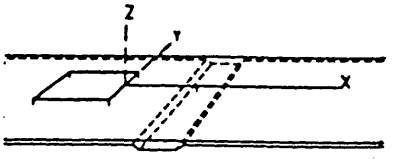

RESISTIVE VALLEY IN OVERBURDEN OV:3

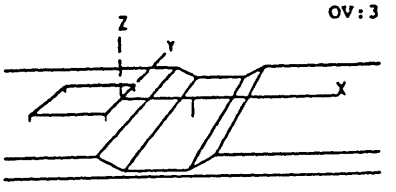

RESISTIVE RIDGE IN OVERBURDEN OV:4

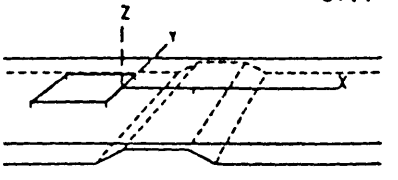

STEP DOWN OV:5

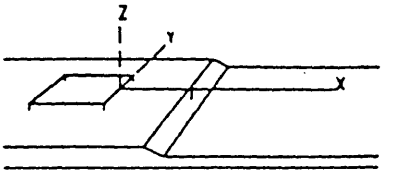

STEP UP OV:6

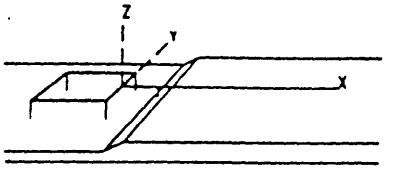

IRREGULAR OVERBURDEN SERIES

PLUNGING ANTICLINES AS:A

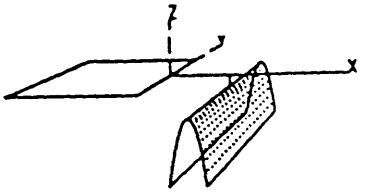

PLUNGING SYNCLINES AS:S

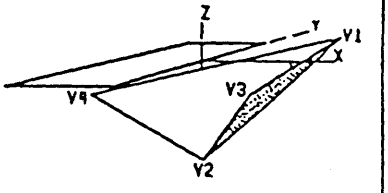

ANTICLINE AND SYNCLINE SERIES

FIG. 3-1c

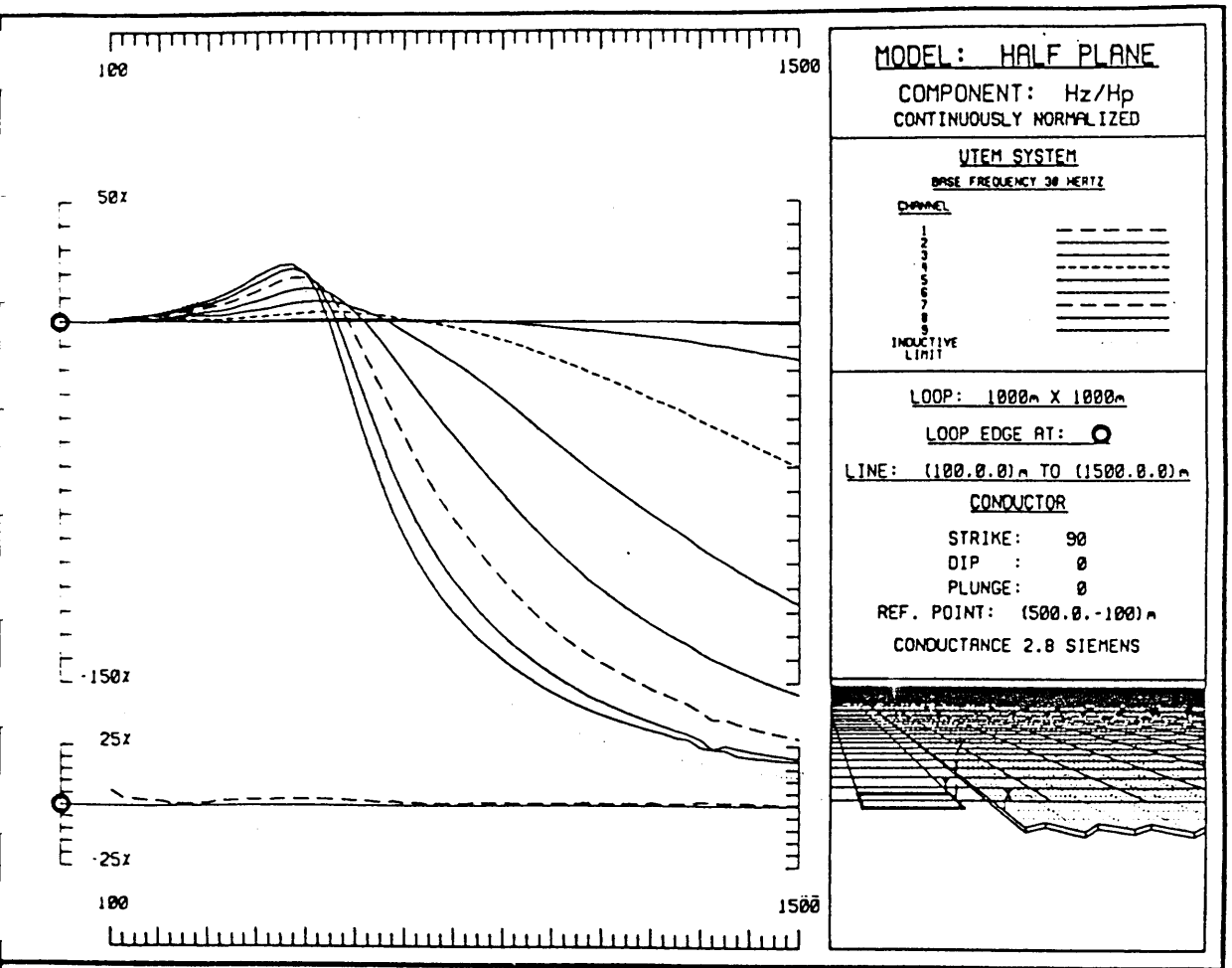

FIG. 3-2a

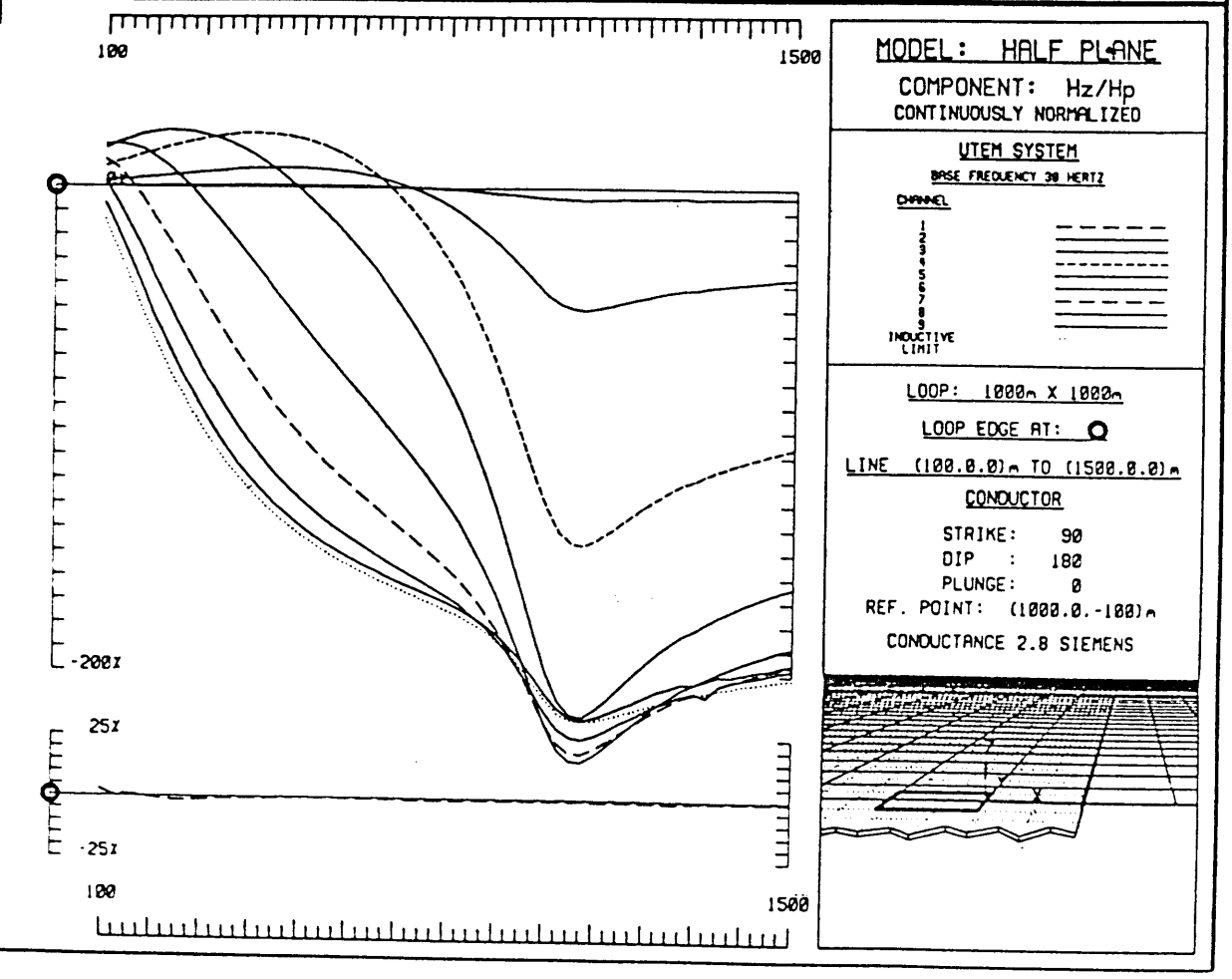

FIG. 3-2b

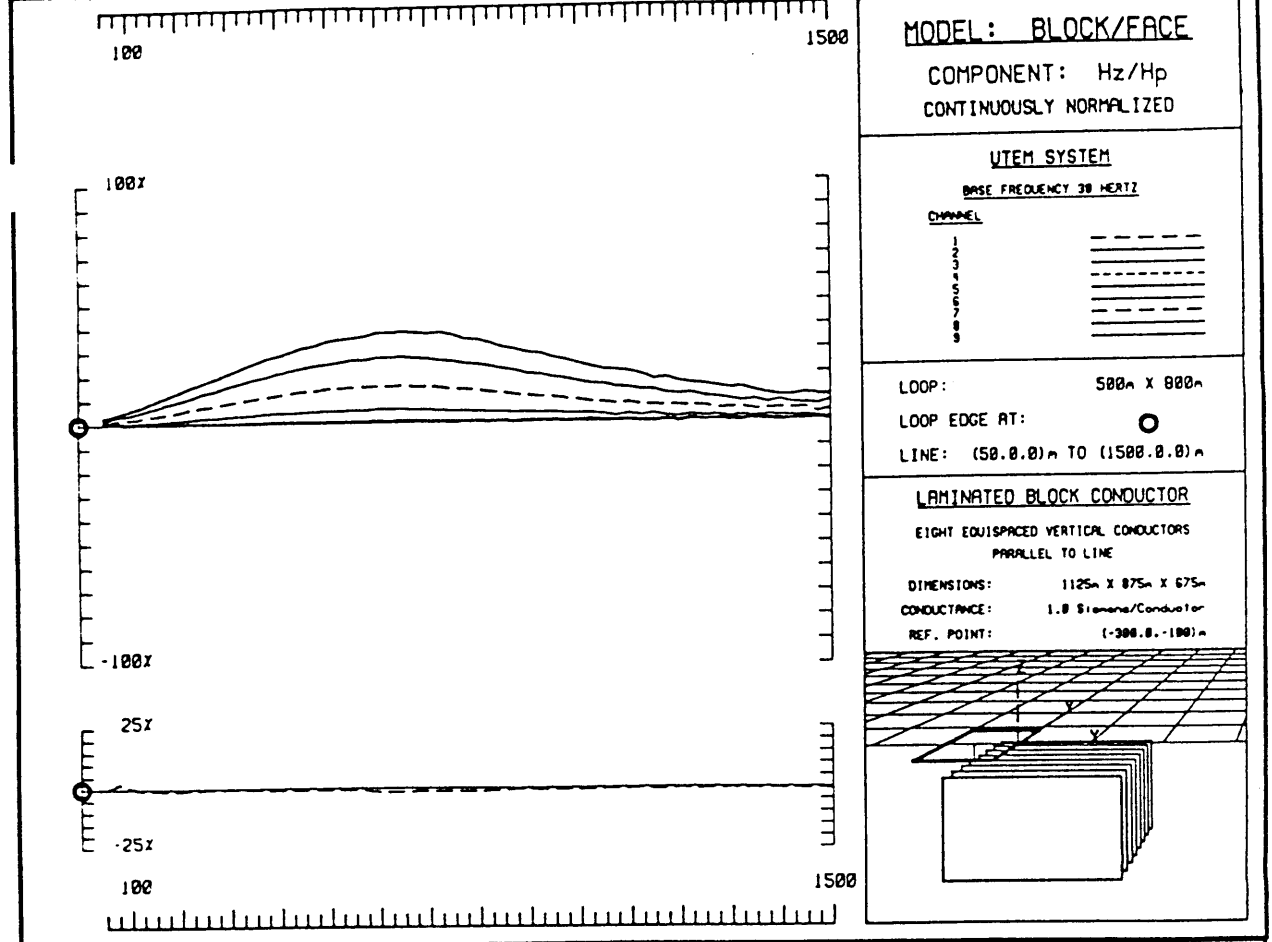

FIG. 3-3a

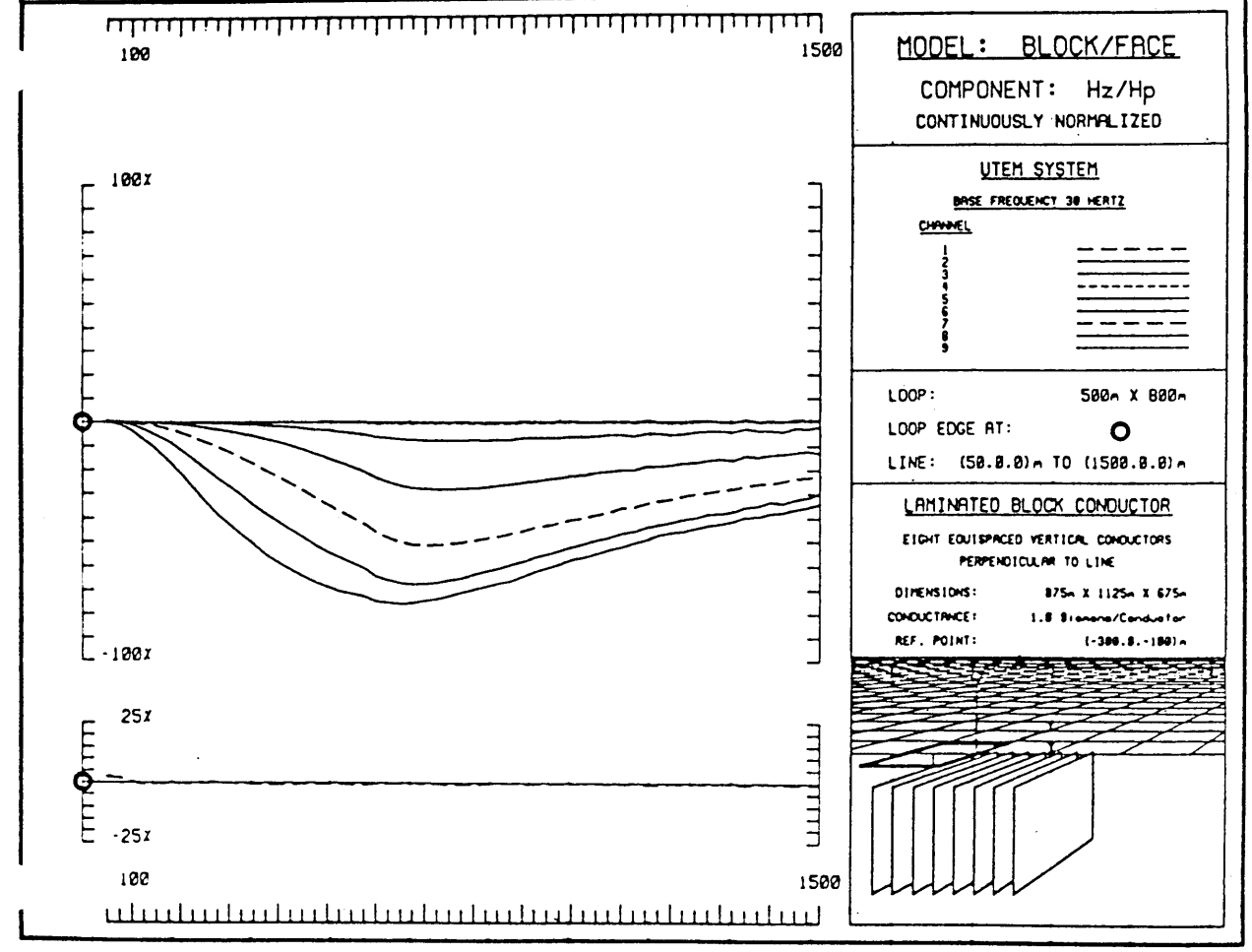

FIG. 3-3b

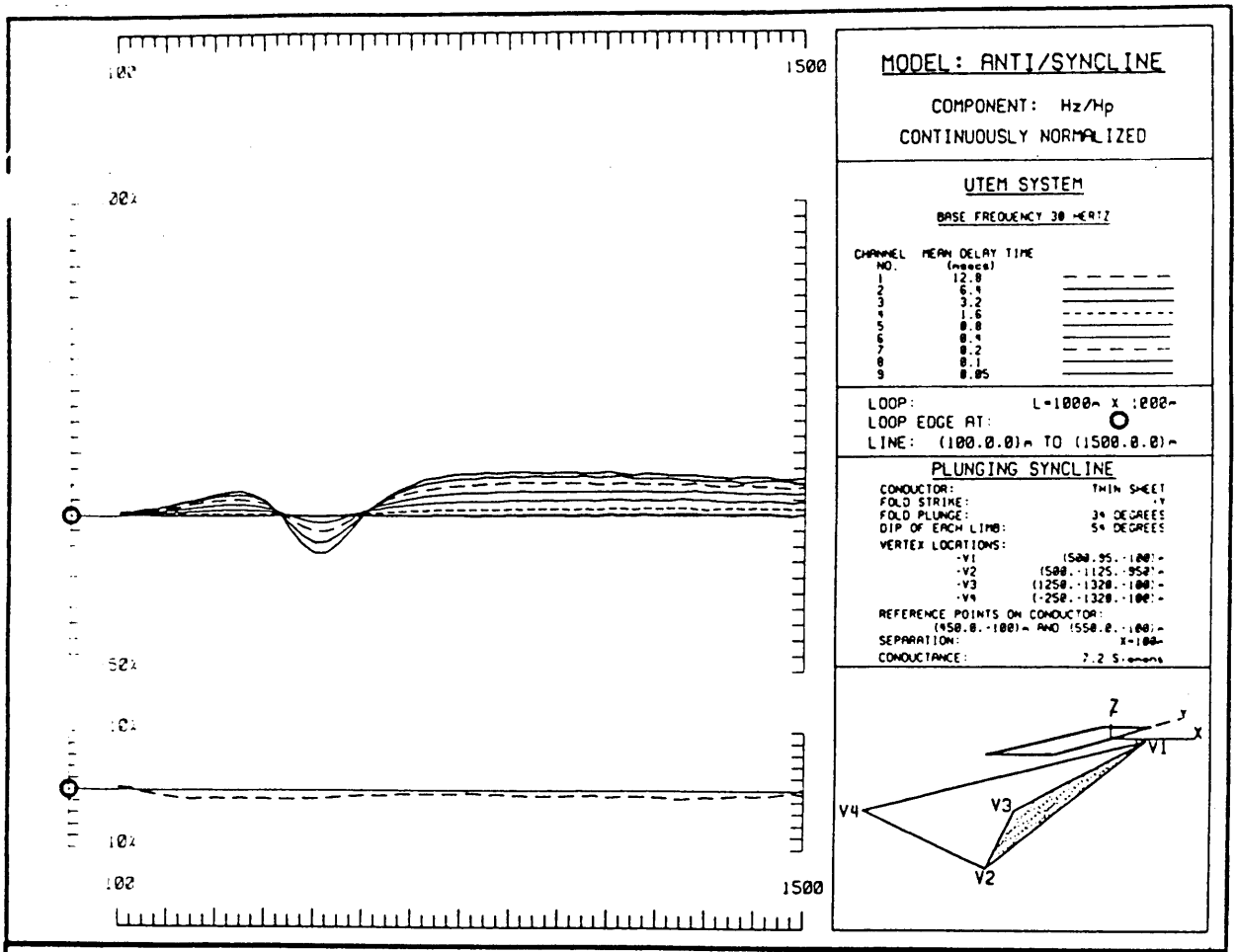

FIG. 3-4a

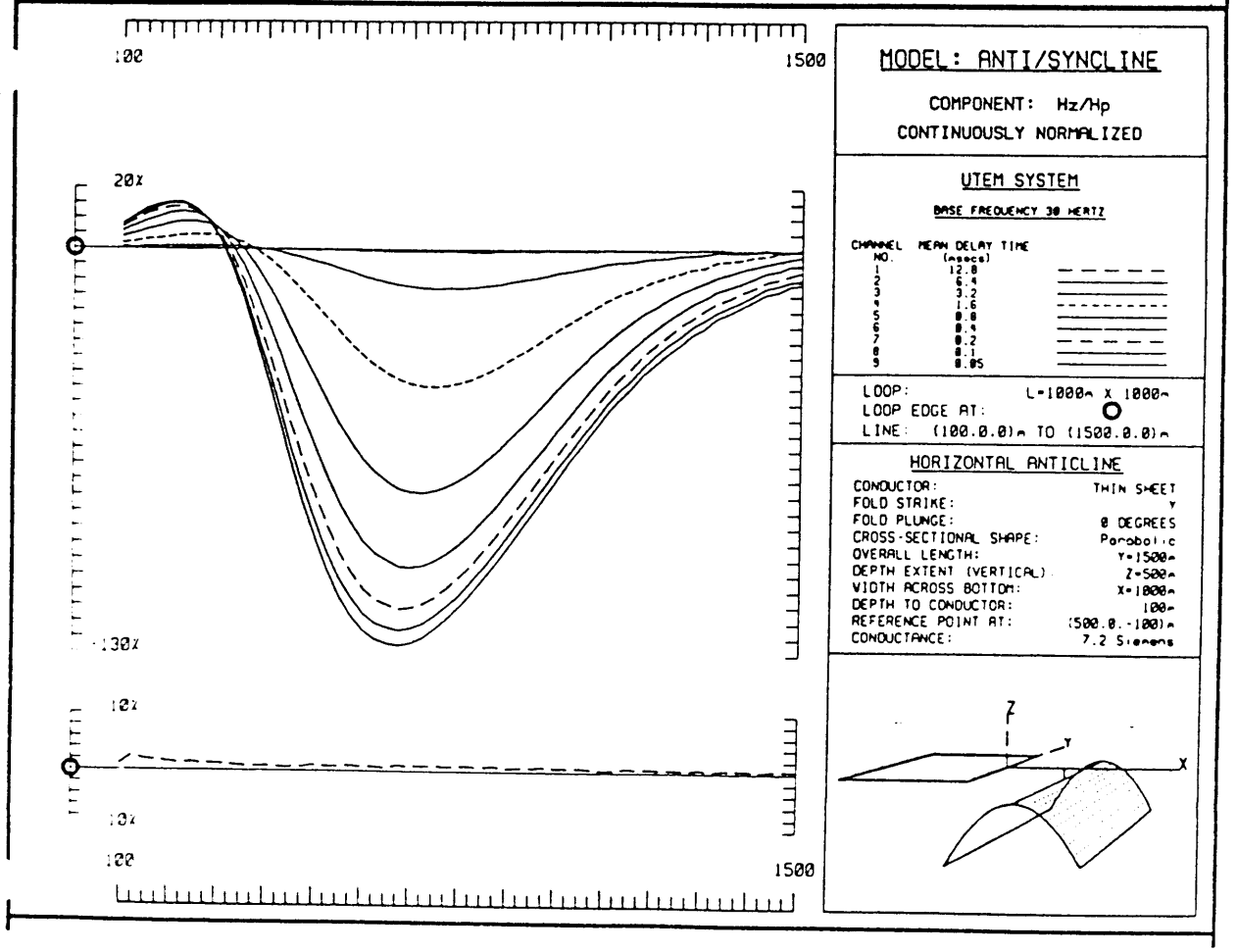

FIG. 3-4b

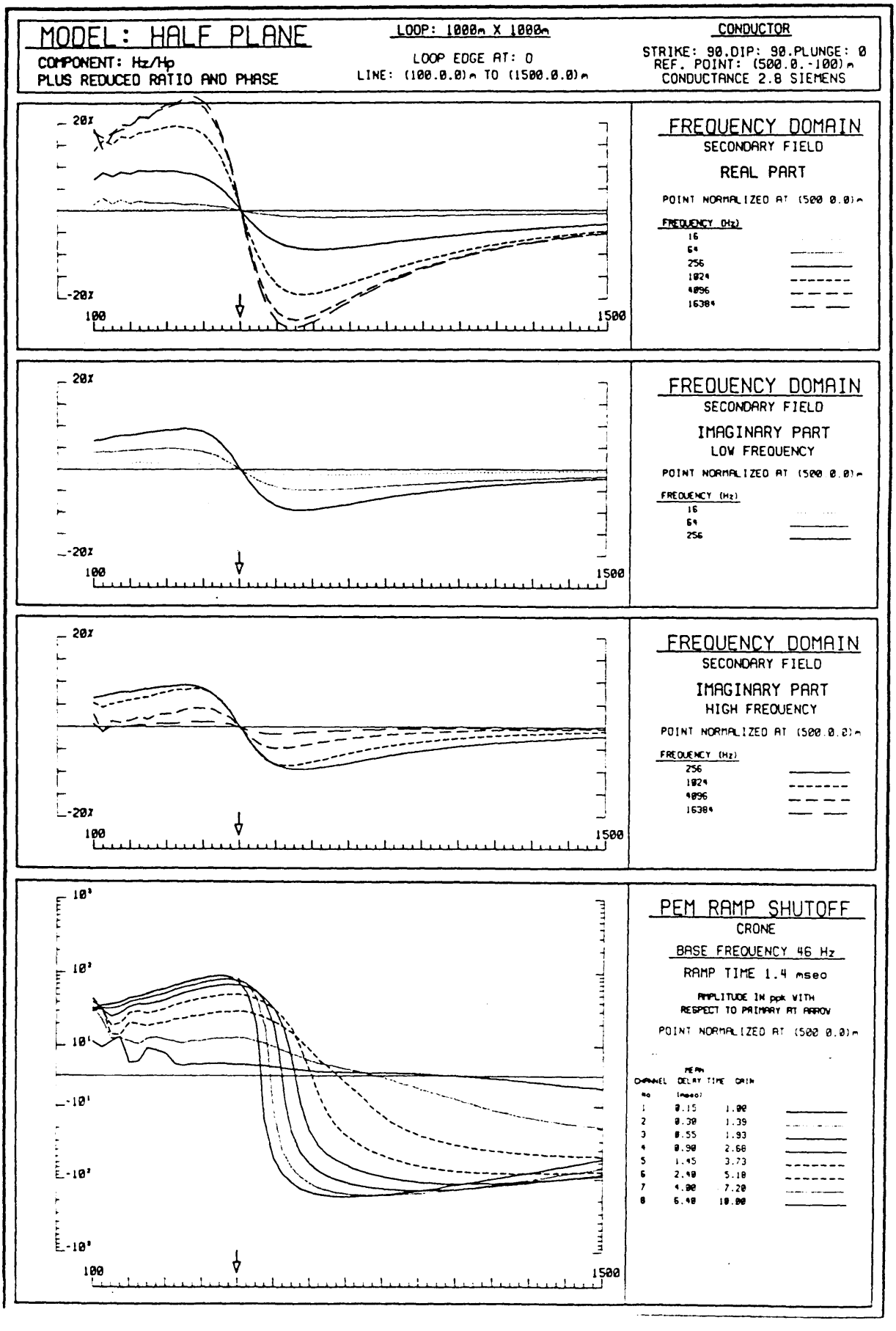
MODEL: HALF PLANE
COMPONENT: Hz/Hp
PLUS REDUCED RATIO AND PHASE
LOOP: 1000m X 1000m
LOOP EDGE AT: 0
LINE: (100.0.0)m TO (1500.0.0)m
CONDUCTOR
STRIKE: 90.DIP: 90.PLUNGE: 0
REF. POINT: (500.0.-100)m
CONDUCTANCE 2.8 SIEMENS
20%
-20%
100
1500
FREQUENCY DOMAIN
SECONDARY FIELD
REAL PART
POINT NORMALIZED AT (500 0.0)m
FREQUENCY (Hz)
16
64
256
1024
4096
16384
FREQUENCY DOMAIN
SECONDARY FIELD
IMAGINARY PART
LOW FREQUENCY
POINT NORMALIZED AT (500 0.0)m
FREQUENCY (Hz)
16
64
256
FREQUENCY DOMAIN
SECONDARY FIELD
IMAGINARY PART
HIGH FREQUENCY
POINT NORMALIZED AT (500.0.0)m
FREQUENCY (Hz)
256
1024
4096
16384
PEM RAMP SHUTOFF
CRONE
BASE FREQUENCY 46 Hz
RAMP TIME 1.4 mseo
AMPLITUDE IN ppk WITH
RESPECT TO PRIMARY AT ARROW
POINT NORMALIZED AT (500 0.0)m
CHANNEL No
PEAK DELAY TIME (mseo)
GAIN
1 0.15 1.00
2 0.30 1.39
3 0.55 1.93
4 0.90 2.68
5 1.45 3.73
6 2.40 5.18
7 4.00 7.20
8 6.40 10.00

FIG. 3-5

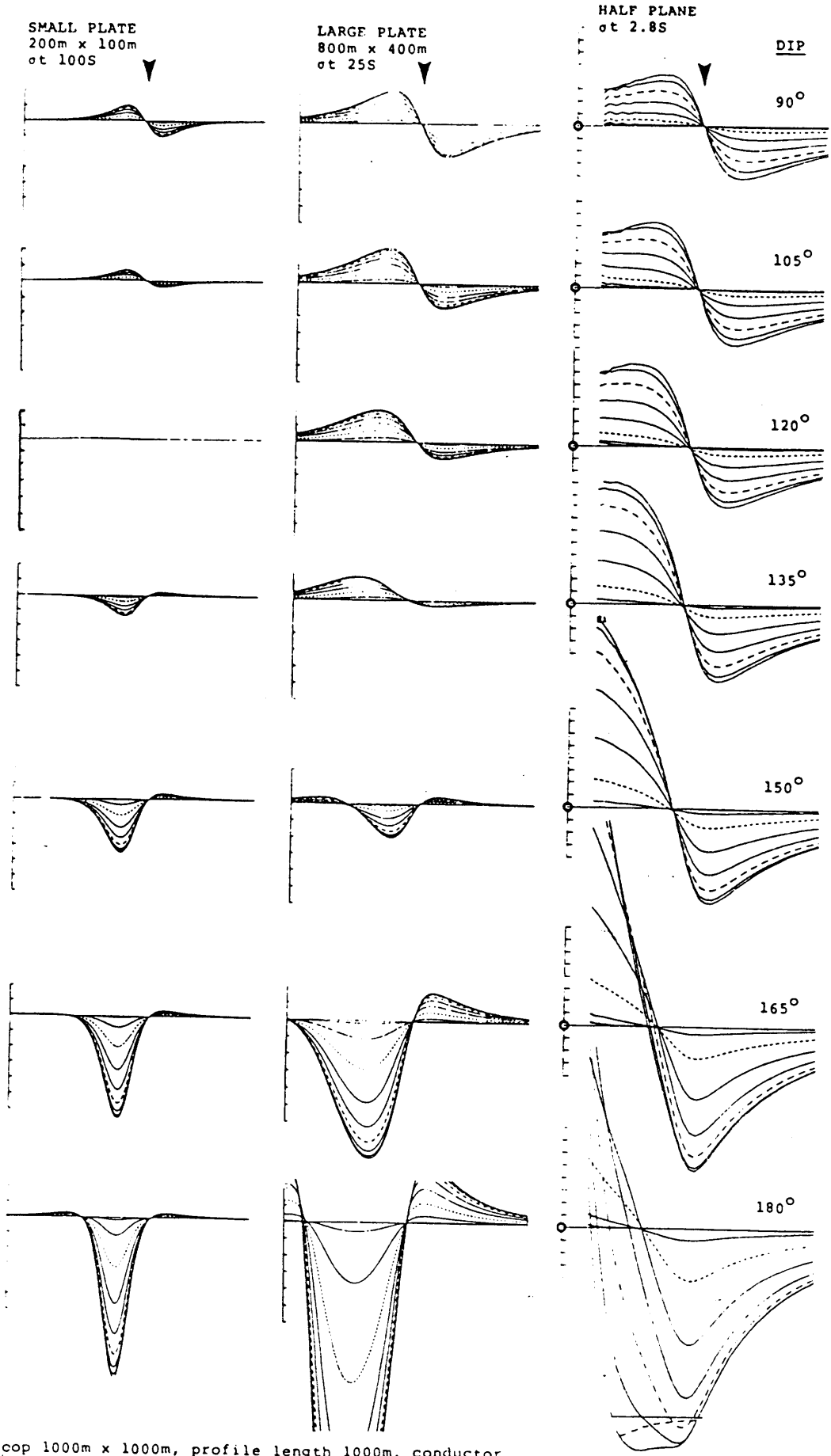

FIG. 7

Variation of response shape with dip showing also the effect of size. The amplitude scale for each size of conductor is different (but kept constant as a function of dip) and was chosen to have equivalent response in the vertical component at 0 degree dip. The model conductances were chosen to show the full range of decy from inductive to resistive limit.

Tx loop 1000m x 1000m, profile length 1000m, conductor edge at depth 100m located 500m from front of Tx loop. Amplitudes point normalised at arrow (conductor edge).

NOISE PROCESSING TECHNIQUES FOR TIME-DOMAIN EM SYSTEMS

James C. Macnae *%, Y. Lamontagne %, and G.F. West *

Presented at the 52nd Annual International SEG meeting,
October 19, 1982 in Dallas.

*Geophysics Laboratory, Dept. of Physics, University of Toronto,
Toronto, Canada, M5S 1A7.

%Lamontagne Geophysics Ltd., 740 Spadina Ave.,
Toronto, Canada, M5S 2J2.

ABSTRACT

A variety of signal processing techniques can be used to minimize the effects of noise on linear, Wideband, EM systems operating in the time-domain. All systems use repetetive waveforms with polarity reversal in alternate half cycles. Exponential averaging or digital integration (stacking) is employed to increase signal-to-noise ratios by limiting the noise acceptance to narrow frequency bands centered on odd harmonics of the repetition frequency, the width of the acceptance bands being inversely proportional to stacking time. For certain types of non-stationary noise (e.g. occasional transients) or coherent noise (e.g. powerlines) it is possible to increase signal-to-noise ratios above those obtained by simple stacking for an equal time by use of techniques such as pruning, tapered stacking or randomized stacking. With some system waveforms and when the noise spectrum is not "white", use of pre-emphasis filtering in the transmitter and a corresponding de-emphasis filter in the receiver may significantly improve the input signal-to-noise ratio before stacking. Specific applications of the various techniques are discussed with reference to one particular time-domain EM system, the UTEM 3 system. By their use, improvements in signal-to-noise ratio of as much as 6 to 1 have been regularly achieved without any increase in transmitter power, depending on the nature of the local noise.

INTRODUCTION

The aim of this paper is to present a general description of some processing techniques that have been found to be useful for rejecting noise in time-domain EM systems. One major difference between the type of signal processing used in EM systems and that used in other areas, such as seismic surveying, is that EM system processing is usually constrained to be primarily in real time. This is not a fundamental requirement, of course, but arises because the field crews required to perform a survey are typically quite small, and usually have limited access to major computers and mass data storage at the data acquisition point.

Virtually all controlled source EM systems transmit a repetetive signal and use some form of synchronous detection and averaging (stacking) to enhance the signal relative to the noise background. Because the sensors, amplifiers, and signal conditioning circuits in a time-domain EM system EM system are broadband, it is sometimes assumed that any time-domain EM system must have signal-to-noise characteristics which are inferior to a frequency domain unit. This is not so, however, because the averaging procedures reduce the effective acceptance of the system for incoherent noise while still performing a broadband measurement of signal. Basically, synchronous averaging causes the instrument's spectral response to be collapsed to a multitude of narrow spectral lines centred on odd harmonics of the signal's base frequency. The object of this paper is to show how the system response to different types of noise may be calculated

for various processing techniques, and to discuss some of the trade-offs that must be made in designing a practical signal acquisition system. Most of the analytical basis for this paper is contained in the PhD thesis of Lamontagne (1975).

Synchronous detection is a powerful rejector of incoherent noise that has a stationary statistical character. However, not all noise has this characteristic. Steady powerline noise has high phase coherency. Powerline transients and local sferic activity often occur sporadically on the time scale of a single EM measurement, and when the total number of noise events is small, the resulting noise is not stationary in a statistical sense.

When a coil sensor is used to measure the magnetic field, it is found that much of the natural electromagnetic field noise energy is from sferic sources, and is not uniformly distributed throughout the system bandwidth. Rather, it is concentrated mostly in the high frequency part of typical EM systems' bandwidth. When wideband noise is "coloured", a standard technique to improve signal-to-noise ratios consists of adding a filter to the receiving circuitry to "whiten" the noise, with a corresponding inverse filter being applied to the transmitted waveform. In audio recording, it is usual to "pre-emphasize" certain parts of the recorded spectrum and then perform a reciprocal de-emphasis in the playback system. In numerical Fourier transforms, the technique is used to increase precision; however, there the "whitening" filter is applied first, and the output later "deconvolved" to remove the effect of the prewhitening

(Kanasewich, 1975). In this paper we discuss the application of a class of realizable filters to wideband EM instruments.

EM NOISE

There are a several sources of EM noise that affect EM prospecting. There are substantial differences in the noise spectrum at different places on the earth and at different times of day and year. Many authors have discussed one or more aspects of EM noise (e.g. Watt, 1967; Strangway et al., 1973; Koziar, 1976; Gamble et al., 1979).

Common inductive EM systems work in the frequency range 5Hz to 25kHz, although some of the large scale systems for sedimentary basin and geothermal sounding operate down to about 0.1Hz. The natural noise spectrum in the 5Hz - 25kHz range is primarily due to sferics, which are natural EM transients generated by lightning discharges. A sferic generally propagates to the survey site directly if the lightning is nearby or by multiple reflection in the earth-ionosphere (E-I) waveguide if it is at a large distance. Schumann resonances occur when the ELF components of sferics travel completely around the earth and interfere constructively or destructively. Attenuation with distance in the E-I waveguide is frequency selective, and it is minimal in the 2.5kHz to 10kHz range and below 500Hz. Thus, distant (even world-wide) lightning often contributes much to the average noise power at any site, while occasional very strong transients usually come from nearby or

intermediate distances (<1000km). A typical moderately distant sferic noise pulse and the distant sferic spectrum are shown schematically in Fig. 1. Actual noise amplitude varies considerably with density, location and severity of thunderstorms relative to the survey site, and often a regular diurnal variation is present. The attenuation band at about 500Hz to 2.5kHz is very clear only for distant storm activity. Frequency limits of the attenuation band depend on ionospheric conditions; in particular, the abrupt upper frequency limit shifts with ionosphere height. Watt(1967) reproduces charts of worldwide noise probabilities as a funtion of diurnal and annual time. Secondary source mechanisms of auroral, ionospheric and other origin are present in the audio-frequency band, with descriptive names such as "whistlers", "hiss", and "dawn chorus". All these contribute considerably less energy in the audio-frequency band than sferic sources.

Below about 6Hz, the natural EM noise field is primarily of geomagnetic and ionospheric origin, with relatively little noise present in the range 1Hz to 6Hz. Long oscillatory signal trains called PC's often appear below about 1Hz. They are the bane of IP surveys and they likewise harass any ultra-low frequency EM measurement.

The conductivity of the survey area has a strong effect on the natural EM field, just as on the field of the system transmitter. (This is of course the basis of the AFMAG and magnetotelluric exploration methods). In terrain that is more or less uniformly

conductive, the natural magnetic EM field is nearly horizontal. Lateral irregularity in the conductivity structure (particularly irregularity in any near surface conductor) may cause a strong vertical noise component to appear.

Man-made noise in the EM prospecting band comes mainly from the power distribution grid. The long term average frequency of mains power is usually highly stable (1 in 100,000), with short term variations that may rarely be as much as 1% and are better described as phase modulation.

The power line voltage waveform is usually quite accurately sinusoidal. However, the current waveform is often complicated. Motor loads operate non-synchronously and can produce sidebands and subharmonics of the mains frequencies. Simple switching of current loads, and electronic cycle-by-cycle switching of rectifiers or silicon controlled rectifiers produces broad-band transients and high frequency harmonics. Generally, the powerline EM field consists of a series of steady spectral lines at the mains frequency and its odd harmonics, and then a multitude of much weaker but more damaging non-stationary components.

Motion induced noise is of a different character, but just as important to EM systems as the natural EM field. The earth's steady magnetic field is usually more than 100,000 times the intensity of the fields used in EM prospecting. Any angular motion of a coil or magnetometer will produce an output from the sensor. Thus a

receiver may be an effective seismometer or microphone, and steps must be taken to minimize such disturbance. Undamped mechanical resonances can be particularly troublesome.

The point of the foregoing dissertation on noise is that there is more than one kind of noise problem in EM, and the severity of the different kinds varies with local circumstances. Consequently, there is no single optimum method of noise rejection. A well designed apparatus should be able to handle all types of noise in a reasonably satisfactory way.

In the following sections, we first discuss the theory of how instrument averaging or stacking rejects random but statistically stationary noise signals such as might be caused by system electronics or distant spheric activity. This provides a basic framework for all noise considerations.Then the problem of non-stationary, intense transients such as local sferics or power line transients is considered and a data rejection (pruning) procedure is recommended. Thirdly, modifications to standard uniformly weighted stacking are described which can improve the rejection of coherent (line spectrum) noise such as steady power line interference but do not severely degrade the rejection of stationary random noise. Fourthly, a technique of signal modification (pre-emphasis/de-emphasis) is described which accommodates to the non-white character of the sferic noise spectrum. Finally, practical experience with use of the methods in the UTEM system is described.

SIGNAL EXTRACTION

Most time-domain EM systems have a transmitted primary field which exactly repeats at a base frequency f_0 and has equal half cycles of alternating polarity. The receiver operates as a synchronous detector, stacking average amplitude measurements in time windows, with the negative half cycles being sign reversed and added to the positive half cycles. The output measurement is essentially a summation of signal components, so its output may be considered to be a linear transformation of the input signal.

It is useful to think of a synchronous detector as operating in two successive modes, first forming an average waveform at the base frequency by stacking over many periods, and then cross-correlating the stacked signal period with a reference waveform R(t) (Figure 2). The order of the two operations is not fundamental. In fact, analogue electronic apparatus usually performs the two operations concurrently or in reverse order. In time-domain EM systems, the reference waveforms for the various measuring channels are usually paired windows of unit amplitude. For extraction of single frequency in-phase and quadrature components, sine and cosine reference functions would be used.

In most digital EM systems, all cycles of signal within a specified time interval T contribute equally to the final result. In most analogue systems, the output measurement is continually updated, and contributions to the current output from sample windows

in earlier time periods are progressively deweighted. This happens because the output signal is stored as a voltage on a continuously discharging capacitor (RC filter). Thus we can express the un-normalized output A_x of the system at an arbitrary time at the end of a signal period (t=o) due to an input signal x(t) as

$$A_x = \int_{-\infty}^{o} x(t)\ S(t)\ dt \qquad (1)$$

where S(t) is called the sampling function of the instrument, and is usually expressible as

$$S(t) = R(t)\ W(t) \qquad (2)$$

where R(t) is the reference waveform which defines the sampling time windows and repeats periodically in an infinite time interval, and W(t) is the weighting function applicable to the measuring scheme. W(t) represents the relative contribution to the output measurement of the sampling window at a time t prior to the end of the last sampled signal period. For a simple digital stacker working for n transmitted periods

$$W(t) = 1 \quad \text{when} \quad o < t < T, \quad \text{otherwise} = o \qquad (3)$$

For an idealized RC averager with time constant Tc

$$W(t) = \exp. - t/Tc,\ t > o;\ = o,\ t < o \qquad (4)$$

Figure 3 shows the form of R(t) for some of the channels of the UTEM system.

It is easy to write down the output of the measuring system for a signal input s(t) which is periodic and synchronized with the reference waveform. It is necessary only to do direct integration of (1). If the average value of s(t) in the time window of width Δ_n centered at delay time t_n in the positive half cycle is $\bar{s}(t_n)$, then A^n is

$$A_s^n = 2f_o\Delta_n \bar{s}(t_n) \int_{-\infty}^{o} W(t)dt \qquad (5)$$

In the case of simple stacking for N waveform periods, the integral is just N/f_o , giving

$$A_s^n = 2N\Delta_n\bar{s}(t_n) \qquad (6)$$

When the instrument output is to be calibrated so that a square wave input signal of unit amplitude gives the same output in each measuring channel (which is the case for almost all EM systems except the Crone PEM instrument), the required measurement is the normalized quantity A_s^n/N^n where

$$N^n = 2f_o\Delta_n \int_{-\infty}^{o} W(t)\ dt \qquad (7)$$

NOISE REDUCTION

It is more complicated to estimate the output of the measuring system for a random noise input n(t). Each measurement of n(t) will lead to a different value of A_n, even if the statistical properties of n(t) are unchanged. Conceptually, what is wanted is the variance of A_n when inputs are drawn from a statistical ensemble of noise signals having a given power spectrum $|\bar{n}(\omega)|^2$.

Rigourous derivation of the statistical properties of the output of an arbitrary linear signal averager is lengthy, and is therefore left to Appendix 1. A key result is that the output variance is a property which is localizable in the frequency domain; that is, it depends only on the power spectrum of the noise input. However, in some continuous averagers designed to detect periodic signals, the statistical properties of the output are non-stationary; that is, they vary systematically during each signal period. Stationarity applies only to the period averaged output. However, for simple discrete measuring schemes such as are described by (1) and where the output measurement is at most updated once per signal period or at the end of the stackup period, the variance σ^2 of A_n is stationary and given by*

$$\sigma_n^2 = \int_{-\infty}^{\infty} \bar{K}^2(\omega)\,|\bar{n}(\omega)|^2\,d\omega \qquad (8)$$

where $\bar{K}^2(\omega) = \hat{S}(\omega)\,\hat{S}^*(\omega)$

and where $\hat{S}(\omega)$ is the Fourier transform of the sampling function S(t). $\bar{K}(\omega)$ is named the noise spectral sensitivity of the measuring

* Refer to Appendix 2 for a complete Table of the symbols used in this paper.

system; defined as the first power of $\bar{K}$ because it is σ which ultimately is wanted.

Equation (8) can be justified by a simple heuristic argument. We may consider successive noise measurements A_n to be discrete values of a conceptual, continuous, output signal $A_n(t)$. The conceptual continuous output is, by extension of (1)

$$A_n(t) = \int_{-\infty}^{t} n(\theta)\ S(t-\theta)\ d\theta \qquad (9)$$

which is a convolution $A_n(t) = n(t) * S(t)$. Real measurements can, at best, be extracted only at times t which are at the end of reference signal periods.

Equation (9) has the immediate consequence that if n(t) is a stationary random noise with power spectrum $|\bar{n}(\omega)|^2$, the power spectrum of the conceptual, continuous, output signal $A_n(t)$ is

$$|\bar{A}_n(\omega)|^2 = \hat{S}(\omega)\ \hat{S}^*(\omega)\ |\ \bar{n}(\omega)|^2 \qquad (10)$$

Since a stationary random noise has no time correlation with the reference signal waveform, the actual measurements are just a random sample of values from $A_n(t)$ and their variance is just the <u>power</u> of $A_n(t)$, which by Parseval's theorem is the total power in the spectrum.

$$\sigma_n^2 = \langle A_n^2(t) \rangle = \int_{-\infty}^{+\infty} |\ \bar{A}_n(\omega)\ |^2\ d\omega \qquad (11)$$

$$= \int_{-\infty}^{+\infty} \bar{K}^2(\omega)\ |\ \bar{n}(\omega)\ |^2\ d\omega$$

The noise spectral sensitivity $\bar{K}(\omega)$ is easily calculated when S(t) is given by (2). Then

$$\bar{K}(\omega)^2 = |\hat{R}(\omega) * \hat{W}(\omega)|^2 \qquad (12)$$

where $\hat{R}(\omega)$ and $\hat{W}(\omega)$ are Fourier transforms of the reference signal and measurement weighting functions. Because R(t) is periodic, $\hat{R}(\omega)$ consists of a comb of delta functions. For channel n of UTEM

$$\hat{R}(\omega) = \sum_{m=1,3,5\cdots}^{\infty} \frac{2}{m\pi} \sin\left(\frac{m\pi}{2^{n+1}}\right) \delta(\omega - m\omega_o) \qquad (13)$$

$\omega_o = 2\pi f_o$, f_o = base frequency

For simple stacking or averaging, as described by (3) or (4)

$$|\hat{W}(\omega)| = \frac{\sin(\omega T)}{\omega T} \qquad \text{simple stacking, } T = \text{total stacking time} \qquad (14)$$

$$|\hat{W}(\omega)| = \frac{(1-\omega^2 T_c^2)^{\frac{1}{2}}}{1+\omega^2 T_c^2} \qquad \text{simple averaging, } Tc = \text{time constant} \qquad (15)$$

Since T(or Tc) is generally much larger than the signal base period, $|\hat{W}(\omega)|$ is generally a function that falls off in amplitude very rapidly from ω = o. Thus the nature of the noise spectral sensitivity $\bar{K}(\omega)$ is easy to discern. It is a comb of spectral lines (ω_m) located at odd harmonics of f_o; each line having its shape and width set by $|\hat{W}(\omega)|$ and its relative amplitude by $\hat{R}(\omega_m)$. Examples of this type of structure are shown in Figures 4, 5, 6, and 12, and the relative merits of various averaging schemes are discussed in the following sections.

Equations (12), (13) and (15) purport to express the noise sensitivity of a continuous averager, and are correct if the averager updates its output once per signal cycle when the sampling window is closed. The common RC window averager consists of a switch which executes the sampling window operation followed by a resistor R in series with a capacitor C. The input is a voltage applied to the switch, the output is the voltage on the capacitor (read by a device with very high input resistance). This circuit has a time constant RC when the switch is closed, and holds the voltage unchanged when the switch is open. If the switch is on for $2\Delta_n$ in each period of the signal, the apparent time constant is $RC/(2\Delta_n f_o)$. The difference between the response of this circuit and that of a discrete averager with a simple time constant of the same size can be significant, particularly for high frequency noise components. The variance of the switching averager's output for a stationary noise input is localizable in the frequency domain but is not constant because it varies with time throughout each measuring period. Specifically, it differs markedly while the switch is closed. However, the period averaged variance is a measure which is stationary and it has a spectral sensitivity $\overline{K}(\omega)$ which is calculated by Equations A-8 to A-11 of Appendix 1.

SENSITIVITY TO STATIONARY NOISE: EXAMPLES

The first example, shown in Fig. 4, is the spectral sensitivity (period averaged variance) of a simple, switching mode, continuous RC averager with an apparent time constant of $60/f_o$. Spectra are plotted for two different UTEM channels, and the general character described above is evident. The shape and width of all lines is the same, since all data are similarly averaged, but the relative amplitude of the lines depends on the sampling.

To show the effects of changing the amount of averaging or stacking, Fig. 5 shows the UTEM noise spectral sensitivity with a ditital stacker having uniform weighting, for two different stacking lengths: 10 cycles and 100 cycles. In this figure, the spectra are plotted with a linear amplitude scale, so that the concentration of signal acceptance into spectral lines is more readily apparent. With longer averaging, the lines become sharper and their shoulders more attenuated. Fig. 6 shows the same data as Fig. 5 but amplitude plotted logarithmically, as in Fig. 4, so that performance of the RC averager and the digital stacker may be compared. The main difference is the digital averager has a complex structure of sid-lobes between the peaks, whereas the continuous averager has a smooth shoulder structure.

As stated previously, the amplitude of the peaks depends on the sampling pattern R(t), and the variation between different UTEM channels can be seen in the foregoing examples. Channel 1 shows

a monotonic decrease inversely proportional to frequency from low harmonics to high. Higher numbered channels show an oscillatory structure.

Figures 5 and 6 show the spectral sensitivity only up to about 20 times the system base frequency. Typically, the bandwidth of EM systems extends to several decades times the base frequency, for example with the UTEM system, the pass band extends up to 45kHz, or 1500 times the usual base frequency of 30Hz. It is difficult to show the full "comb" function graphically over such bandwidth on a linear frequency plot.

To show the spectral sensitivity to uncorrelated noise at higher frequencies, Figures 7 and 8 plot the envelope of the sensitivity, i.e. only the amplitude of the acceptance peaks. All channels have a comb (series of equispaced lines) structure, and all except Ch. 1 and 10 have envelope notches within the instrument passband, for example the plot of Ch. 4 on Figure 4 should be compared with the beginning of the Ch. 4 envelope on Figure 7. Different channels give rise to quite different envelopes, with a regular character from one channel to the next as can be seen in the figure.

To gain a better understanding for how wideband noise will affect output after sampling, it is best to plot the noise acceptance as a spectral density with logarithmic amplitude and frequency scales. It is then desirable to consider line density as well as

line amplitude in summarizing the noise acceptance of the sampling channels. Figure 9 shows amplitude density (expressed) as the square root of sum of total power) in each fifth decade of frequency. The plot shows that the wide, long delay time channels admit primarily low frequency noise, while the narrow, early delay time channels have maximum acceptance at progressively higher frequencies. For example, Ch. 8 has its noise acceptance maximum at frequencies around $100f_o$. There is a clear high frequency limit, with a simple $1/\omega$ falloff to which all channels tend. The complicated structure seen in any individual channel reflects the wide spacing of the low order harmonics on this logarithmic frequency scale, as well as the notched structure of the sensitivity envelope.

On all the amplitude density plots we note that Ch. 10 appears to have a noise acceptance much less than Ch. 1. However we should also keep in mind that the window width of Ch. 10 is 512 times shorter than that of Ch. 1, and therefore the signal acceptance is also 512 times smaller (or 54dB down). It is generally true in the case of white noise and constant signal amplitude that the output signal/noise ratio for any channel with a small window width will always be worse than for one with a larger window width.

In the electronic implementation of an instrument, it is very difficult to achieve exact equality in processing the plus and minus half cycles. The resulting zero bias may be eliminated by interchanging processing paths in the receiver at regular intervals during stacking. The output is then a sum of several smaller

stacks, rather than one continuous stack. As will be discussed under pruning, this procedure has no effect on the spectral sensitivity for uncorrelated noise. However, if the instrument is off for a finite time during each interchange, the sensitivity to coherent noise may be altered.

PRUNING

Large amplitude transient noise such as local sferic activity or nearby powerline transients often occurs only occasionally on the time scale of a single measurement. Such noise is not stationary with respect to system averaging time, and it is easy to show that signal/noise ratios after stacking can be improved if during the time of the transient all input is totally rejected rather than added to the stack. However, the difficulty with any data rejection scheme is the possiblility of introducing bias into the final result.

Optimal noise spike rejection during stacking depends on the precise nature of the spikes. A typical sferic transient was shown in Figure 2, and it can be noted that its duration is much less than the time for one cycle (33ms) of a system operating at a base frequency of 30Hz. Powerline transients have quite a different character.They may often have a less abrupt onset than a sferic spike, and last for a much longer time. The simplest criterion for identifying a transient is to have an adjustable amplitude threshold which triggers the rejection mechanism. The threshold is best set according

to experience at the survey site. Typical useful thresholds set according to experience with the UTEM system, vary from 30% above "steady" input level for sferic noise, to 200% above "steady" input level if powerline transients are the major source of noise. "Steady" is defined as a threshold that causes triggering in more than about half the waveform periods.

Some sferic and powerline transients have a precursor or gradual onset. To reject this part of the non-stationary noise, it is necessary to have a two stage process. In the UTEM system, data undergoes A/D conversion, and the digital output remains in temporary storage for one complete cycle before being added to the main stack. If the threshold has been exceeded at any time during a half cycle, then both the current and the previous half cycle of data are rejected. Rejection then continues for a time which is dependent on the amplitude and duration of the overload, and includes at least one complete cycle after the threshold is no longer exceeded to prevent any "tail" of the transient from biasing the stacked data. It is essential to reject equal numbers of plus and minus cycles to avoid introducing a zero bias.

Some instruments merely clip spikes at the threshold level, leading to much poorer overall signal/noise ratios than complete rejection. This may also create low frequency noise components from a strong but purely high frequency event, and introduce bias if the noise events have non-random polarity. In continuously averaging instruments, it is common to set the exponential averaging

time low enough that the instrument operator can make a selective long term average of those short term averages that seem uncontaminated by transients.

Since pruning is neither a linear nor a stationary process, in that its effect is strongly data and threshold dependent, the quantification of its effects is complex and will not be discussed here. Experience has shown that it can greatly improve signal/noise of data, however it is also found that in some cases it can reduce precision.

WEIGHTED STACKING

It is well known (e.g. Kanasewich, 1975) that power spectral estimates based on Fourier transformation of a time series are quite heavily dependent on the weighting factors used. Most spectral estimators use tapered windows (e.g. Hanning, Bartlett, Parzen windows) to minimize the width of acceptance sidelobes and obtain an improved estimate of the power at one frequency. The same techniques can be applied to noise rejection. However for simplicity only linearly tapered stacking will be discussed here.

Figure 10 shows schematically how such linearly tapered stacking can be applied to input data. Figure 11 shows a plot of the amplitude of the function $\hat{W}(\omega)$ which is the Fourier transform of the stacking window. To obtain the noise rejection spectrum of this method of stacking, $|\hat{W}(\omega)|$ above can be convolved with the appropriate channel

amplitude comb functions given in equation (4). From the figure it is clear that linearly tapered stacking has a wider central acceptance peak than simple stacking for equal time, but that the side lobe amplitude is much reduced. Figure 12 presents the spectral gain in the same format as that on Figure 6 for direct comparison of simple and tapered stacking. Quite clear is the greater breadth and depth of the acceptance lows.

If the noise is "white", it is easy to show that normal stacking for an equal time will result in a better signal/noise ratio than tapered stacking, for the example in Figure 10 an effective averaging time of tapered stacking is 12/16 of simple stacking. However, reduction of sidelobes may be very advantageous if strong nearly monochromatic noise is present. For example, at a frequency 20/T away from a main peak, the tapered window shown in Figure 12 has an acceptance power about 20dB less than the simple window, and if moderately narrow band noise lies in this vicinity, tapered stacking will do a much better job of rejection. In practice, the harmonics of steady powerline noise are usually suited to rejection by a tapered window, and the procedure is particularly suited to rejecting signal from other geophysical surveys in the area.

The effect of tapering can be understood quite simply in that it reduces the dependance of the stack on exact starting and finishing points. It has a simple physical analogue: if the output from some continuing averaging process is being monitored on a meter, and the noise is such as to produce a beat about a fixed value,

linearly tapered stacking will substantially attenuate the beating, because its effect is to average the output of the simple averaging process over the taper interval. This is easily demonstrated by noting that a linearly tapered window may be thought of as the convolution of an abruptly terminated sampling window with a window equal to the taper length.

It is possible to apply both pruning and tapered stacking to the same data set, but because pruning is a switching operator, it reintroduces the power sidelobes that tapered averaging is designed to remove, and may so lead to a bias in the output. In cases where both strong transients and narrowband noise are present, another stacking scheme has been devised. If the sampler is switched randomly on and off as shown in Figure 10, the system coherency with respect to narrowband noise is removed (except for noise exactly at odd harmonics of the base frequency f_0). Pruning is obviously allowed to take priority over the random shut offs. To maximize the signal, the actual ON time in any implementation much exceeds the stacking OFF time. To avoid zero bias and sensitivity to even harmonics of the transmitter base frequency, it is necessary that equal number of plus and minus cycles be stacked.

Unfortunately the analytical treatment of such processes is much more difficult. Randomized sampling and pruning are both processes whose properties are not localisable in the frequency domain. The effect of a randomized averaging process in practice is to avoid occasional large measurement errors caused by fortuitous

coherence of strong artificial signals. These would often show as "single point" anomalies scattered every few points on a profile, or as a sudden jump in the averager output in a long stack. The strategy of randomized averaging is to tolerate greater short term fluctuations in order to eliminate large occasional errors.

PRE-EMPHASIS/DECONVOLUTION

Analogue bandpass filtering techniques are commonly used in all EM systems. For example, if system design characteristics require a linear bandwidth for signal only up to a certain limit, a high cut filter eliminates noise above this frequency. It is also possible to redistribute the power in the transmitted spectrum and compensate in the receiver by filtering of the signal and noise. Such techniques, known as pre-emphasis, prewhitening, deconvolution, etc. are well known in many fields such as audio engineering. The main obstacle to their use in EM is the necessary preservation of phase characteristics in filters.

In a linear EM system consisting of a transmitter and receiver, the noise free output $V_o(\omega)$ of the receiver can be related to the transmitter current $I_o(\omega)$ through a transfer impedance $Z(\omega)$ in:

$$V_o(\omega) = Z(\omega) I_o(\omega).$$

If noise $N(\omega)$ is present then we measure:

$$V_m(\omega) = V_o(\omega) + N(\omega).$$

If we have a filter $A(\omega)$ with a realizable inverse $A^{-1}(\omega)$ and we

filter $I_0(\omega)$ by $A(\omega)$, the transmitter output is now:

$$I_1(\omega) = A(\omega)I_0(\omega)$$

Inserting the filter with response $A^{-1}(\omega)$ in the receiver we obtain a new measurement $V_n(\omega)$ in:

$$V_n(\omega) = A^{-1}(\omega)\left[\underline{Z}(\omega)A(\omega)I_0(\omega) + N(\omega)\right]$$
$$= V_0(\omega) + N(\omega)A^{-1}(\omega).$$

The new output has signal $V_0(\omega)$ unchanged while the noise has been filtered by $A^{-1}(\omega)$. A trivial example of such filters would be to increase the transmitter current by a constant $A(\omega) = C$ say, in which case the inverse filter $A^{-1}(\omega) = 1/C$ in the receiver will give rise to noise reduced by a factor of C. In reality, pre-emphasis filtering is a practical procedure only when the pre-emphasis gain can be applied within the capabilities of the existing transmitter unit. In the case of UTEM, strong high frequency pre-emphasis requires only a marginal increase in the peak transmitter current. The modified waveform can therefore be transmitted with only a marginal reduction in low frequency current.

For real time operation of complex filters, the major constraint is realizability. There are only a few classes of filters whose inverses can be exactly realized. Figure 13 shows the amplitude response of one pair of realizable filters, with a high:low frequency gain of 10:1, and time constant τ. The gain product of both filters at any frequency is unity. Pre-emphasis/deconvolution has wideband effects, and as a result is best understood by looking at the response of the averaged noise sensitivity of each time channel. Figure 14 shows the sensitivity of a system with pre-emphasis, using a filter

with 10:1 high:low frequency gain and time constant $.003/f_o$. The effect of the filter in reducing noise in the high frequency part of the spectrum is evident. Making a comparison with Figure 9 shows that this particular example of prewhitening has little effect at low frequencies, but the high frequency noise sensitivity is reduced 20dB.

Optimization of pre-emphasis is a complex process for any EM system, as the actual noise spectrum is far from constant, as discussed earlier. As well, it is necessary to take account of achievable voltage or current limits when redistributing the power within the transmitter waveform. With the UTEM system, signal/noise ratio improvements of 3:1 on long delay time channels and 6:1 on short delay time channels have been achieved routinely without any increase in peak transmitter voltage or power, for the same stacking time. Since stacking generally improves signal/noise with a $\sqrt{T}$ factor, use of pre-emphasis corresponds to the increase in precision that would be obtained by stacking 9 to 36 times longer! An improvement of this order required implementation of filters with multiple rather than single time constants to more closely match the transmitted spectrum to the noise spectrum.

The optimization process for the UTEM system was done empirically by trial and error over a period of two years, but the trials were inspired by the noise spectrum. Although optimization can be formalized, the conditions for this are that the noise spectrum is known and constant, the relative precision sought on the different

channels be stated, and a norm of transmitter output be fixed. It was found more effective to compare a number of different filters with an unfiltered case in a variety of noise conditions and select the one with the best average performance. The limiting constraint for the transmitter is the peak output voltage since the load is inductive and the pre-emphasis is at high frequencies. In fact, the "optimum" waveform determined has a slightly lower peak current and average signal power than the pure triangular waveform. For moderate levels of pre-emphasis, the choice is simple since the precision of both early and late channels improve in almost all noise conditions. The level of pre-emphasis and the poles of the filters were changed until the improvement on late channels was maximum for average sferic noise. This also corresponds to the case where the precision for predominent power line noise is degraded by no more than 15% on the late channels. The end result in the presence of distant sferic noise is very similar to ideal prewhitening where the precision varies by factors of $\sqrt{2}$ between adjacent channels (because the channel widths vary by 2) except for the channels narrower than 240μs.

CONCLUSIONS

Even with the constraints of system portability and cost imposed on practical EM prospecting instruments, it is now possible to tailor the type of real-time signal processing to the local noise characteristics to achieve significant signal/noise improvement. A brief summary of how the techniques discussed in this paper have worked out in practice in application to the UTEM system is presented in Table 1. It shows the advantages which may sometimes be gained and also cautions against indiscriminate application.

TABLE OF PRACTICAL APPLICATION TO UTEM SYSTEM

STACKING for time T

Noise type	Effect: At best	Effect: At worst
Stationary broadband	$\sqrt{T}$ x better	$\sqrt{T}$ x better
Narrowband	T x better coherent noise away from acceptance peak	no improvement noise at odd harmonic of f_0 e.g. instrumenta

50% TAPERED STACK compared to SIMPLE STACK of equal time

Noise type	At best	At worst
Stationary broadband	13% worse	13% worse
Narrowband noise away from acceptance peak	>100 x better	13% worse
"Typical powerline"	x2 or x3 better*	x2 or x3 worse* if pruning allowed
Interference from other geophysical system	20 x better	3 x better

PRUNING compared to NO PRUNING

Noise type	At best	At worst
Stationary broadband	no effect	decreases effective averaging time T and eliminates benefits of tapering
Occasional transient	many x better depending on relative amplitude/frequency of spikes	x2 worse* if threshold set too close to "steady" limit
Narrowband	no effect	reduces xT improvement with stacking time to a x$\sqrt{T}$ factor

CLIPPING (not used in UTEM)

Similar to pruning, but somewhat less effective, as precursor/ leading edge of transient is not rejected, and will usually introduce undesirable bias.

TABLE OF APPLICATION TO UTEM SYSTEM CONTINUED

RANDOMIZED STACKING compared to SIMPLE STACKING WITH PRUNING

(20% off time, distributed in ½ to 3½ cycle breaks)

Noise type	At best	At worst
White	10% worse	10% worse
narrowband	x10 better	10% worse
powerline with or without transients	x1.5 to x2 better*	10% worse

PREWHITENING compared to NO PREWHITENING
(UTEM Level 2 implementation)

Noise type	At best	At worst
Typical sferic	x6 better# at early delay times	x3 better# at late delay times

* Implementation dependent, based on qualitative observation over several years in the field

Based on statistical data collected at Milton, Ontario

ACKNOWLEDGEMENTS

This paper is in part a review of results obtained during the course of other research during about a decade. Support for the work thus came from various sources at different times. Initial support was through the National Research Council (now NSERC) of Canada for work by YL, GFW. Further developments by JCM, YL were partially supported by the Ontario Geological Survey through an ETDF grant to Lamontagne Geophysics Ltd. JCM acknowledges NSERC support through an Industrial Research Fellowship. Computing expenses were met through an NSERC grant to GFW. We thank Khader Khan for some of the drafting.

REFERENCES

Blanc-Lapierre, A. and Fortet, R., 1953, Théorie des fonctions aléatoires, Paris: Masson et Cie. Editeurs.

Gamble, T.D., Goubau, W.M., and Clarke, J., 1979, Error analysis for remote reference magnetotellurics: Geophysics v.44, no. 5, p. 959-968.

Kanasewich, E.R., 1975, Time series analysis in geophysics: Edmonton, The University of Alberta Press.

Koziar, A., 1976, Applications of audio frequency magnetotellurics to permafrost, crystal sounding, and mineral exploration. PhD thesis, Department of Physics, University of Toronto.

Lamontagne, Y., 1975, Applications of wideband, time-domain EM measurements in mineral exploration. PhD thesis, Department of Physics, University of Toronto, published as Research in Applied Geophysics no. 7, Geophysics Laboratory, Department of Physics, University of Toronto.

Strangway, D.W., Swift, C.M., and Hohmer, J.R., 1973, The application of audio-frequency magnetotellurics (AMT) to mineral exploration: Geophysics v. 38, no. 6, p. 1159-1175.

Watt, A.D., 1967, VLF radio engineering, Oxford, Pergamon Press.

LIST OF FIGURE CAPTIONS

Fig. 1: Components in the electromagnetic noise spectrum (schematic), plus detail on one sferic pulse. The amplitude and shape shown is based on typical published vales, and will vary with location, time of day/year etc.

Fig. 2: The two conceptual stages of synchronous detection; stacking/averaging and cross-correlation. In a fully digital system, the operations are usually performed in the order described here. In an analogue system, the correlation is done cycle-by-cycle and the result is averaged.

Fig. 3: UTEM binary sample windows shown for one complete cycle of a periodic waveform.

Fig. 4: Spectral sensitivity to uncorrelated noise as a function of frequency, for a continuous, exponentially weighted averager. The sensitivity spectra of two sampling channels are shown. The time constant of the exponential averager is 60 waveform periods.

Fig. 5: Spectral sensitivity to uncorrelated noise as a function of frequency for a uniformly weighted stacker. Sensitivity spectra for two sampling channels are given, plotted on linear scales. Data for stacks of 10 and 100 cycles are shown. They correspond to 0.33s and 3.3s averaging times at a waveform period of 30Hz. All functions are plotted at the same scale.

Fig. 6: Spectral sensitivity from fig. 5, plotted in decibels for the Ch 1 data.

Fig. 7: Envelope of the spectral sensitivity in dB for later time channels of the binary sampling scheme. The actual sensitivity has a comb-like structure; the envelope describes the height of the teeth and is determined by the sampling scheme within a period. The structure of the lines depends on the length and weighting scheme of the averaging.

Fig. 8: Envelope of the spectral sensitivity in dB for earlier time channels. (Continuation of Fig. 7).

Fig. 9: Noise sensitivity of UTEM channels, shown as averaged amplitude density (root sum power per fifth decade) vs frequency.

Fig. 10: Different averaging methods. Normal stacking accepts data continuously. Tapered stacking accepts data with a weighting dependent on time; the example shown here is linearly tapered. To ensure that no zero bias is introduced, randomized stacking must contain equal numbers of positive and negative half cycles.

Fig. 11: Absolute amplitude of the Fourier transform of normal and linearly tapered stacking windows. These functions, when convolved with an individual channel comb function will give the spectral gain for an individual channel and stacking type, as shown in Figures 6 or 12. Note that the linearly tapered stack has a wider main sensitivity peak, but much reduced sidelobe amplitude.

Fig. 12: Sensitivity vs frequency for data averaged with a linearly tapered stack. This plot can be directly compared with Figure 6 which is for simple stacking.

Fig. 13: Amplitude spectra for a pre-emphasis filter and its realizable inverse. The example if for a low:high frequency gain factor of 10 and time constant τ. To have a total gain of unity, each filter has a different amplitude scale.

Fig. 14: Noise sensitivity of UTEM channels showing the effects of pre-emphasis/deconvolution. The deconvolution filter has a low:high gain ratio of 10:1 and a time constant $0.003/f_o$. Compare with Fig. 9.

SYNCHRONOUS DETECTION OF PERIODIC SIGNALS

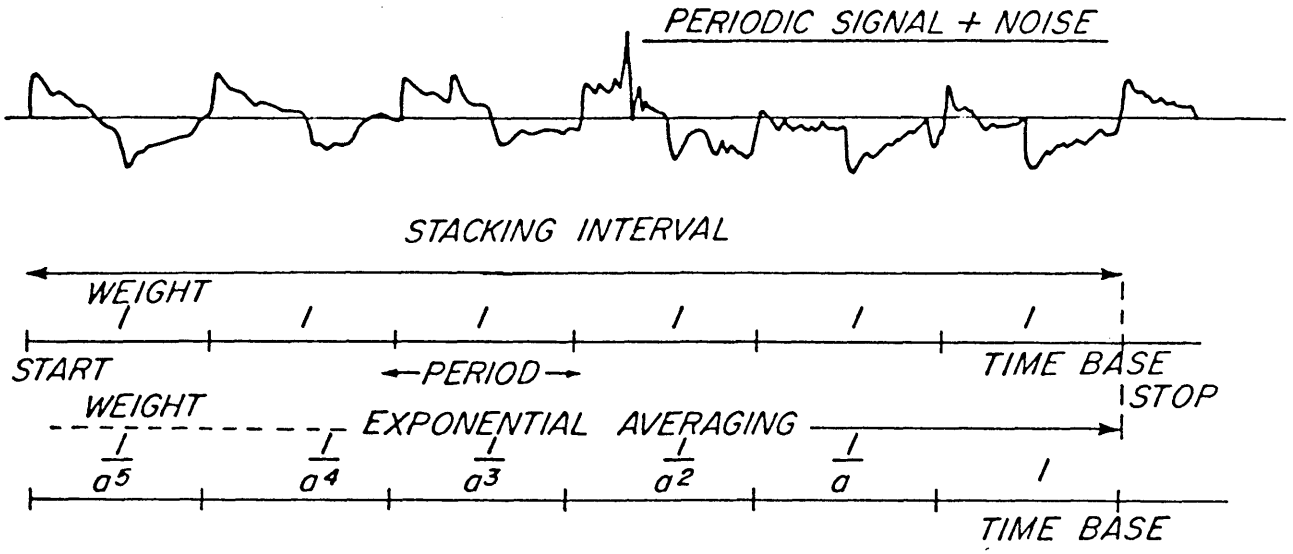

(A) SIGNAL ENHANCEMENT BY STACKING OR AVERAGING

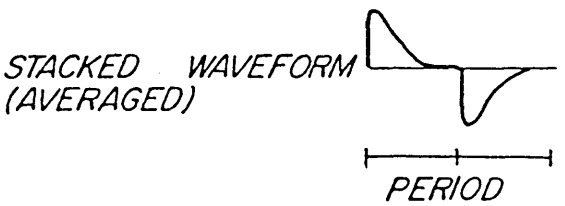

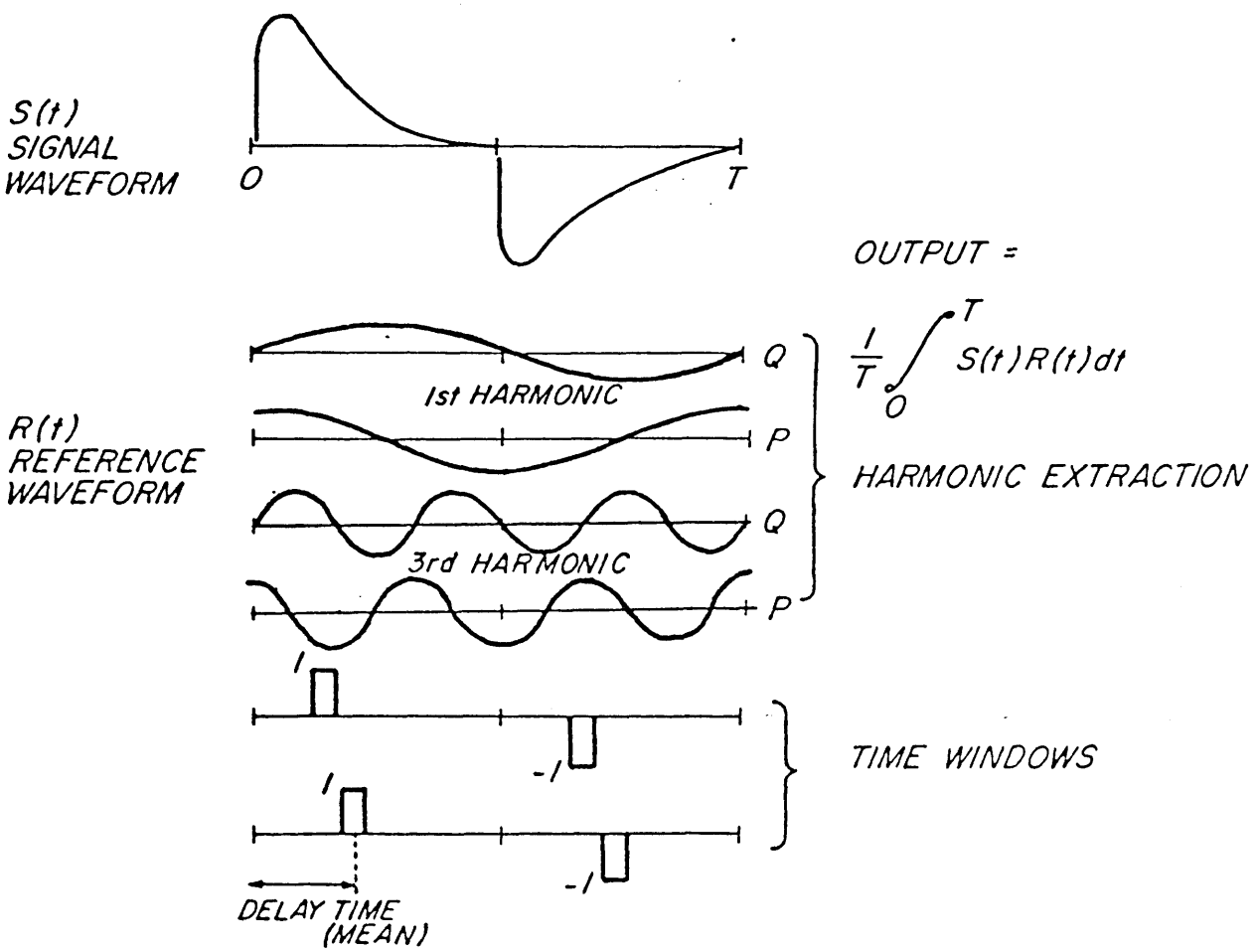

(B) SIGNAL MEASUREMENT BY CROSS-CORRELATION

ELECTROMAGNETIC NOISE

(COMPONENTS IN THE SPECTRUM)

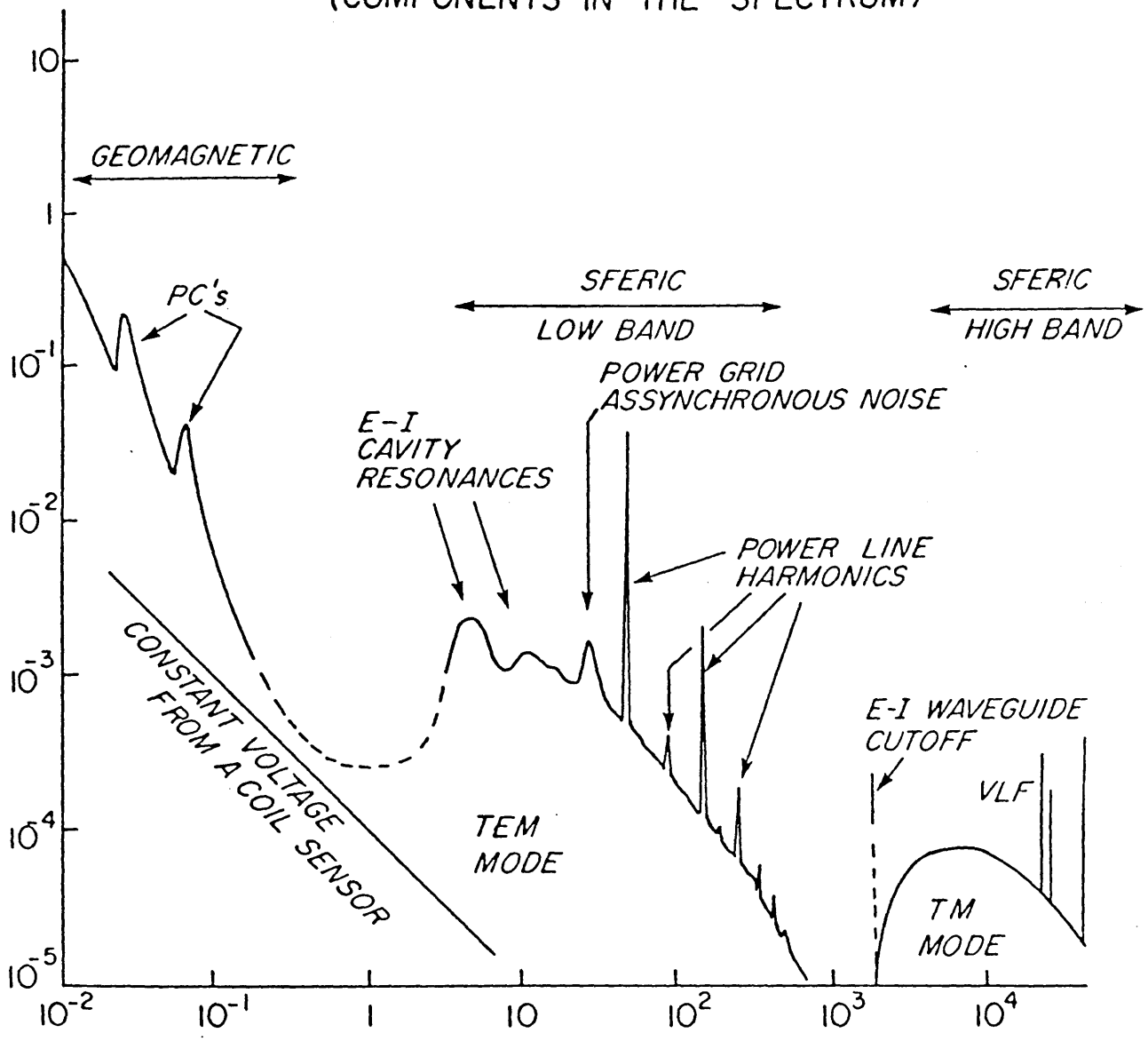

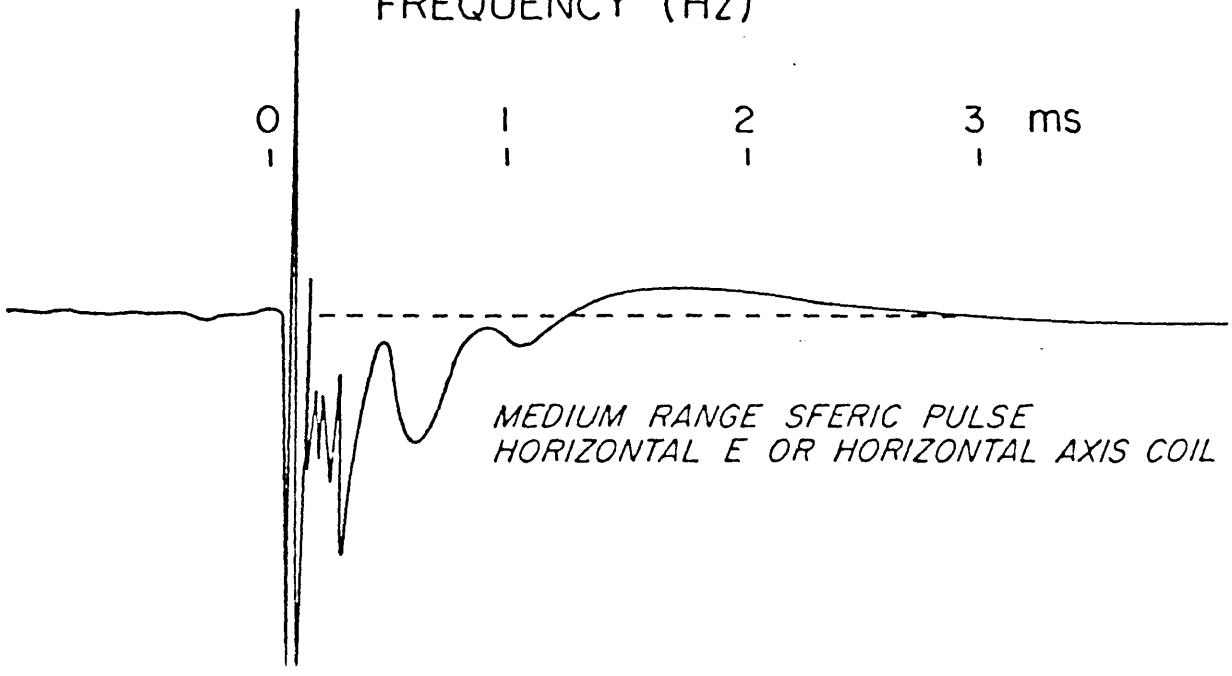

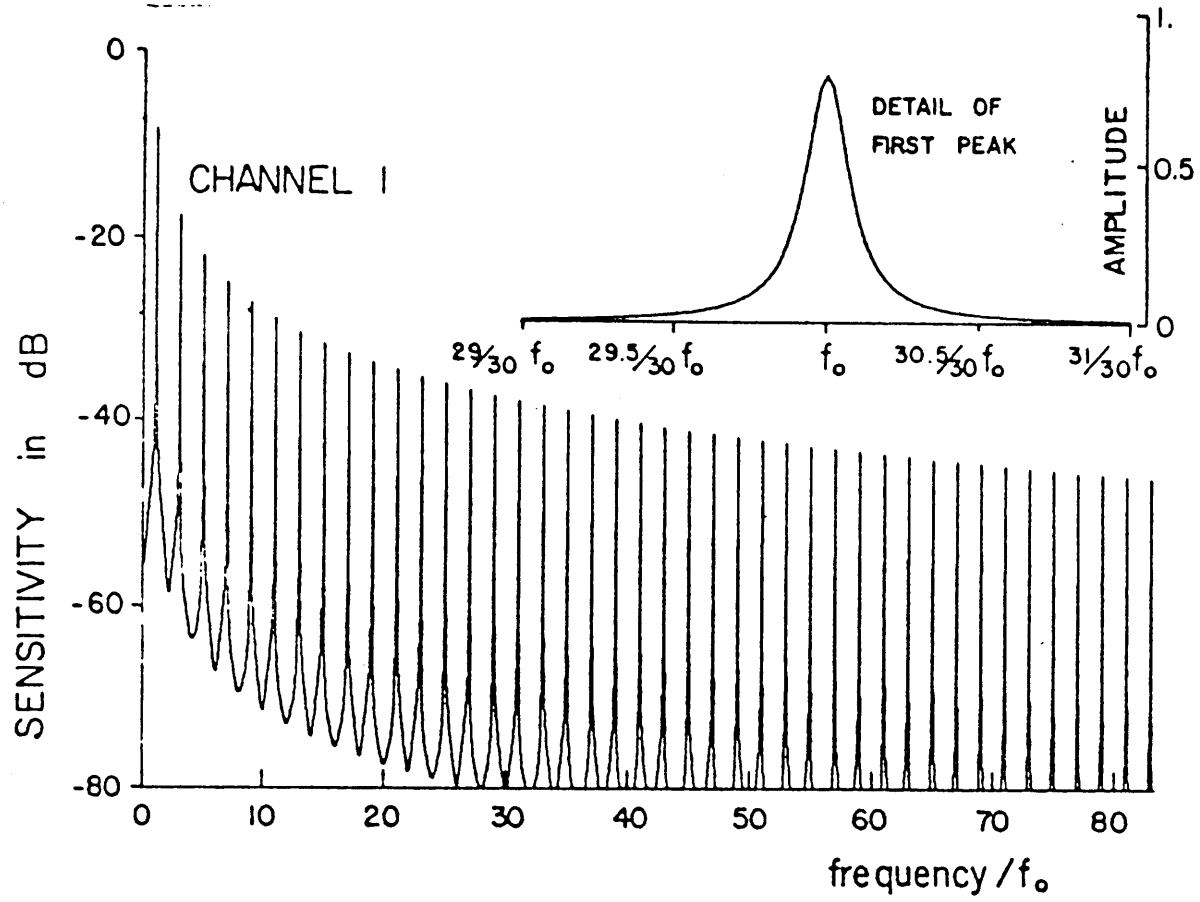
CHANNEL 1
DETAIL OF FIRST PEAK
AMPLITUDE
1.
0.5
0
29/30 f₀
29.5/30 f₀
f₀
30.5/30 f₀
31/30 f₀
SENSITIVITY in dB
0
-20
-40
-60
-80
0
10
20
30
40
50
60
70
80
frequency / f₀

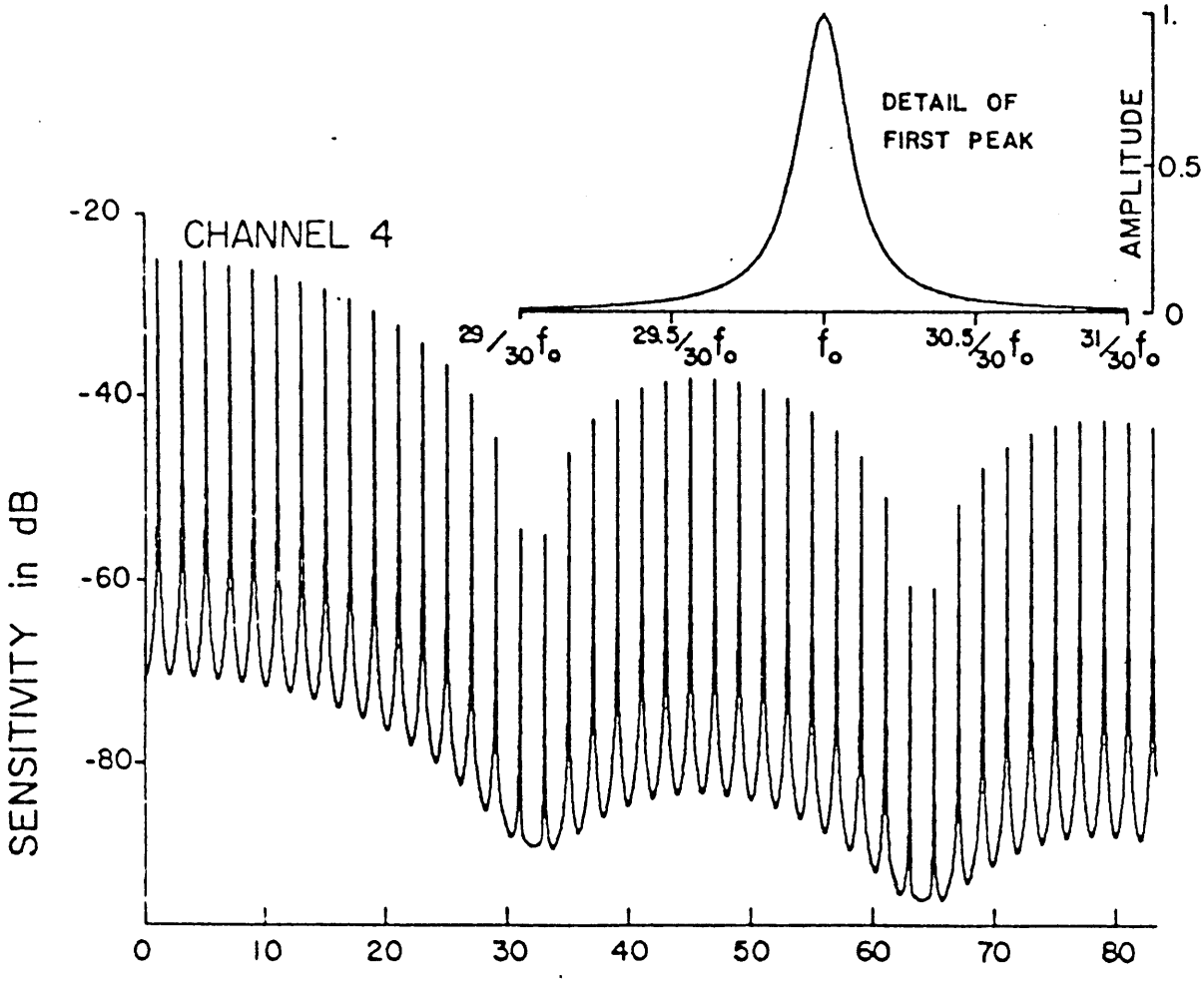
CHANNEL 4
DETAIL OF FIRST PEAK
AMPLITUDE
1.
0.5
0
29/30 f₀
29.5/30 f₀
f₀
30.5/30 f₀
31/30 f₀
SENSITIVITY in dB
-20
-40
-60
-80
0
10
20
30
40
50
60
70
80

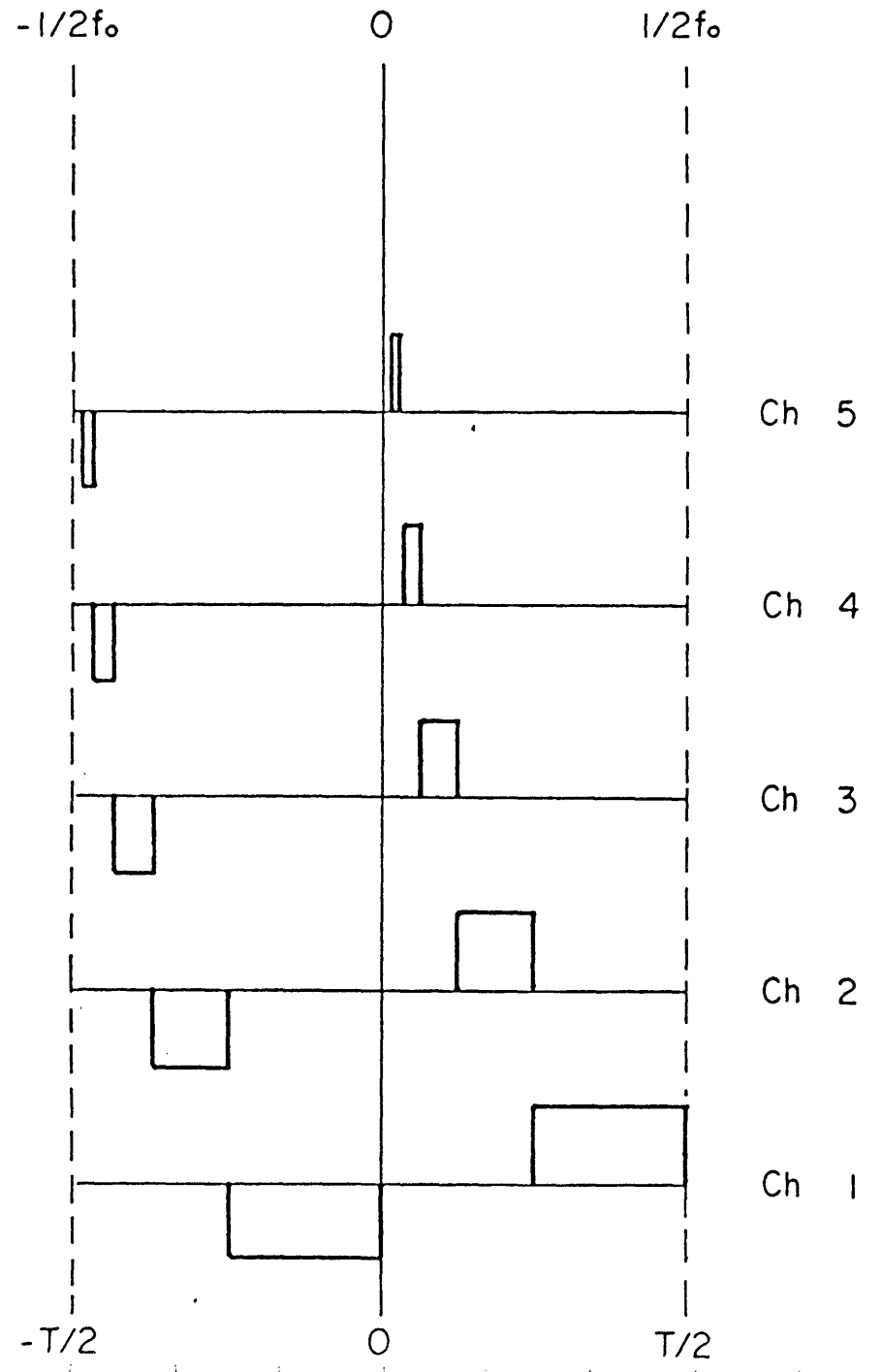

BINARY SAMPLE WINDOWS

FOR CHANNEL n

WINDOW FROM : $T/2^{n+1}$

TO : $T/2^{n}$

MEAN DELAY : $3T/2^{n+2}$

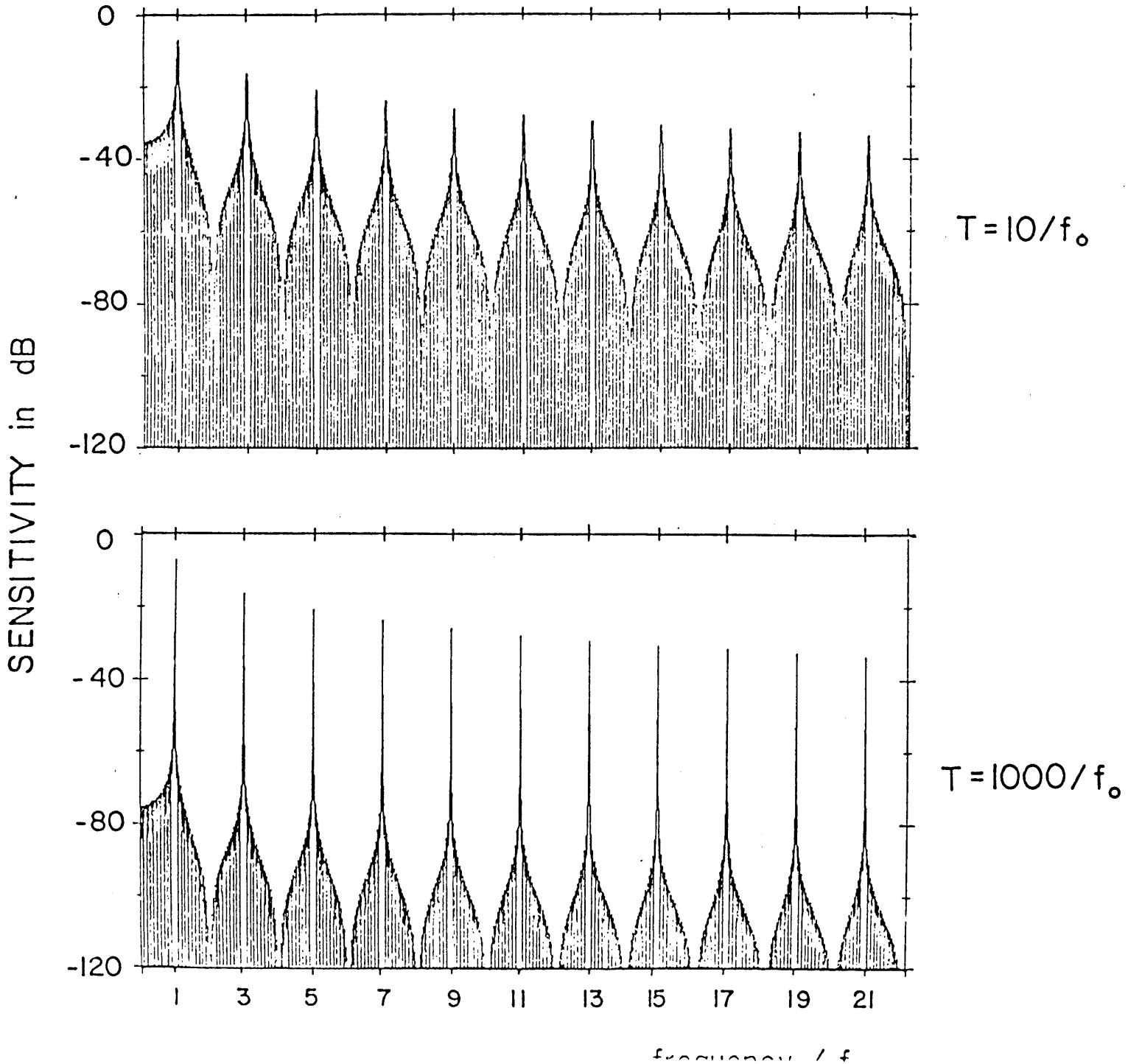
0
-40
-80
-120
SENSITIVITY in dB
T = 10/f₀
0
-40
-80
-120
T = 1000/f₀
1
3
5
7
9
11
13
15
17
19
21

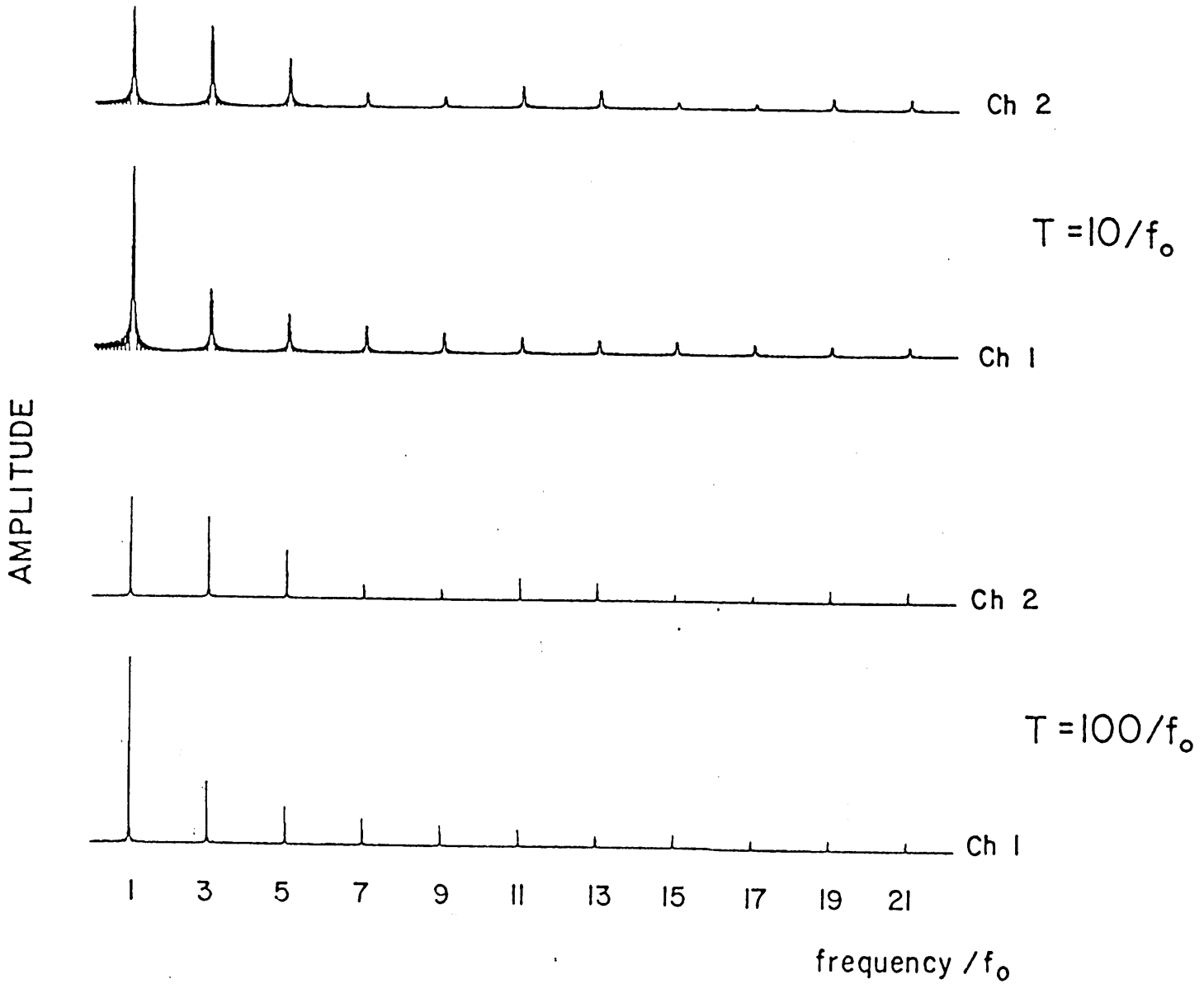
Ch 2
T = 10/f₀
Ch 1
AMPLITUDE
Ch 2
T = 100/f₀
Ch 1
1 3 5 7 9 11 13 15 17 19 21
frequency / f₀

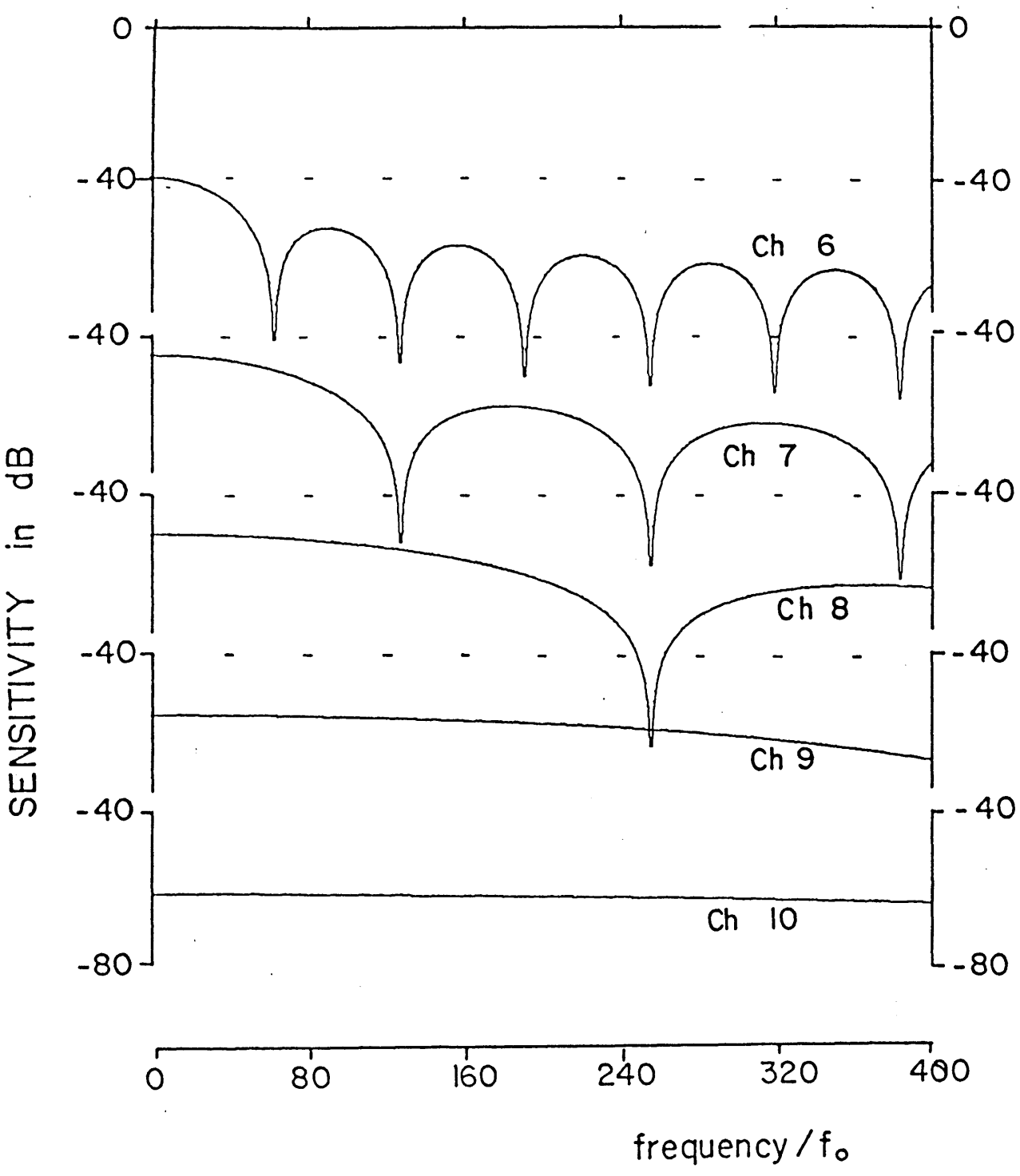
0
-40
-40
-40
-40
-80
0
-40
-40
-40
-40
-80
Ch 6
Ch 7
Ch 8
Ch 9
Ch 10
SENSITIVITY in dB
0
80
160
240
320
400
frequency / f_o

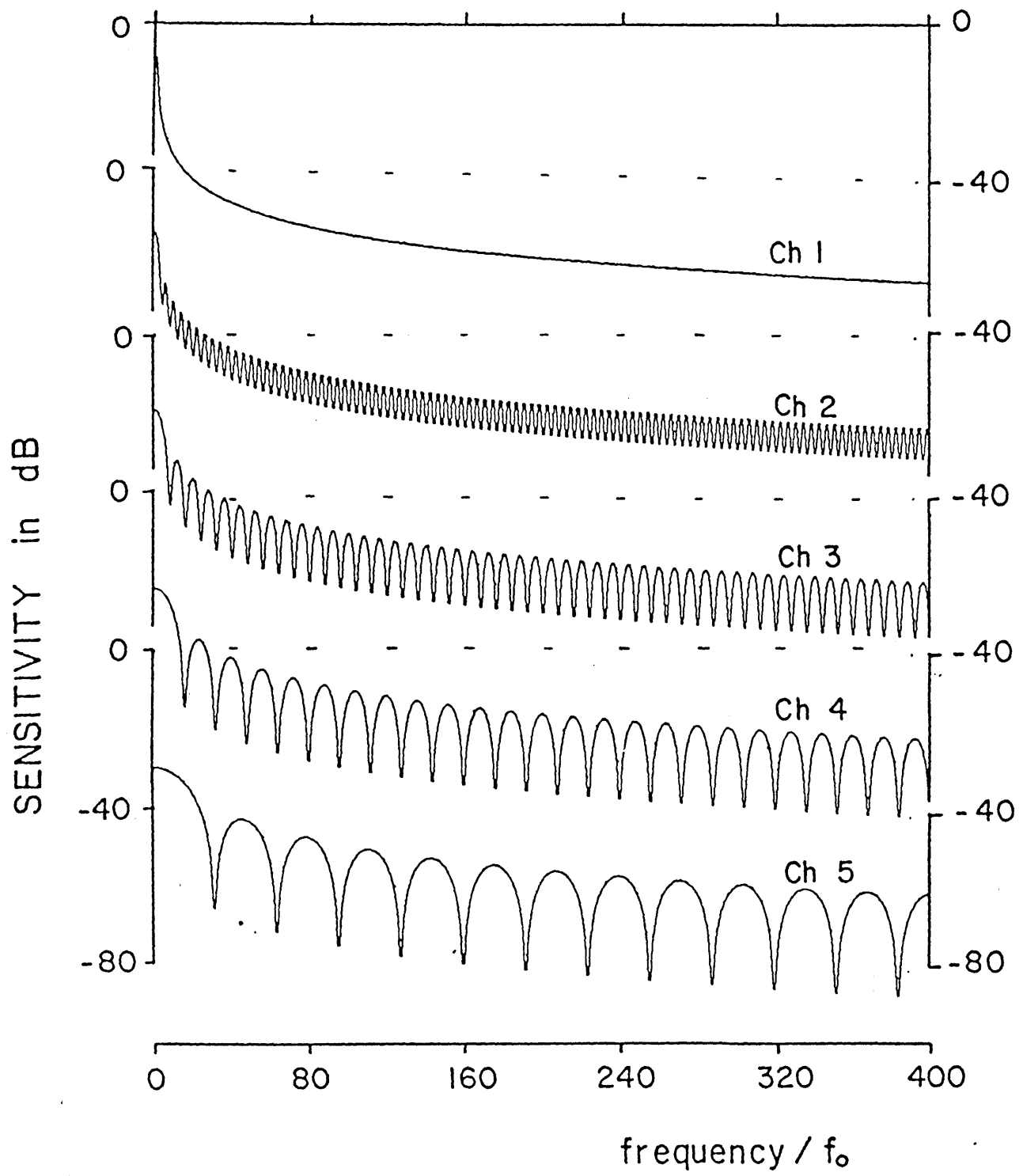
SENSITIVITY in dB
0
0
0
0
0
-40
-80
0
-40
-40
-40
-40
-40
-80
Ch 1
Ch 2
Ch 3
Ch 4
Ch 5
0
80
160
240
320
400
frequency / f_o

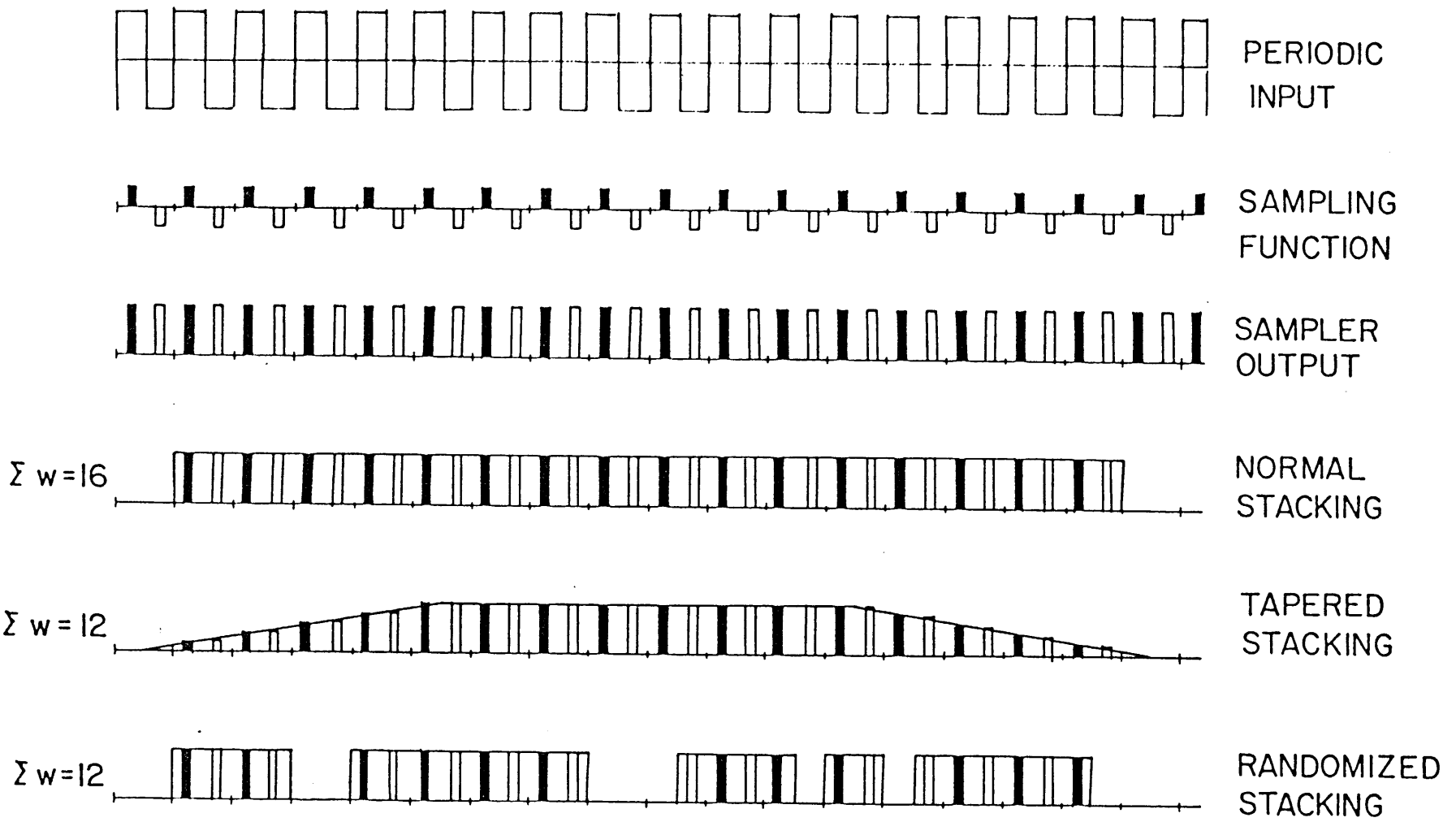
PERIODIC INPUT
SAMPLING FUNCTION
SAMPLER OUTPUT
Σ w=16
NORMAL STACKING
Σ w=12
TAPERED STACKING
Σ w=12
RANDOMIZED STACKING

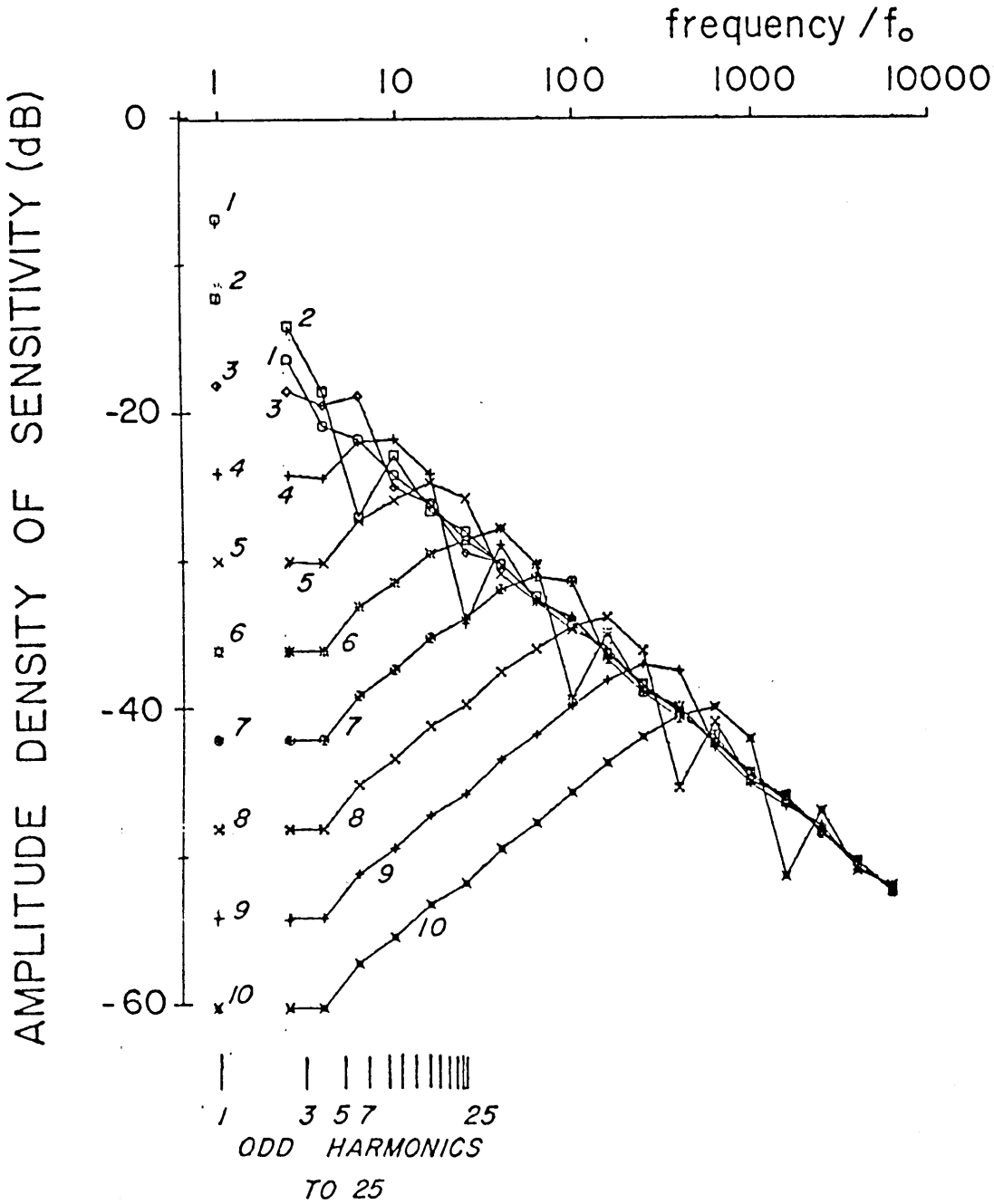
frequency / f_o
1
10
100
1000
10000
0
-20
-40
-60
AMPLITUDE DENSITY OF SENSITIVITY (dB)
1
2
3
4
5
6
7
8
9
10
1 3 5 7 25
ODD HARMONICS
TO 25

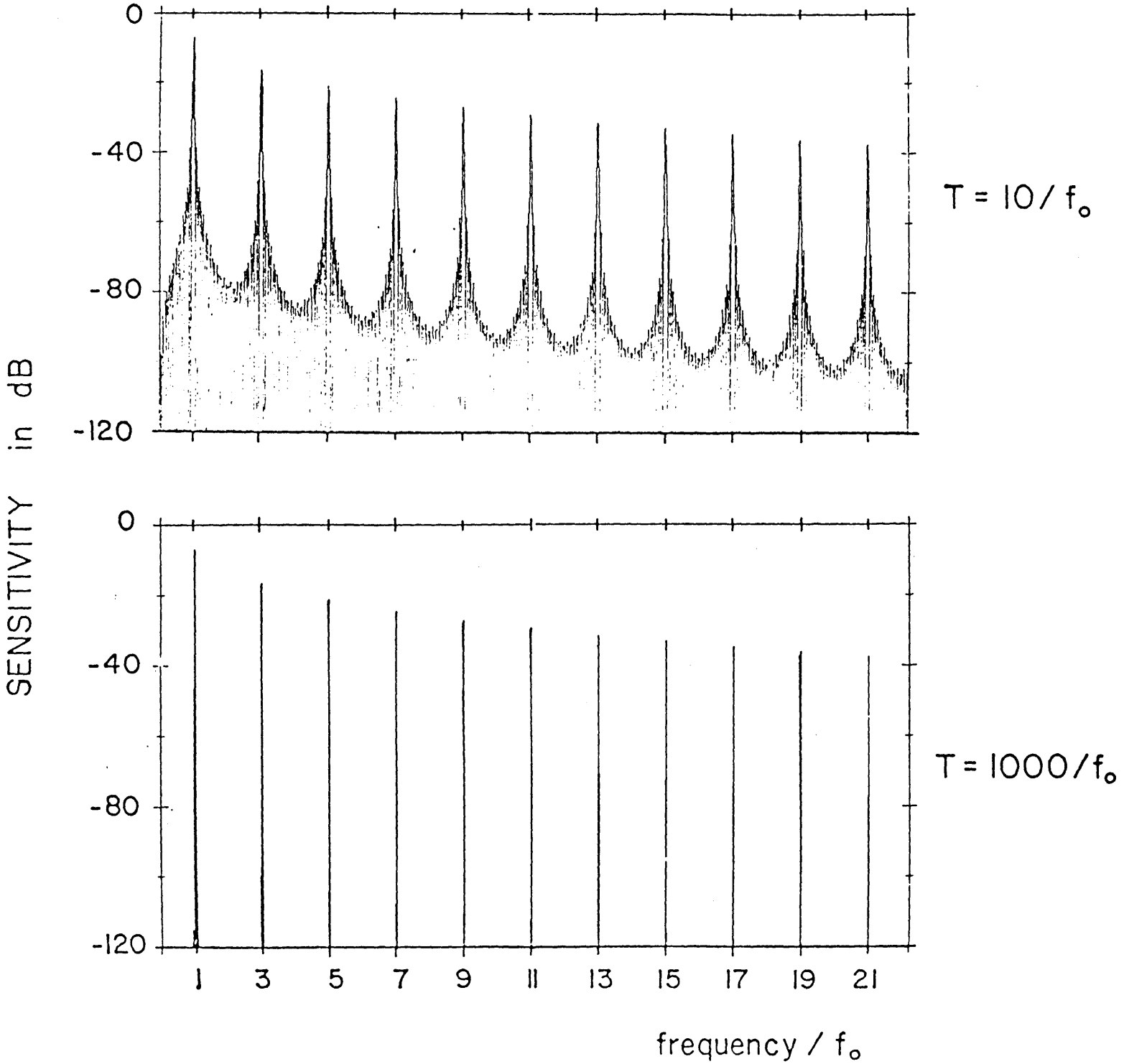
0
-40
-80
-120
SENSITIVITY in dB
T = 10/ f₀
0
-40
-80
-120
T = 1000/f₀
1
3
5
7
9
11
13
15
17
19
21
frequency / f₀

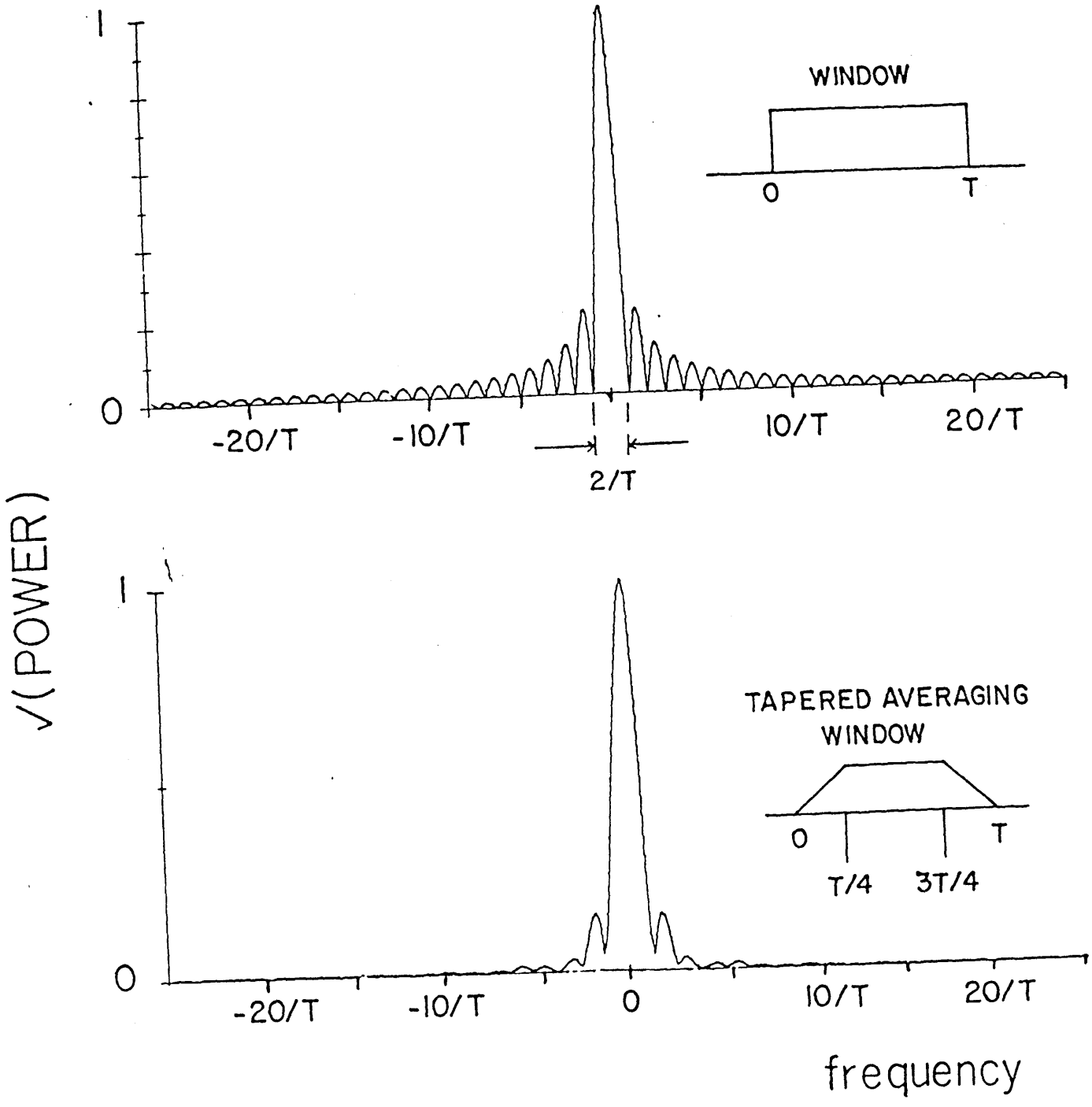
1
0
WINDOW
0
T
-20/T
-10/T
2/T
10/T
20/T
√(POWER)
1
0
TAPERED AVERAGING
WINDOW
0
T
T/4
3T/4
-20/T
-10/T
0
10/T
20/T
frequency

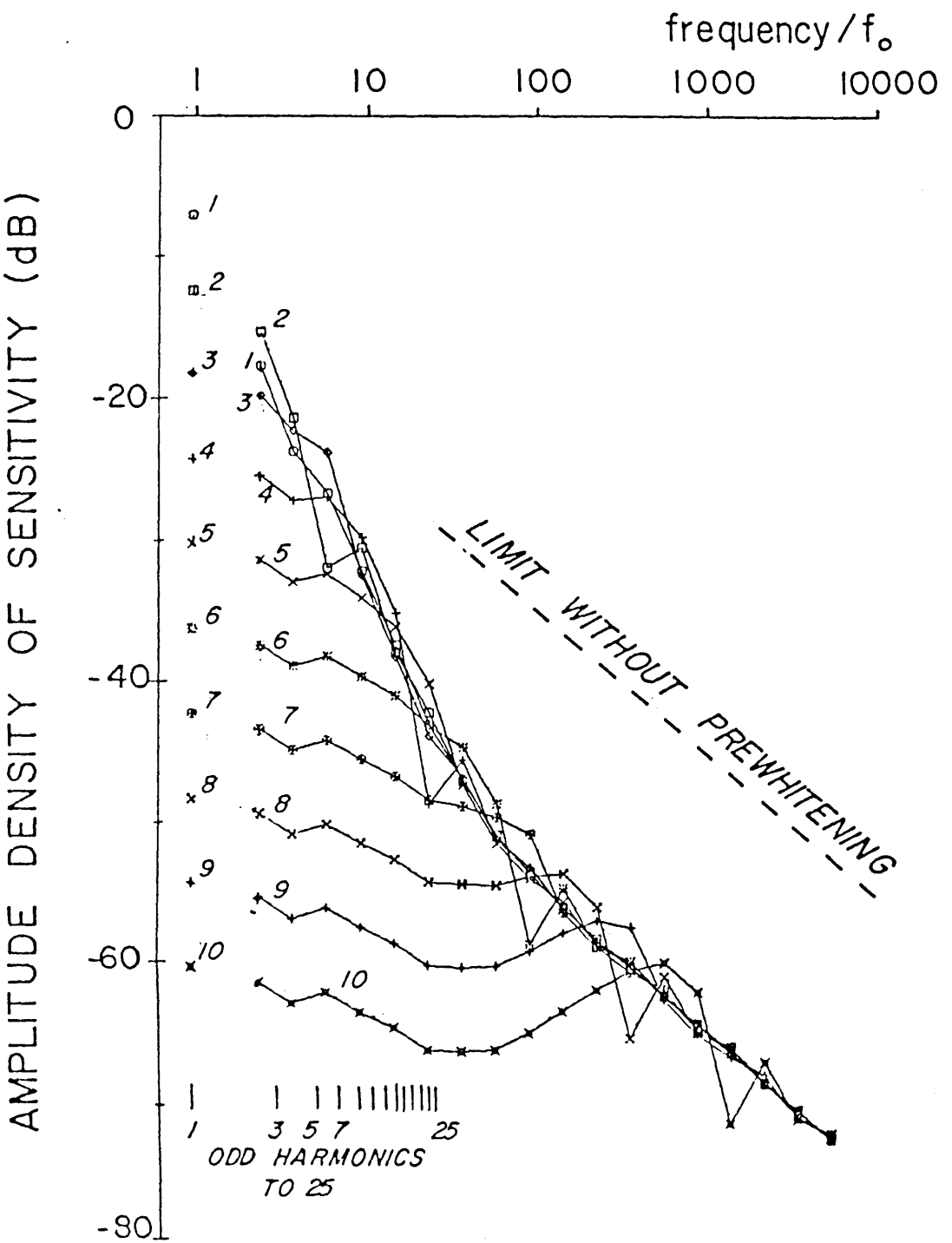
frequency / f_o
1
10
100
1000
10000
0
-20
-40
-60
-80
AMPLITUDE DENSITY OF SENSITIVITY (dB)
LIMIT WITHOUT PREWHITENING
1
2
3
4
5
6
7
8
9
10
1 3 5 7 25
ODD HARMONICS TO 25

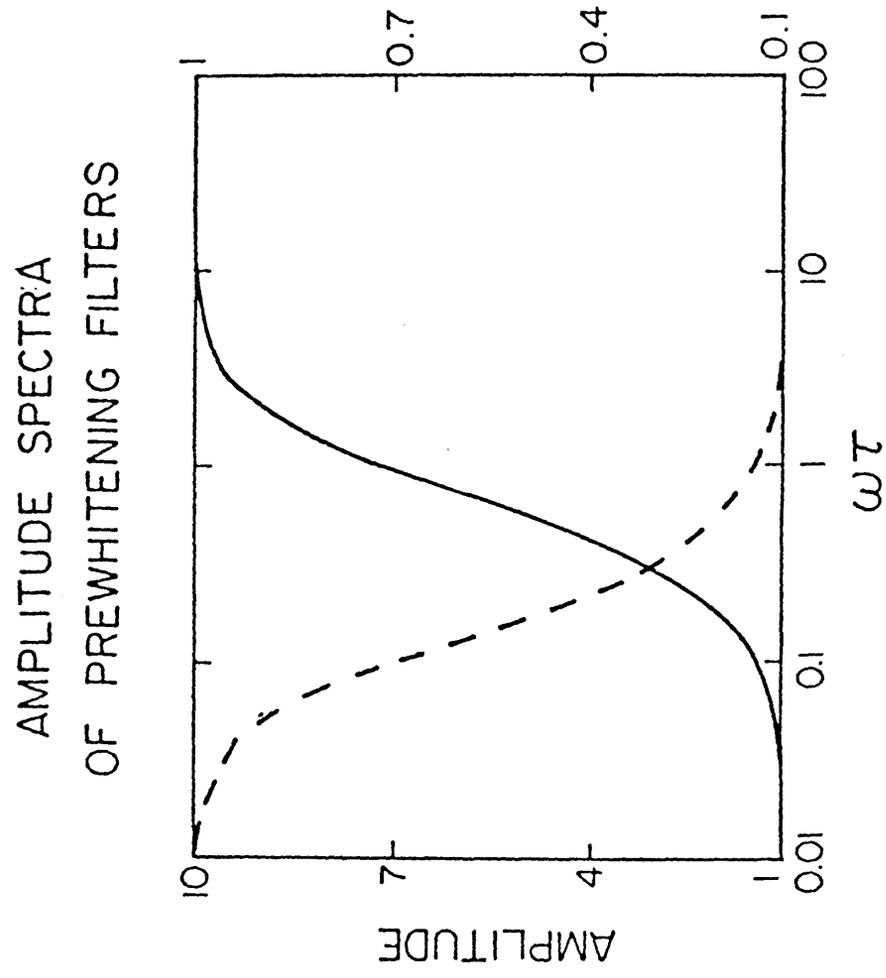
AMPLITUDE SPECTRA
OF PREWHITENING FILTERS
AMPLITUDE
10
7
4
1
0.01
0.1
1
10
100
0.1
0.4
0.7
1
ωτ

APPENDIX 1: NOISE RESPONSE OF A GENERAL MEASURING SYSTEM

A continuous linear sampler is a measuring device which associates an output $y(t)$ with an input $x(t)$ by means of a general linear transformation $G\{\}$ written as follows: *

$$y(t) = G\{x(t)\}$$

$$= \int_{-\infty}^{\infty} x(\theta)S(t,\theta)d\theta \qquad (A\text{-}1)$$

where $S(t,\theta)$ is called the sampling function and it describes the output at time t due to a spike input (delta function) at time θ. If the averaging process were a linear filter, the sampling function would be a function of lag $t-\theta$ instead of the independent time variables. In an averager designed to detect periodic signals, $S(t,\theta)$ may be periodic; i.e. describable in terms of lag $t-\theta$ and input or output time modulo the sampling period.

The transformation defined by A-1 is linear but non-stationary, and as such it does not belong to the class of transformations usually called <u>linear filtering operations</u>. It is linear in the sense that to a sum of inputs corresponds a similar sum of outputs. It is non-stationary, since from

$$y(t) = G\{x(t)\}$$

does not necessarily follow the relation,

$$y(t+\tau) = G\{x(t+\tau)\}$$

As a result of the non-stationarity, the energetic properties of the

*Refer to Appendix 2 for a complete Table of the Symbols used in this paper.

sampling operation may not be localizable in the frequency domain, as are, for example, those of linear filtering. Localizability is an important property treated in the mathematical theory of measures. If a measure is localizable, all its statistics are uniquely determined by the spectrum of the input.

Conditions for a localizable measure

A measure A_x of $x(t)$ defined by a general transformation

$$A_x = T\{x(t)\}$$

is localizable in frequency if it can be put in the form (Blanc-Lapierre & Fortet, 1953, p. 380)

$$A_x = \int_{\infty}^{+\infty} \bar{a}_x(\omega)\, d\omega$$

and if, for any given u obtained from x by linear convolution filtering

$$u(t) = \int_{\infty}^{t} g(t-\tau)\, x(\tau)\, d\tau \quad \leftarrow FT \rightarrow \quad \hat{u}(\omega) = \hat{g}(\omega)\, \hat{x}(\omega)$$

the same measure of u, A_u can be expressed in the form

$$A_u = \int_{-\infty}^{+\infty} |g(\omega)|^2 \bar{a}_x(\omega)\, d\omega$$

We will show in the following that a periodic measuring process can be considered localizable in the frequency domain for uncorrelated noise inputs, but not for signal inputs.

Signal and Noise

We consider that the input is a sum of a periodic signal

s(t) and a noise n(t)

$$x(e,t) = s(t) + n(e,t)$$

To emphasize the fact that the input is not deterministic, an ensemble variable e is written explicitly. In the above, t is system time defined by the receiver time base, and it can be re-enacted any number of times simply by repeating a measuring sequence. For a particular measuring sequence (i.e., for fixed e), n(e,t) is one realization of an infinite set of noise functions.

If we assume that the noise n(t) has zero mean, then the expected value of x(t) is the pure signal since computing an expectation is essentially an averaging of n(e,t) over the whole domain D of the expectation variable e. Thus

$$E\{x(t)\} = \int_D x(e,t)\ p(e)\ de = s(t) \qquad \text{(A-2)}$$

in which p(e) is the normalized probability distribution associated with n(e,t) as a function of the variable e and the integration covers the domain D of e. Integral A-2 can be regarded as generalisation of a linear combination. Consequently, the linear sampling operation defined by A-1 has an expected value of its output y(t) given by

$$E\{y(t)\} = \int_D y(e,t)\ p(e)\ de = G\{E\{x(t)\}\}$$

Therefore, if E{n(t)} is zero, the output of the sampler will be unbiased.

Covariance of Output

The covariance of the output is estimated

$$E\{y(t_1)\ y(t_2)\} = \int_{-\infty}^{+\infty}\int_{-\infty}^{+\infty}\int_{A} S(t_1,\theta_1)\ S(t_2,\theta_2)\ x(e,\theta_1)\ x(e,\theta_2)\ d\theta_1 d\theta_2 de$$

which is equivalent to

$$\int_{-\infty}^{+\infty}\int_{-\infty}^{+\infty} S(t_1,\theta_1)\ S(t_2,\theta_2)\ \left\{E\{n(\theta_1)n(\theta_2)\}+ s(\theta_1)s(\theta_2)\right\}\ d\theta_1 d\theta_2 \qquad (A\text{-}3)$$

since the other terms of $E\{x(\theta_1)x(\theta_2)\}$ are null because the noise is uncorrelated with the signal and has zero mean. Uncorrelated here means that $E\{n(\theta_1)s(\theta_2)\} = 0$ for any θ_1 and θ_2.

Separating y into parts due to signal and to noise

$$y = y_S + y_n$$

one finds that

$$E\{y(t_1)y(t_2)\} = y_s(t_1)y_s(t_2) + E\{y_n(t_1)\ y_n(t_2)\}.$$

The effect of noise is represented by the second term of the covariance. If we can assume that the noise is stationary, i.e., that its statistics and in particular its covariance do not depend on system time, we can write

$$E\{n(\theta_1)n(\theta_2)\} = c_n(\theta_1-\theta_2) = c_n(\tau)$$

c_n being the autocorrelation of the noise. Extracting from A-3 the term in n, one finds

$$E\{y_n(t_1)y_n(t_2)\} = \int_{-\infty}^{+\infty}\int_{-\infty}^{+\infty} S(t_1,\theta_1)S(t_2,\theta_1+\tau)c_n(\tau)\ d\theta_1 d\tau$$

Carrying the integration with respect to θ_1, the expression becomes

$$E\{y_n(t_1)y_n(t_2)\} = \int_{-\infty}^{+\infty} \Phi(t_1,t_2;\tau)\ c_n(\tau)\ d\tau$$

where $$\Phi(t_1,t_2;\tau) = \int_{-\infty}^{+\infty} S(t_1,\theta_1)S(t_2,\theta_1+\tau)\ d\theta_1 \qquad \text{(A-4)}$$

Using Parseval's formula, this expression can be put in the equivalent form

$$E\{y_n(t_1)y_n(t_2)\} = \frac{1}{2\pi} \int_{-\infty}^{+\infty} \hat{\Phi}(t_1,t_2;\omega)\ \hat{c}_n(\omega)\ d\omega \qquad \text{(A-5)}$$

where $\hat{\Phi}(\omega)$ and $\hat{c}_n(\omega)$ are respectively the Fourier transforms of $\Phi(\tau)$ and $c_n(\tau)$.

A similar demonstration can be made for noise filtered by a linear filter of gain $g(\omega)$, since this input would also be stationary. In such a case, one would obtain in formula (A-5)

$$c'_n(\omega) = |g(\omega)|^2\ \hat{c}_n(\omega) \qquad \text{(A-6)}$$

instead of $\hat{c}_n(\omega)$. Therefore, the covariance of the sampler output is a measure which is localisable in the domain of frequencies, and it can be evaluated knowing only the power spectrum of the noise.

In particular, (A-5) permits one to evaluate the variance of the sampler output

$$\sigma_y^2 = E\{y_n^2(t)\} = \frac{1}{2\pi} \int_{-\infty}^{+\infty} \hat{\Phi}(t,t;\omega)\ \hat{c}_n(\omega)\ d\omega \qquad \text{(A-7)}$$

which helps to determine the effect of noise on the precision of measurements. The variance may not itself be stationary, being possibly tied to the system time base; but if it is not stationary its dependence on t is usually small and periodic with the sampling

period. The time dependence can be removed from it and from the covariance by averaging $\hat{\Phi}$ over one period

$$\hat{\Psi}(\tau;\omega) \equiv \frac{1}{P}\int_{O}^{P}\hat{\Phi}(t,t+\tau;\omega)\,dt \qquad (A-8)$$

giving a stationary estimate for c_y

$$c_y(\tau) = \frac{1}{2\pi}\int_{-\infty}^{+\infty}\hat{\Psi}(\tau;\omega)\,\hat{c}_n(\omega)d\omega \qquad (A-9)$$

where $c_y(\tau)$ is the period averaged covariance of the output and

$$\bar{\sigma}_y^2 = c_y(O) = \int_{-\infty}^{+\infty}\hat{\Psi}(O;\omega)c_n(\omega)\,d\omega \qquad (A-10)$$

is the time averaged variance. In the above, the function $\hat{\Psi}$ is the noise sensitivity power spectrum. In the notation of the main text

$$K^2(\omega) \equiv \hat{\Psi}(O;\omega) \qquad (A-11)$$

If $S(t,\theta)$ is stationary, i.e. $S=S(t-\theta)$ as is the case with a discrete digital stacker or averager, Φ is time invariant since (A-4) reduces to the autocorrelation of S.

$$\Phi(\tau) = \int_{-\infty}^{\infty}S(t-\theta)S(t-\theta+\tau)\,d(t-\theta)$$

The Fourier transform of $\Phi(\tau)$ $(\hat{\Phi}(\omega))$ which is real because $\Phi(\tau) = \Phi(-\tau)$ is then the energy spectrum of S, and thus

$$K^2(\omega) = \hat{\Phi}(\omega) = \hat{S}(\omega)\,\hat{S}^*(\omega)$$

as given in Equation (8).

APPENDIX 2: SYMBOL TABLE

$x(t)$, $y(t)$, $u(t)$	Time varying signals; respectively an input to and an output from a measuring system, and a filtered version of an input.
$T\{x(t)\}$	An arbitrary linear transformation of $x(t)$.
$G\{x(t)\}$	A linear transformation producing $y(t)$ as its output and representing operation of a continuous measuring system.
t, θ	Time variables; specifically, time of output, time of input (where a distinction is necessary).
τ, δ	Time differences (lag); related to t, θ.
$\hat{x}(\omega)$ $\hat{y}(\omega)$ $\hat{u}(\omega)$	Fourier transforms of signals x,y,u.
ω	Angular frequency.
$g(t)$, $\hat{g}(\omega)$	An arbitrary linear filter, and its transform.
$s(t)$, $n(t)$	Periodic signal, random noise.
$\hat{s}(\omega)$	Fourier transform of $s(t)$.
$\lvert\overline{n}(\omega)\rvert^2$	Power spectrum of $n(t)$.

$S(\theta - t)$	Sampling function of a discrete averager; relative contribution of an input spike at time t to output at time θ.
$S(t,\theta)$	Sampling function of a general linear averager; relative output at time t due to a spike input at time θ.
$\hat{S}(\omega)$	Fourier transform of S(t).
A_x, A_u	A measure of time series x,u.
σ_x^2	Variance of Ax.
e, as in n(e,t)	Ensemble variable, signifying different realizations of n(t).
p(e)	Probability distribution in the ensemble.
$E\{x(t)\}$	Expectation of x(t); i.e., integral of x(e,t) weighted by p(e) over the domain D.
$c_n(\tau)$, $\hat{c}_n(\omega)$	Autocorrelation and power spectrum of n(t) $\hat{c}_n(\omega) \equiv \lvert\bar{n}(\omega)\rvert^2$
$\Phi(t,\theta;\tau)$, $\hat{\Phi}(t,\theta;\omega)$	An autocovariance and corresponding energy spectrum related to $S(t,\theta)$ by (A-4).
$\bar{K}(\omega)$	Spectral sensitivity to uncorrelated noise of the discrete sampler S(t), or the period averaged spectral sensitivity of sampler $S(t,\theta)$.

Δ_n	Time duration of the nth channel's sampling windows.
f_o	Base frequency of the signal s(t).
$R^n(t)$	Periodic reference waveform describing the sampling windows for the nth channel. (Base frequency f).
$W(t)$	Relative weighting in A of sampling windows at time t prior to the end of the last sampling period.
$T = N/f_o$	Measuring period lasting N base periods.
t_n	Mean delay time of the nth channel's sampling window.
$\bar{s}(t_n)$	Mean signal amplitude in the nth channel's positive sampling window.

SURVEY DESIGN FOR MULTICOMPONENT EM SYSTEMS

James C. Macnae *

REVISED JULY 1983, SUBMITTED TO GEOPHYSICS

*Geophysics Laboratory, Dept. of Physics, University of Toronto,
Toronto, Canada, M5S 1A7.

and Lamontagne Geophysics Ltd., 740 Spadina Ave,
Toronto, Canada, M5S 2J2.

ABSTRACT

A roving coil receiver is employed by several modern EM exploration systems to measure various spatial components of the time derivative of the magnetic field set up by a fixed transmitter. The absolute instantaneous secondary field measured above the surface of the earth is a potential field in this case, and, using well established potential field theory, it is known to be possible to predict the response of both horizontal components on any plane from a complete knowledge of the vertical component on the same plane. The required operation is simply performed in the wavenumber domain and is an amplitude invariant quadrature phase translation. In practice, errors are introduced in this transformation by spatial aliasing effects which depend on the sampling density and by windowing effects which depend on the areal extent of data coverage.

The major souce of noise in EM survey data collected in remote areas is sferic activity, which arises from the worldwide distribution of lightning discharges. Sferic noise, although time-varying, is predominantly uniform in a spatial sense, with local spatially varying anomalies near conductive inhomogeneities. Since the horizontal component noise amplitude is typically an order of magnitude greater than the vertical component noise amplitude, a strong case can be made that it is advantageous in routine surveys to increase the spatial coverage of vertical component data rather than to read both horizontal components.

INTRODUCTION

Large loop, time-domain, fixed-transmitter EM systems are currently in extensive use for mineral exploration. These include the UTEM® system manufactured by Lamontagne Geophysics, the Geonics EM37, the Crone DEEPEM, the Newmont EMP system and the Australian SIROTEM in roving receiver mode. Typical survey practice is to read the vertical component and sometimes one or both horizontal components of the EM system's magnetic fields at evenly spaced stations on picketed survey lines. Interpretation of the conductivity structure of the ground is then based on the detected secondary fields.

Horizontal component data may be collected because they aid in the interpretation process. However, in any particular prospecting situation, the benefits of horizontal component collection have to be weighed against the benefits of increased spatial coverage that could be obtained at equal cost if the vertical component alone were read. This paper will examine the factors that should be considered when making this choice. We will by examining the relationship between horizontal and vertical components to see how much independant information is contained in each.

® Registered trademark of Lamontagne Geophysics Ltd.

THE RELATIONSHIP BETWEEN VERTICAL AND HORIZONTAL COMPONENTS

We will denote magnetic field vectors with cartesian components (H_x, H_y, H_z) by the symbol $\vec{H}$. If we have a transmitter of fixed location, then the secondary time-varying magnetic field $\vec{H}^s$ may be mapped out on the surface of the earth. From Maxwell's equation we have:

$$\vec{\nabla} \times \vec{H}^s = \vec{J}^s + \partial \vec{D}^s / \partial t \quad . \qquad (1)$$

In the usual quasi-static approximation, $\partial \vec{D}^s / \partial t$ is negligible (Grant and West, 1965), and since all secondary currents lie beneath the surface of the earth we can set $\vec{J}^s = 0$ in the air. Since $\vec{\nabla} . \vec{H}^s = 0$, equation (1) reduces to Laplace's equation for measurements on or above the surface:

$$\nabla^2 \vec{H}^s = 0 \quad . \qquad (2)$$

This equation applies to the secondary magnetic field measured at any frequency or at any instant of time, and also to any linear combination of the fields such as an average of H_z^s in a time window or the difference in field intensity between two time windows. For systems which confine measurements to the transmitter off-time, separation of secondary from primary field is automatic, for UTEM where the primary field is always present separation can be acheived by either calculation and subtraction of the primary field or, more commonly, by use of a late time reference (Lamontagne, 1975).

Thus equation (2) implies that we can directly apply potential field theory well-developed for such fields as gravity and static magnetics to the secondary components of the EM magnetic field, whether in time or frequency domain. It is known for example that on a horizontal plane both horizontal components of a potential field may be derived from a complete knowledge of the vertical component (Skeels, 1947; Skeels and Watson, 1949). The original formulation of the required transformation by Skeels was as a surface convolution integral in the space domain, and Skeels and Watson presented a number of numerical examples of this data transformation. However, most recently published developments in potential field transformation and filtering have used Fourier techniques to perform computationally simpler operations in the wavenumber domain (Bhattacharrya, 1972; Bhattacharrya and Leu, 1977; Mohan et al. 1982; are typical examples).

Defining the two-dimensional Fourier transform to be

$$H_z^s(p,q) = \frac{1}{4\pi^2} \int_{-\infty}^{\infty}\int_{-\infty}^{\infty} H_z^s(x,y)\, e^{ipx}\, e^{iqy}\, dx\, dy$$

$$H_z^s(x,y) = \int_{-\infty}^{\infty}\int_{-\infty}^{\infty} H_z^s(p,q)\, e^{-ipx}\, e^{-iqy}\, dp\, dq$$

where $i = \sqrt{-1}$

represents the relationship between wavenumber (p,q) and space (x,y) domains on any surface of constant z. Taking the Fourier transform of equation (2) leads to the following simple expression defining the relationship between the horizontal (x,y)

and vertical (z) components of H^S to be

$$H_x^S(p,q) = \frac{-ip}{\sqrt{p^2+q^2}} H_z^S(p,q) \quad (3)$$

$$H_y^S(p,q) = \frac{-iq}{\sqrt{p^2+q^2}} H_z^S(p,q) \quad (4)$$

Assuming that there is no variation in the y direction we can rewrite (3) as

$$H_x^S(p) = -i \, sgn(p) H_z^S(p) \quad (5)$$

which is the mathematical statement that in a two-dimensional case H_x^S and H_z^S are the Hilbert transforms of each other. A pertinent discussion of the Hilbert transform relationship for two-dimensional static magnetic fields may be found in Nabighian(1972).

The transformations shown in (3), (4), and (5) are amplitude invariant, quadrature phase operations. The amplitude invariance property in two-dimensions can be taken to mean that the amplitude in a radial wavenumber $r=\sqrt{p^2+q^2}$ decomposition is unchanged by the transformation operator. For example, if random noise is present in data, then the expected value of noise amplitude in transformed horizontal components is identical to that measured in the original vertical component H_z^S data. Complications arise in practice in the transformation of actual data, and sampling density and windowing effects prevent perfect wavenumber decomposition, as will be discussed after an example.

THEORETICAL MODEL EXAMPLE

Program PLATE (Dyck et al., 1980) is a standard computer package for modelling the EM response of thin, rectangular conductors located in a resistive environment. The program was used to compute the reponse in channel 5 (mean delay time 0.8ms) of the UTEM time-domain EM system to a vertically dipping, thin plate conductor of strike length 500m, depth extent 250m, depth to top 50m, and conductance 10S. All three components H_x^s, H_y^s, H_z^s were calculated directly by the program. The vertical component H_z^s data were then Fourier transformed to the wavenumber domain using a standard library FFT routine, the multiplications of (4), (5) performed, and the data inverse transformed to yield predicted horizontal H_x^s, H_y^s components respectively. Figure 1 shows the results over a 1000m by 1000m grid, with 25m line/station spacing. The normalization used to express secondary fields as a percentage is division by the value of the primary field on the surface at a point located directly above the centre of the conductor. The difference at any point between transformed and directly modelled horizontal components is less than 3% of the peak H_x^s amplitude.

A close examination of this transformed data shows that the error mostly occurs as a "ripple" which can be seen near the grid edges on the H_x^s plot. This ripple (or ringing) is an artifact of discrete Fourier Transforms when any discontinuities exist at the edge of the data grid. Having seen one example of transformation of vertical component to horizontal component

data, we will now consider what areal coverage and sampling density is required to transform ideal data within required error bounds.

PRACTICAL TRANSFORMATION OF NOISE FREE DATA

In practice, vertical component data are usually collected on a grid, and consist of a discrete set of points on the surface of the earth which may not necessarily be a plane. Assuming a planar earth, errors will be introduced into the prediction of horizontal comonents using (4) and (5) both by inadequate sampling (aliasing) and windowing effects (e.g. Kanasewich, 1975). Aliasing effects arise when anomalies have high wavenumber (small wavelength) contributions, and the station/line spacing is not dense enough to sample the characteristics of the response. Windowing effects arise since the grid area is limited. This results in an inability to characterize the contribution of small wavenumber components.

Two common simplified EM models are the line current and the magnetic dipole. In space domain, the vertical component H_z^s of the magnetic field of a wire at depth z below the y axis (x=0) is given by:

$$H_z^s(x) = \frac{Ix}{2\pi(x^2+z^2)}$$

where I is the current in the wire. The Fourier transform of

this may be obtained from tables (Gradshteyn and Ryzhik, 1980, p. 1147) to be:

$$H_z^s(\rho) = \frac{-iI}{8\pi z^2}\,\rho z\, e^{-z|\rho|} \qquad (6)$$

The field of a horizontal dipole at depth z below the origin $\varsigma = \sqrt{x^2+z^2}$ of moment πIb^2 is given by Grant and West (1965) to be:

$$H_z^s(x) = \frac{Ib^2}{4}\left[\frac{3\varsigma z}{(\varsigma^2+z^2)^{5/2}}\right]$$

The corresponding wavenumber domain expression along the line y=0 can be obtained to be (Oberhettinger, 1957, p. 6; Abramowitz and Stegun, 1964, p.255):

$$H_z^s(\rho) = \frac{-iIb^2}{\pi z^2}\,\rho^2 z^2 K_1(\rho z) \qquad (7)$$

where $K_1(\rho z)$ is a modified Bessel function. Figure 2 shows the wavenumber variation of equations (6) and (7), plotted against a dimensionless wavenumber a=pz. Most amplitude in wavenumber domain is concentrated around the value a=1 or at wavenumbers equal to the inverse of the depth of burial. The amplitude drops off fairly sharply to both high and low wavenumbers.

Reconstruction of a space domain profile is ideally an integral with infinite limits, in practice an upper and lower limit on wavenumber must be used when the reconstruction is performed numerically. If we define a space domain error expectation k, then we can calculate the limits u,v of dimensionless wavenumber required to reconstruct a profile in space domain by integrating equation (6) to get:

$$\int_0^u a e^{-a}\,da = \int^{\infty} a e^{-a}\,da = k/2 \int^{\infty} a e^{-a}\,da = k/2$$

Numerical substitution with k=1% for example leads to values u=0.1z, v=8.0z. In field practice this requirement would be for a station spacing 10 times smaller than the depth to source, and a symmetrically placed survey line of length 8 times greater than the depth to source; or a total of 80 equally spaced stations! This will almost never be realized in routine surveys since there are typically only 20 to 40 stations on a survey line, and conductors may lie at any depth or location.

The model example shown in Figure 1 can be seen to have been chosen just about optimally for transformation on a 40 by 40 point grid, and is thus not representative of typical transformations ~~from~~ of anomalies from randomly positioned bodies. If all anomalies were detailed over their centres with logarithmic rather than equally spaced stations, then it would be possible to characterize the response in wavenumber domain with much fewer points, however such a procedure is totally unrealistic for routine field use.

TRANSFORMATION OF FIELD DATA

Figures 3 and 4 show examples of field data selected to show what problems may occur in routine transformation of field data. Both examples show profiles taken to be in the horizontal x direction. Figure 3 shows some UTEM data from the Cavendish test site, plotted as a secondary field normalized to the constant

primary field at the station closest to the conductor. The original plots of the UTEM multichannel response on six lines of the grid may be found in Macnae(1980). (The data there are plotted with a different convention, viz. continuous normalization to local primary field at each station rather than to a fixed value, and as such are not treatable as a potential field without renormalization.) Shown is the channel 5 response (mean delay time 0.8ms) and it is clear that the H_z^s anomaly is undersampled near the [illegible] crossover. Also shown is the transformed H_x^s data which was computed using equation (3) in the two-dimensional wavenumber domain, and based on six parallel lines of field data, all of which showed significant differences from each other, the differences indicating that sampling in the y direction was probably also inadequate. The difference between transformed and measured H_x^s amounts to about 20% of the peak-to-peak H_z^s response. What clearly has occurred here is that the station spacing is too large to permit accurate estimation of the high wavenumber components. The depth to top of conductive material is known to be only a few metres in this case.

Figure 4 shows an example from a much deeper conductor, with an anomaly extent much greater than the survey line length of 1500m. In this case eleven lines of data were used for the transformation, all of which were very similar to the H_z^s profile shown, implying that the detected conductor appeared was uniform over a strike length much greater than the survey dimensions. Thus, this example has reasonable sampling in the y direction.

The main problem in this case is that the low wavenumber components of the anomaly in the x direction cannot be well determined. The simply transformed H_x^s data are significantly different from the measured H_x^s data. In cases such as these, as is discussed in many texts, e.g. Kanasewich (1975), a discrete Fourier transform applied directly to the data assumes a spatial repetition of the survey data that is obviously unrealistic. To avoid this problem, a common practice in two-dimensional Fourier processing of airborne magnetic data is to predict and taper the data outside the survey area. However, depending on how tapering is done, there may still be significant effects in the estimation of the amplitude of long wavelength (low wavenumber) components. Figure 4 shows the change in predicted H_x^s response when the actual data was empirically "tapered" on the left (large discontinuity) side by simply folding the response about the leftmost point on the plot. The calculated H_x^s response is now much closer to the measured response than before, and essentially differs from measured H_x^s only by a monotonically decreasing amount of about 10% per km. The difference corresponds to a poor estimate of the amplitude of only one very low wavenumber, which if added would significantly reduce the difference between the actual and predicted data.

These above two examples show that H_x^s data may often be poorly estimated from undersampled H_z^s data by the transformation technique described. However, the essential object of any survey is not the measurement of the data itself, but rather the interpretation of this data in terms of a reasonable geological

model.

INTERPRETATIONAL VALUE OF HORIZONTAL COMPONENTS

Techniques for EM magnetic component interpretation have been developed in the spatial domain and to a lesser extent in the wavenumber domain as has been done for gravity and static magnetic responses. A full interpretation includes consideration of the frequency or time dependance of the response, and the nature of the induced eddy current system. For the moment, we will continue to consider only the independent interpretation of one channel of data. Although no attempt will be made to prove this, it is very reasonable to assume that proper interpretation cannot be achieved unless sufficient detail has been measured on the response to characterize it in both space and wavenumber domains, since perfect knowledge of one implies perfect knowledge of the other. Interpretation is in fact a non-unique operation, considerably more dificult than the simple transformation of vertical to horizontal data discussed here, and whose success relies heavily on the amount of detail in the data.

Interpretational error is, ~~however~~ of course, closely tied to data noise level. To estimate quantitatively the benefits of additional horizontal component data we will assume that the interpretational error is proportional to the data error as

measured in the amplitude and phase of a wavenumber decomposition, and confine the discussion to the two-dimensional (no y variation) case. The reason for choosing the wavenumber domain representation is that we know the response of both horizontal and vertical components is characterized by ~~the same~~ an identical amplitudes at each wavenumber as given in equation (5). At n space domain data points with separation Δx we can obtain by Fourier transformation two independent estimates of n discrete wavenumbers spaced $1/\Delta x$ apart. If both H_x^s and H_z^s data have equal noise levels, then the expected value of noise in an averaged estimate at each wavenumber is reduced by a factor of $\sqrt{2}$, and under our assumption then interpretation should be improved by this factor.

If we had read twice as many H_z^s values on a given profile, either twice as long or twice as detailed, then (Oppenheim and Schafer, 1975) we can either have 2n estimates at different wavenumbers, or combine these to yield n estimates at the original wavenumbers with noise expectation again $\sqrt{2}$ smaller than if just n data points were used. Depending on whether the profile is twice as detailed or twice as long, the advantage of this data over additional H_x^s data is that it is possible to estimate the amplitude of one wavenumber at twice(half) the previous largest(smallest) value respectively.

Under our assumption then, an interpretation made in wavenumber domain using both horizontal and vertical components with equal noise amplitudes is likely to have identical error expectation to that made from twice as many vertical component

data points. However some additional feature may be interpretable from the extra wavenumber data point which is only obtained from extra vertical coverage. Actual noise levels in horizontal and vertical components averaged for equal time are not in fact identical, as will be discussed.

NOISE

Noise affecting coil measured magnetic EM fields, and methods of minimizing its effects on data have been described by Macnae et al. (1983). For a coil receiver measuring the time derivative of the magnetic field, the most significant noise in areas remote from powerline systems is at high frequencies, and is a combination of wide-band sferic and narrow-band VLF transmissions in origin. Both VLF and natural sferic sources have themselves been used for EM prospecting in the past, so that we can turn to the literature on VLF and AFMAG techniques to see what the relationship of vertical and horizontal components of what for this discussion we will call "noise" is likely to be. AFMAG has been reviewed by Ward(1966), and VLF by Paterson and Ronka(1971).

For distant sources, the primary magnetic field measured by a coil receiver is predominantly horizontal, with a local anomalous vertical component response if any vertical inhomogeneity is present. Over uniform sedimentary basins with

flatly dipping strata, the vertical component of the "noise" is generally less than 1% of the total field. In vertically inhomogenous terrain, the amplitude of the vertical component of the "noise" will vary, and may locally become the predominant component of the total "noise" at the peak of a crossover anomaly.

Figure 5 shows a plot of the VLF amplitude (which may be considered linearly proportional to the expectation amplitude of other noise with a source in the same direction as the VLF transmitter) in the horizontal and vertical components along a line also surveyed with UTEM. All data were collected on Line C of the Cavendish test site in Ontario, Canada. The UTEM data are again channel 5 data, plotted as a secondary field with amplitude normalized to the primary field at station 16W. The scaling was chosen to create similar anomalous amplitude at zone A.

On the plot, the presence of the primary field in the horizontal component VLF or "noise" response is evident as a baseline shift. At zone A, both "noise" and Ch 5 response have the same form: a sharp crossover in the vertical component and a positive peak in the horizontal component. On zone B however, the "noise" and Ch 5 response are quite different. The UTEM Ch 5 response corresponds to a smooth crossover-type anomaly, interpreted to be caused by a good conductor at depth, whereas the "noise" response arises primarily from what is interpreted to be a poorer, near-surface conductor. The anomaly of this poorer conductor can be seen at earlier delay times in the UTEM response which are not plotted here but may be found in Macnae(1980). Locally increased noise levels with little coincident signal

response even at the earliest delay times are actually quite commonly observed in the field near steeply dipping or sharp-edged poor conductors such as fault/fracture zones.

This example shows that we cannot in general simply define the signal/noise ratio for one time channel in a survey area as it may vary from point to point depending on the local conductivity structure. However, it is almost invariably true that the noise in the horizontal component will significantly exceed that in the vertical component. For equal precision in averaged data, it is necessary to stack for a time equal to the square of the noise ratio between the two components.

IMPLICATIONS FOR SURVEY DESIGN

We have discussed the relationship between vertical and horizontal components of the secondary magnetic field, and the different effects of noise on each. An obvious question that needs careful consideration relates to survey design. Given certain geological and economic constraints, what is the optimum line/station spacing to read, what reading precision should be obtained by averaging, and which components should be read?

In massive sulphide exploration, the geological constraints typically include a probable strike direction and dip of the target, and the thickness and conductivity of overburden cover. Mathematically, a uniform strike implies that spatial variation in this direction will be much less than in that perpendicular to strike. This has led to the standard practice of surveying reasonably close stations on lines spaced somewhat further apart. Thick overburden cover indicates that the predominant wavelengths of any anomalies of interest will likely be large, and hence a wider station/line spacing can be tolerated. However in this case, the expected signal amplitudes will be smaller so that longer averaging times may be required. If moderately conductive inhomogeneities are present in the overburden it may be necessary to shorten the station spacing to permit recognition and stripping of nearer surface responses than those of interest. Economic constraints include such factors as the minimum size for a target to be of interest (which may well be a function of depth) and the total budget available for surveying.

Under such considerations, it is usual to choose as coarse a line/station spacing as feasible for reconnaissance so as not to miss any desirable target, and allow for detailing whenever any feature of interest is detected. In the reconnaissance mode, if station spacing is close enough, the routine reading of horizontal as well as vertical components will likely not lead to the discovery of any significant additional features and thus do little more than increase the cost of the survey. If sufficient detailing is done to characterize any detected anomaly, then the

previous discussion indicates that little additional interpretational benefit will result since the horizontal components can now be predicted from the vertical component. In particular, since the general horizontal noise is much greater than the vertical noise (an order of magnitude at times), greater averaging times are needed for equal precision in horizontal components, which further tips the balance in favour of reading the vertical component alone at a closer spacing or over a larger area.

A simple quantitative example may clarify this. Within a total budget \$B, we can calculate the distribution of costs as:

$$a(\$H_z^s) + b(\$H_x^s) + c(\$L) + \$Fixed = \$B$$

where a,b,c are coefficients,

$\$H^s$ is cost per reading,

\$L is cost of moving over

L km of line.

For readings of equal time, experience over the years indicates that with the UTEM system if both H_x^s and H_z^s are read at the same stations survey time increases about 35%, or b=0.35a. If readings of equal precision are taken, then survey time is generally doubled or b=a. The interpretational improvement as defined earlier from this additional horizontal H_x^s data can be estimated to be a factor of 1.15 to 1 and 1.4 to 1 for equal averaging time (assuming a 3:1 horizontal:vertical noise ratio) and equal precision respectively. The interpretational improvement of spending the extra time in collecting additional H_z^s data can either be an increase of 35% or 100% in areal

coverage, or in improving interpretation by detailing any detected anomaly to better characterize its high and low wavenumber components. If, for example, anomalies are present over 25% of the survey grid, detailing of H_z^s at one quarter of the station spacing would lead to an interpretational improvement of 2 in the same time that routine reading of H_x^s led to an improvement of 1.4. Of course, reading H_x^s only over anomalous areas would also lead to similar interpretational improvement at reduced coat.

However, there are a number of applications where the routine measurement of horizontal components may be extremely useful. These are mostly in cases where sufficient detailing is not feasible because access is limited. In borehole surveys, coverage on a plane is virtually never possible, and here multicomponent surveys would be extremely useful for interpretation (Dyck, 1981). Unfortunately in this case the severe technological problems of measuring components perpendicular to the hole and obtaining probe orientation currently prevent routine collection of this data. In rough terrain where access between lines is limited , reading of the horizontal components can be of great use in deciding which side of the survey line the conductor extends (a check of the relative shapes and amplitudes of the three component data of Figure 1 demonstrates this). As well in mountainous or very rough terrain, the vertical component will not be measured on a horizontal plane so that the Hilbert transform relationship will not apply and thus horizontal components are of greater use in

interpretation. For any moving transmitter/ moving receiver system such as Slingram or most airborne EM systems, the secondary field data are not a potential field, but rather are a set of readings each from a different potential field, and thus the reading of horizontal components can add significantly to the interpretability of the data.

CONCLUSIONS

Interpretation per se has not been discussed in this paper, neither of single time (frequency) channels measured over a grid, nor of the variation of response with delay time (frequency). We rather have considered only the nature of the data on which interpretation may be based. We introduced the existing knowledge that the horizontal and vertical components of any secondary EM magnetic field from a fixed transmitter are simply related through an amplitude invariant transform, which in the two-dimensional case reduces to a simple quadrature phase shift relationship with a variable sign transfer in the wavenumber domain. Because of this amplitude invariance, ~~the~~ wavenumber domain interpretation of any response in terms of a physical model can be identically performed whether the space domain data consisted of ~~were~~ vertical or horizontal components.

Under the assumption that interpretational error is proportional to the estimated error in a wavenumber decomposition of space domain data, the benefit of equally precise H_x^S data collected in addition to H_z^S data at the same stations is a $\sqrt{2}$ reduction in expected error. However, such a decrease in expected error is also easily obtainable from increased H_z^S coverage (detail, greater area) with the added benefit of additional estimates at different wavenumbers. Since readings of equal precision take a time proportional to the square of the signal to noise ratio, and the general noise level in the horizontal component is much greater than that in the vertical component, the cost/benefit balance is further tipped in favour of collecting additional H_z^S data. It should be reiterated that this conclusion applies only to fixed transmitter EM surveys where the data are collected on a plane.

ACKNOWLEDGEMENTS

This work was partially supported by the Ontario Geological Survey through grant GR10 to Lamontagne Geophysics Ltd, and through an NSERC Industrial fellowship to JCM. The computing was performed at the University of Toronto with support from G.F. West. Nigel Edwards kindly provided the core of the computer program used for transformation of the potential field data. Fruitful discussions with Yves Lamontagne are acknowledged. Khader Khan assisted greatly with the drafting.

APPENDIX: A NOTE ON QUADRATURE PHASE OPERATORS

We will restrict this discussion to two-dimensional fields (no y variation) measured along a single survey line. The space domain Hilbert transform equivalent to equation (5) is in one dimension and can be expressed as a simple filter suitable for convolution with data acquired at a spacing of 2 units as (Claerbout, 1976)

$$q_n = -2/\pi n \qquad n \text{ even} \qquad (8)$$

$$= 0 \qquad \text{elsewhere}$$

This filter is amplitude invariant , and is one example from a whole class of quadrature phase filters. Quadrature phase filters generally transform isolated peaks to crossovers and vice versa, with a reasonable (but not exact) correspondence between the location of inflection points in slope or amplitude. Figure 6 is an example from scale modelling to illustrate this type of behaviour. The plot shows the UTEM secondary field response over a wedge conductor. The wedge is of finite length, but the profile and transmitter loop are placed symmetrically with respect to its centre so that there is little local variation in the direction parallel to strike. It is clear from a careful look that, within experimental error, as the inflection points in the vertical component migrate with time, those in the horizontal component exactly follow. Although this point should be obvious, we note that slope inflection points need not coincide with the zero crossing.

Until recently, it was the practice of some contractors to plot time domain EM data on logarithmic scales. If this is done, it is not possible to locate routinely positions of slope inflection points, as the logarithmic scaling, and any background level shifts, alter apparent slopes dramatically. As a result, zero crossover points have been used rather than true inflection points in some interpretation methods. Inflection points are related to geometrical location of a conductor in a simpler manner than zero crossing points, and thus the interpretation of conductor location based on the position of zero crossings of H_z^s alone may often be in error. Since it is true that peaks of the H component are inflection points, and may be easily identified on a logarithmic plot, an unfortunate misconception has occasionally arisen that horizontal H_x^s data are better at defining the location of conductors than are H_z^s data.

Considering other quadrature-phase filters, perhaps the best known example in mining geophysical use is the Fraser filter, which consists in convolving data with the series (1,1,-1,-1). Figure 7 shows the Fraser filter, and 30 terms of the Hilbert filter of equation (8). Figure 8 shows the amplitude vs wavenumber response of three filters, the Fraser filter, the infinite length Hilbert filter, and a truncated version of the Hilbert filter. The Fraser filter has the great advantage of being very easy to apply, but the great disadvantage of a complicated gain response making its output a strong function of wavenumber. Its main succesful application has been in fairly specific applications for prospecting below a known thickness of

overburden where it can be matched to the expected peak wavenumber response from a subcropping conductor. The practical problem with the use of any Hilbert transform filter can be seen to lie in the great length of filter needed to to produce the amplitude invariance at low wavenumbers. It is necessary for a valid transformation to have either data that tends close to zero away from the area of interest (but is still within the sampled grid) or to use predictive extrapolation techniques outside the survey area to reduce the anomalies to a zero background within a larger grid. This is needed whether the filter is applied in space or in wavenumber domains. As mentioned earlier, all discrete Fourier transforms have implicit data repetition in the space domain and do not automatically solve this problem.

REFERENCES

Abramowitz M. and Stegun I.A., 1964, Handbook of mathematical functions, Dover, New York.

Bhattacharyya, B.K., 1972, Design of spatial filters and their application to high resolution aeromagnetic data, Geophysics v. 37 p. 68-91.

Bhattacharyya B.K. and Leu L.K., 1977, Spectral analysis of gravity and magnetic anomalies due to rectangular prismatic bodies, Geophysics v. 42 p. 376-387.

Claerbout J.S., 1976, Fundamentals of geophysical data processing, McGraw Hill, New York.

Dyck A.V., 1981, A method of quantitative interpretation of wide-band drillhole electromagnetic surveys in mineral exploration, PhD thesis, University of Toronto.

Dyck A.V., Bloore M., and Vallee M.A., 1980, User manual for programs PLATE and SPHERE, Research in appied geophysics #14, Geophysics Laboratory, University of Toronto.

Fraser D.C., 1969, Contouring of VLF-EM data, Geophysics v. 34 p. 958-967.

Gradshteyn I.S. and Ryshik I.M., 1980, Tables of integrals, series and products, Academic Press, New York.

Grant F.S. and West G.F., 1965, Interpretation theory in applied geophysics, McGraw Hill, New York.

Kanasewich E.R., 1975, Time sequence analysis in geophysics, University of Alberta Press, Edmonton.

Lamontagne Y., 1975, Applications of wide-band, time-domain EM in mineral prospecting, PhD thesis, University of Toronto.

Macnae J.C., 1980, The Cavendish test site; a UTEM survey plus a compliation of other ground geophysical data, Research in applied geophysics #12, Geophysics Laboratory, University of Toronto.

Macnae J.C., Lamontagne Y., and West G.F., 1983, Noise processing techniques for time-domain EM systems, Geophysics (submitted).

Mohan N.L., Sundadarajan N. and Rao S.V., 1982, Interpretation of some two-dimensional magnetic bodies using Hilbert transforms, Geophysics v. 47 p. 376-387.

Nabighian M.N., 1972, The analytic signal of two-dimensional magnetic bodies with polygonal cross-section, its properties and use for automated interpretation, Geophysics v. 37 p. 507-512.

Oberhettinger F., 1957, Tabellen zur Fourier transformation, Springer-Verlag, Berlin.

Oppenheim A.V. and Schafer R.W., 1975, Digital Signal Processing, Prentice Hall, New Jersey.

Paterson N.R. and Ronka V., 1971, Five years of surveying with the VLF-EM method, Geoexploration v. 9, p. 7-26.

Skeels D.C., 1947, Ambiguity in gravity interpretation, Geophysics v. 12 p. 43-56.

Skeels D.C. and Watson R.J., 1949, Derivation of magnetic and gravitational quantities by surface integration, Geophysics v. 14 p. 133-150.

Ward S.H., 1966, The electromagnetic method; in Mining Geophysics v. 2, SEG, Tulsa.

LIST OF FIGURE CAPTIONS

Fig. 1: Directly computed vertical H_z^s and horizontal H_x^s, H_y^s UTEM Ch. 5 response over a conductive plate, together with H_x^s, H_y^s components computed from the spatial variation of H_z^s by a two-dimensional, quadrature phase, amplitude invariant filter. The transmitter loop is the same size as the plotted grid and located immediately to the right of each plot.

Fig. 2: Amplitude of the wavenumber (p) variation of a line current (ae^{-a}) and a horizontal magnetic dipole ($a^2K_1(a)$) at a depth z with a=pz.

Fig. 3: Example of transformation of H_z^s data to the horizontal H_x^s component showing the effect of insufficient sampling density. The transformation was performed in two dimensions on six lines of data, of which only one is shown here.

Fig. 4: Example of transformation of vertical H_z^s data to horizontal H_x^s component. The survey line of length 1.5km is too short to map out the anomaly fully. The simple discrete transform applied implicitly assumes a spatial repetition of the H_z^s data which is unrealistic. The transform using an empirical extrapolation to taper the H_z^s data differs from the measured H_x^s data by one wavenumber component corresponding locally to a slope of 10% per km.

Fig. 5: UTEM Ch 5 secondary field and total VLF ("noise") amplitudes on line C at the Cavendish test site.

Fig. 6: Example of scale model UTEM H_z^s and H_x^s multichannel data over a wedge conductor. The secondary fields observed migrate and decay with time. With no spatial variation in the y direction, the extrema in slope and amplitude of H_z^s and H_x^s should closely correspond in location. Normalization of amplitude is to the primary field on surface at the station shown by the arrow.

Fig. 7: Coefficient amplitudes for the Fraser (dashed) and for 30 terms of the Hilbert (solid) filters suitable for convolution in space domain. The quadrature-phase property of both filters is shown by their antisymmetric form.

Fig. 8: Gain vs. wavenumber (p in cycles per station interval) of the Fraser and Hilbert filters. For plotting convenience, the gains of the Fraser and truncated Hilbert filters are only plotted up to a wavenumber of p=2, above this the amplitude oscillations become more and more condensed on the logarithmic scale.

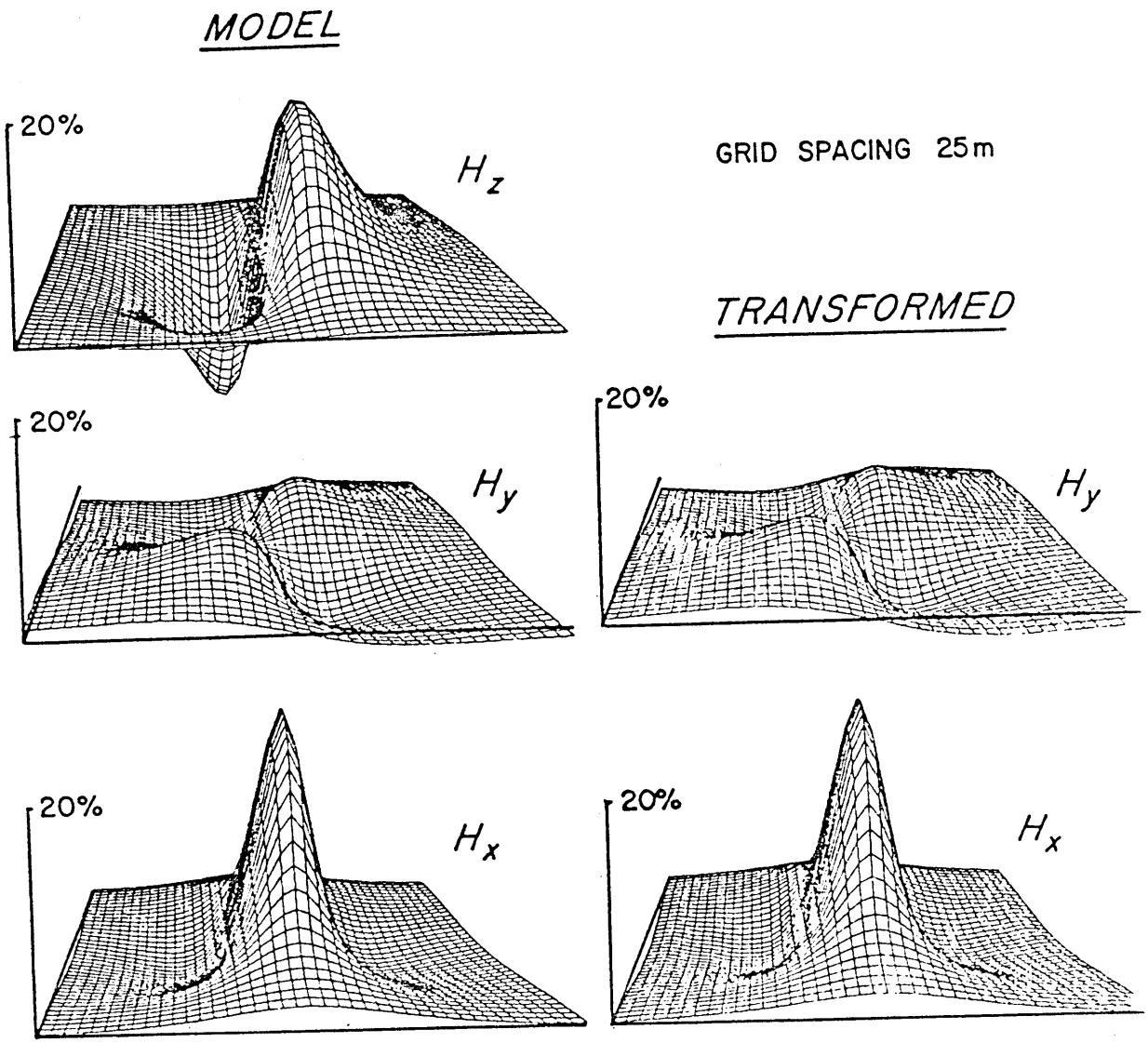
MODEL
20%
H_z
GRID SPACING 25m
TRANSFORMED
20%
H_y
20%
H_y
20%
H_x
20%
H_x

Fig. 1

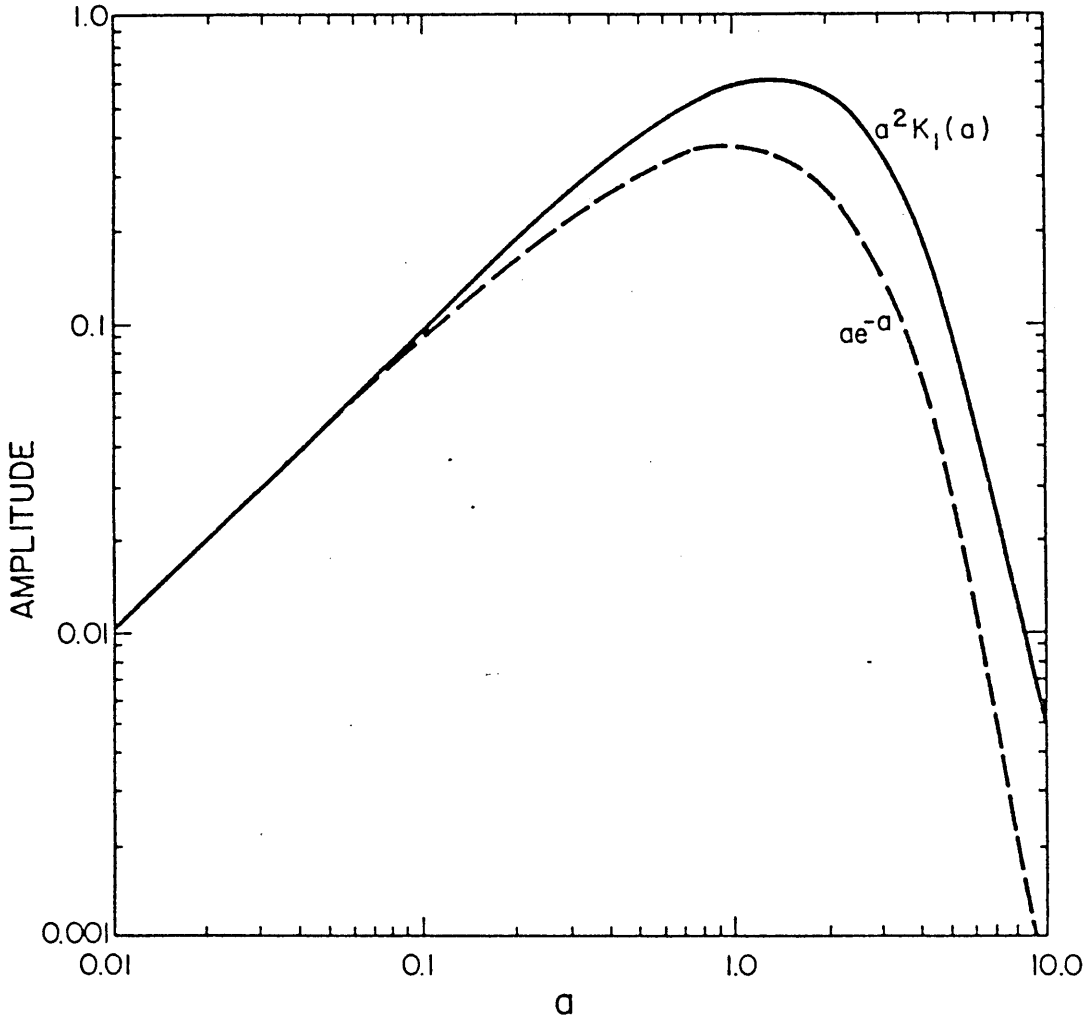

FIG 2.

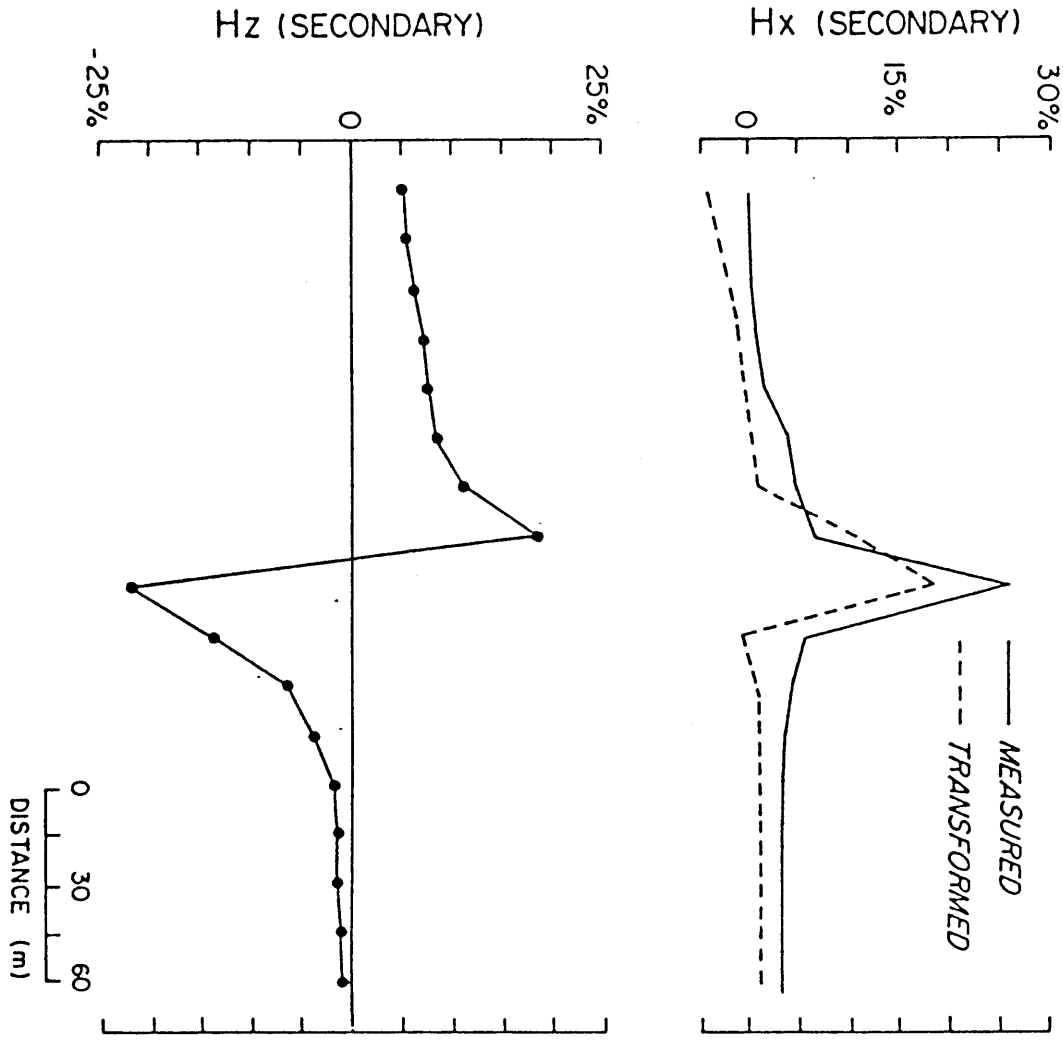
Hz (SECONDARY)
-25%
0
25%
Hx (SECONDARY)
0
15%
30%
MEASURED
TRANSFORMED
0
30
60
DISTANCE (m)

Fig 3

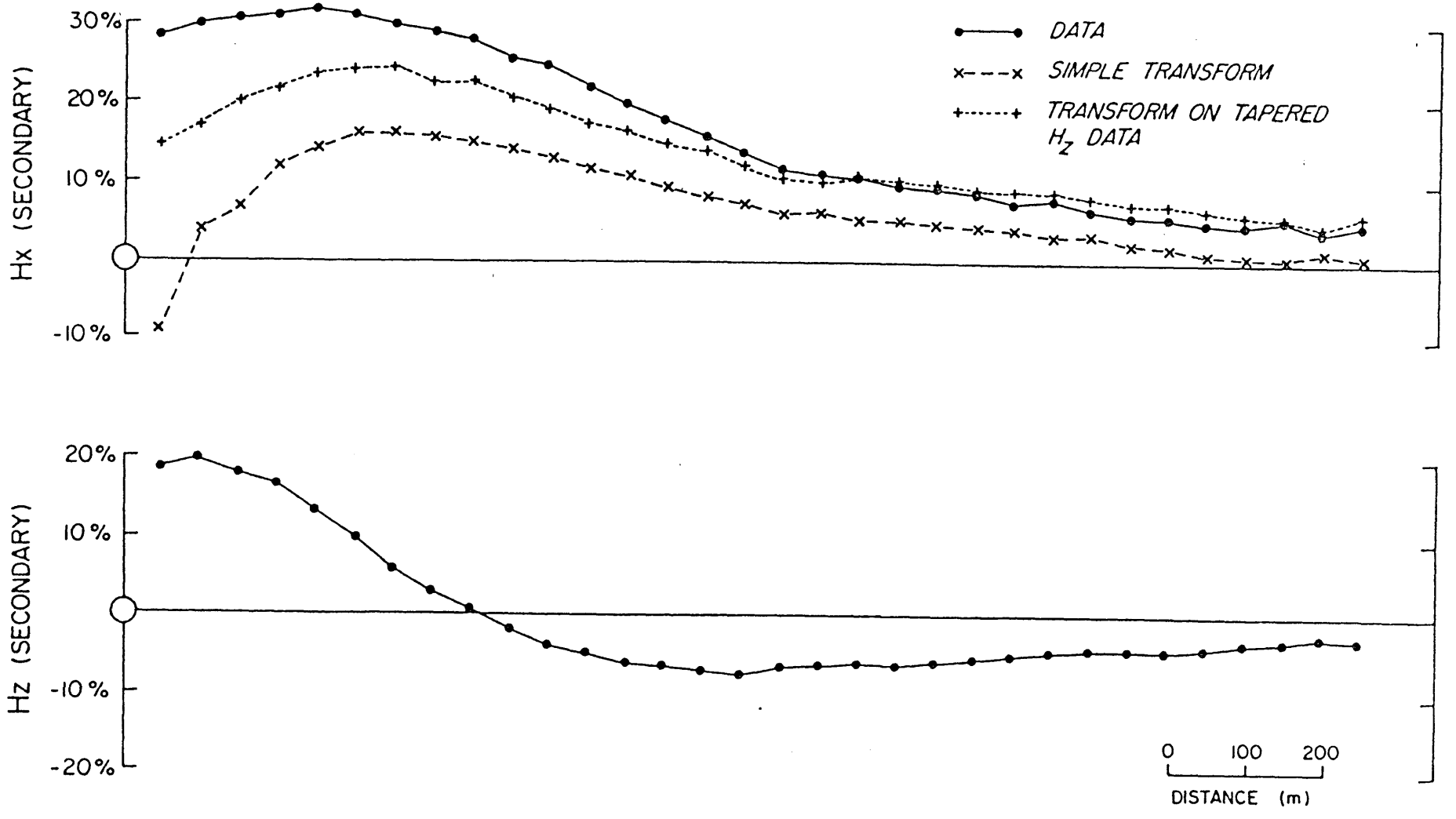
30%
20%
10 %
-10 %
Hx (SECONDARY)
DATA
SIMPLE TRANSFORM
TRANSFORM ON TAPERED
H_z DATA
20%
10 %
-10 %
-20%
Hz (SECONDARY)
0
100
200
DISTANCE (m)

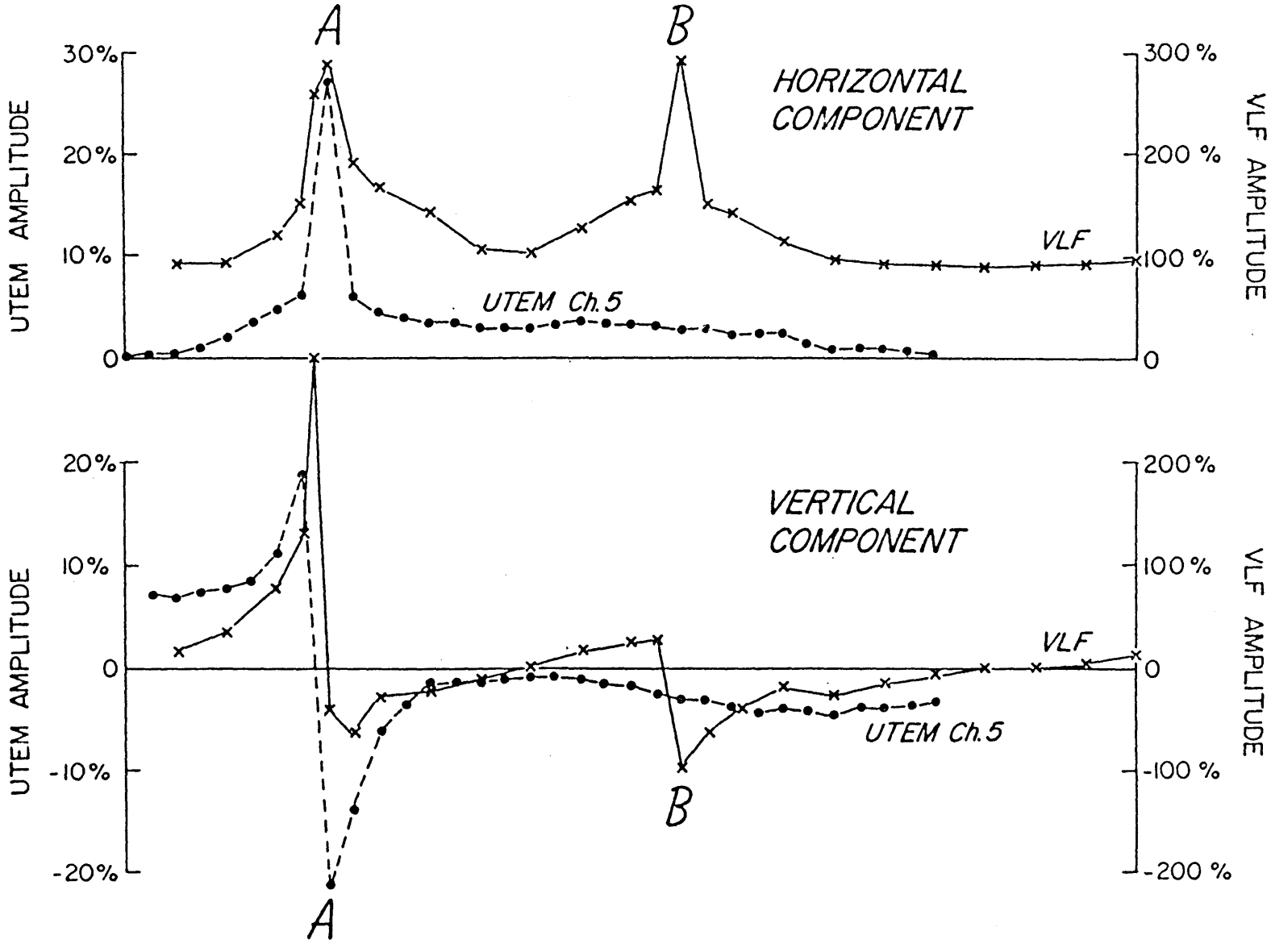
A
B
30%
20%
10%
0
300 %
200 %
100 %
0
UTEM AMPLITUDE
VLF AMPLITUDE
HORIZONTAL
COMPONENT
VLF
UTEM Ch.5
20%
10%
0
-10%
-20%
200%
100 %
0
-100 %
-200 %
VERTICAL
COMPONENT
VLF
UTEM Ch.5
B
A

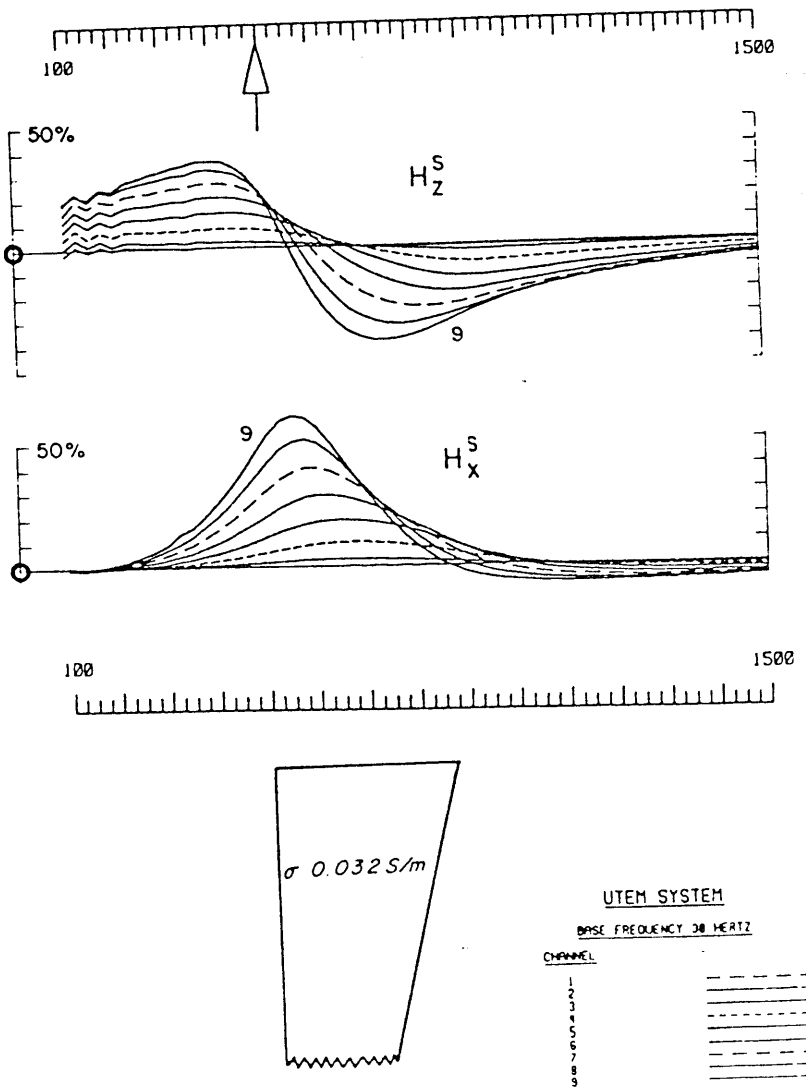
100
1500
50%
H_z^s
9
50%
9
H_x^s
100
1500
σ 0.032 S/m
UTEM SYSTEM
BASE FREQUENCY 30 HERTZ
CHANNEL
1
2
3
4
5
6
7
8
9

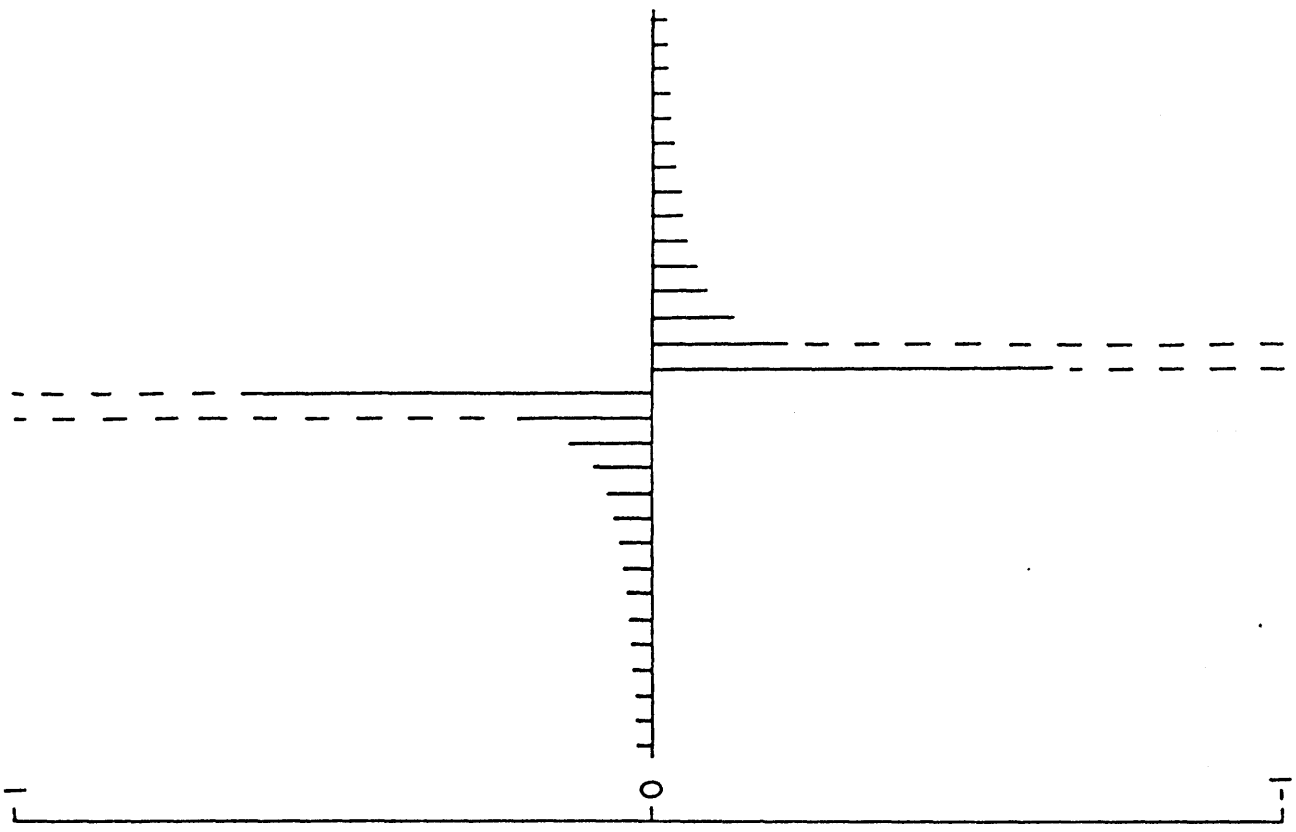

Fig 7

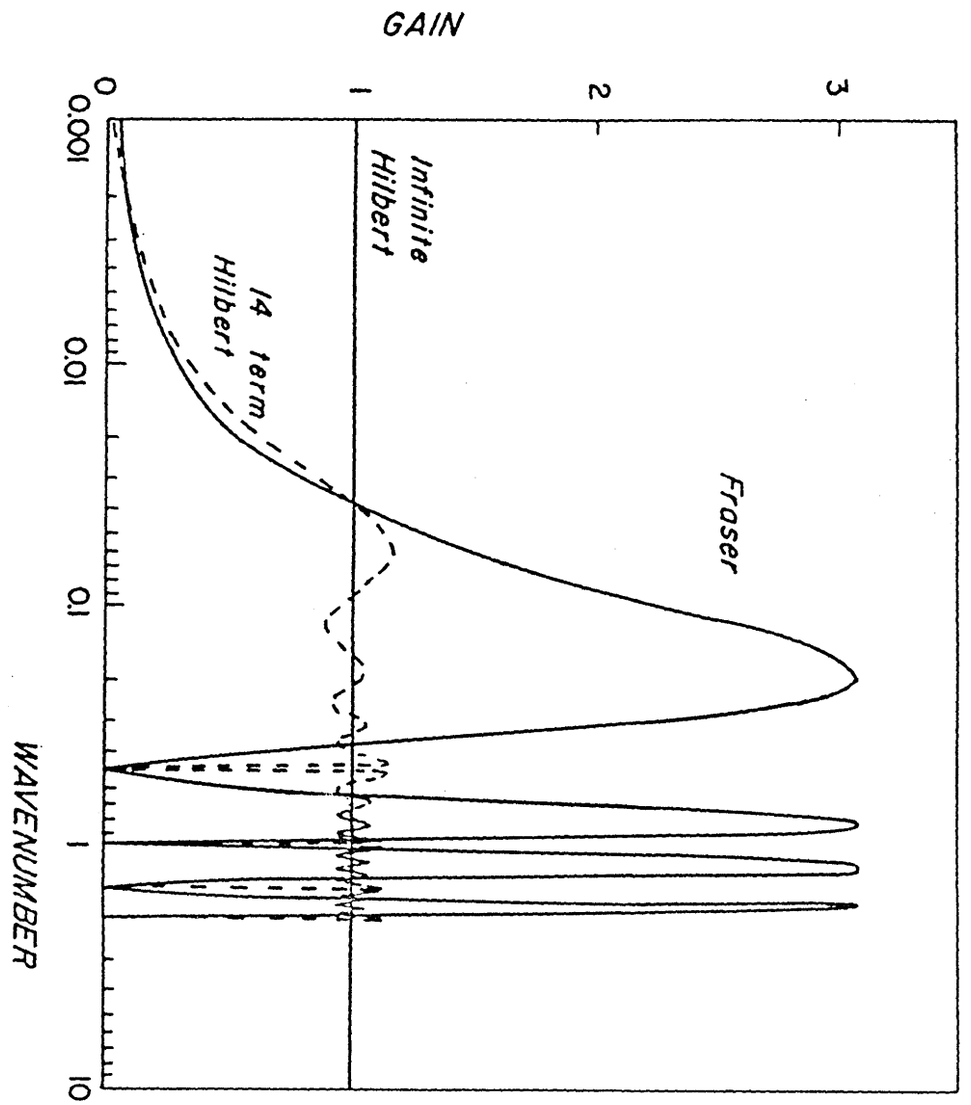
GAIN
0
1
2
3
0.001
0.01
0.1
1
10
WAVENUMBER
Infinite
Hilbert
14 term
Hilbert
Fraser

Fig 8